Field theoretical models of nonsingular compact objects

Marunović, Anja

Doctoral thesis / Disertacija

2013

Degree Grantor / Ustanova koja je dodijelila akademski / stručni stupanj: **University of Zagreb, Faculty of Science / Sveučilište u Zagrebu, Prirodoslovno-matematički fakultet**

Permanent link / Trajna poveznica: https://urn.nsk.hr/urn:nbn:hr:217:766282

Rights / Prava: In copyright/Zaštićeno autorskim pravom.

Download date / Datum preuzimanja: **2024-04-24**

SVEUČILIŠTE U ZAGREBU
PRIRODOSLOVNO-MATEMATIČKI FAKULTET
FIZIČKI ODSJEK

Anja Marunović

MODELI NESINGULARNIH KOMPAKTNIH OBJEKATA U TEORIJI POLJA

DOKTORSKI RAD

Zagreb, 2013.

UNIVERSITY OF ZAGREB
FACULTY OF SCIENCE
PHYSICS DEPARTMENT

Anja Marunović

FIELD THEORETICAL MODELS OF NONSINGULAR COMPACT OBJECTS

DOCTORAL THESIS

Suprvisor: Prof. Dubravko Horvat

Zagreb, 2013

SVEUČILIŠTE U ZAGREBU
PRIRODOSLOVNO-MATEMATIČKI FAKULTET
FIZIČKI ODJSEK

Anja Marunović

MODELI NESINGULARNIH KOMPAKTNIH OBJEKATA U TEORIJI POLJA

DOKTORSKI RAD

Mentor: prof. dr. sc. Dubravko Horvat

Zagreb, 2013.

Modeli nesingularnih kompaktnih objekata u teoriji polja

Anja Marunović

Predložena je metoda za testiranje linearne stabilnosti anizotropnih struktura s de Sitterovom jezgrom i primijenjena na gravastarske objekte. Pokazano je da se iz mikroskopskog pristupa, tj. unutar klasične teorije polja opisane lagranžijanom i (samo)interagirajućim poljima, mogu konstruirati stabilni, visoko kompaktni astrofizički objekti koji, za razliku od crnih rupa, ne posjeduju singularitet u središtu niti horizont događaja na Schwarzschildovom radijusu, a čiji je potpis vanjskom promatraču (u daljini) usporediv s potpisom crnih rupa. Predstavljena su dva modela: 1) lagranžijan skalarnog polja neminimalno vezanog na gravitaciju (tzv. bozonske zvijezde), te 2) lagranžijan više-komponentnog skalarnog polja koji generira topološki stabilan globalni monopol (tzv. D (defektne) - zvijezde). U prvom modelu su dobivene zvijezde slične zvijezdama tamne energije, a u drugom modelu su dobiveni objekti koji zbog jako visoke kompaktnosti predstavljaju dobru alternativu crnoj rupi.

(111 stranica, 111 literaturnih navoda, jezik izvornika engleski)

Field theoretical models of nonsingular compact objects

Anja Marunović

A method for testing linear stability of the anisotropic structures with the de Sitter interior is proposed. It was shown that from a lagrangian, field-theoretic description, one can obtain stable, compact astrophysical objects that at large distances behave as black hole mimickers but, unlike black holes, possess neither curvature singularities nor event horizons. Two models are presented: 1) lagrangian of the scalar field which is nonminimally coupled to gravity (the so called boson stars), and 2) lagrangian of the multi-component scalar field that generates a topologically stable global monopole (the so called D (defect) – stars). In the first model, a dark energy like stars are obtained, while in the second model an object with large compactness is obtained and as such represents a good black hole mimicker.

ACKNOWLEDGMENTS

CONTENTS

CHAPTER 1

PRELUDE

1.1 Motivation and scope

One of the most peculiar predictions of classical general relativity, at least if matter obeys the strong energy condition (SEC) are black holes. (According to the SEC the sum of the energy density and pressures, $\rho + \sum p_i \geq 0$, cannot be negative.) Black holes are stationary, vacuum solutions of the Einstein equations that possess an event horizon and a physical singularity which is *hidden* by the event horizon. This physical singularity represents an as-yet-unresolved problem, since it implies the controversial information loss paradox according to which any information will get completely lost on the singularity of a black hole. The principles of information loss are in conflict with the standard laws of quantum physics. Namely, as a consequence of unitarity of quantum physics, a complete information about a quantum system at one instance of time is sufficient to determine a complete information about the same system at a later time. (In quantum physics the state of a system is described by the wave function defined on a spacelike hypersurface and its evolution is determined by an unitary operator; unitarity of the evolution implies then conservation of the information.) Taking all these considerations into account it is natural to question whether the final stage of a massive star collapse is a black hole, or perhaps some other as-yet-not-understood dense object, that prevents further collapse.

Sakharov was the first that introduced the concept of nonsingular collapse

through the equation of state for the cosmological dark energy (for which the pressure is negative, $p \simeq -\rho$) as a super-dense fluid [1] and then Gliner assumed that such a fluid could be the final state of the gravitational collapse [2]. Inspired by these ideas Mazur and Mottola investigated alternative configurations which led to a solution dubbed the gravastar (*gravitational vacuum star*) [3]. This anisotropic, highly compact astrophysical object consists of a de Sitter core, which through a vacuum transition layer matches on an exterior Schwarzschild space-time by avoiding an event horizon formation. Due to their high compactness (defined as the ratio of the mass to radius) gravastars are perceived by distant observers as black holes, and hence they can be good black hole mimickers. On the other hand, observers that hover near the event horizon and in particular those that enter inside the event horizon of a black hole, can make a clear distinction between a black hole and a gravastar, primarily because black holes contain curvature singularities while gravastars do not.

Depending on their structure, one nowadays distinguishes two types of gravastars. The first type consists of thin shell layers that exhibit discontinuous functions of the energy density and the pressures [4], while the second type of the gravastar exhibits continuous functions of the energy density and the pressures [5]. However, apart from the de Sitter core, both types of gravastars possess the peculiar property of pressure anisotropy. Up to now all proposed models of gravastars have been macroscopic in the sense that they were modeled by fluids characterized by an equation of state and an anisotropy in the principal pressures. The desired physical properties were then obtained by solving the Einstein equations coupled to the fluid. Even though this approach was useful for understanding many gravastar's properties it remained unclear whether these gravastars permitted a more fundamental, microscopic, Langrangian description based on a covariant lagrangian of classical fields. A successful construction of a compact nonsingular object, such as the gravastar, from field theory would have important ramifications. Apart from a better understanding at the fundamental level, this would provide an explanation of the anisotropy in the principal pressures, which naturally occur in the stars made of scalar fields, the so-called boson stars. Furthermore, microscopic models of gravastars would shed light on the above-mentioned problems of curvature singularities and black hole information loss paradox.

The main objective of this thesis is to provide a feasibility study of microscopic models of black hole mimickers, *i.e.* to investigate whether one can obtain stable, compact astrophysical objects from the lagrangian, field-theoretic description that at large distances behave as black hole mimickers but – unlike black holes – possess neither curvature singularities nor event horizons.

The oldest, and accordingly the most studied, astrophysical example based on the Lagrangian formalism, is the boson star, which is a compact object built from a self-interacting, gravitationally bound scalar field [6]. It is known that boson stars coupled to Einstein's general relativity possess some features that characterize gravastars, such as the anisotropy in principal pressures and relatively large compactness ($\mu_{\mathrm{max}} = 0.32$). However, no matter how large the self-coupling is, the ordinary boson star cannot attain arbitrarily large compression and as such does not represent a good black hole mimicker. Furthermore, the principal pressures do not have a de Sitter-like interior - that is, their principal pressures are always positive at the origin. In order to overcome this problem in this work we extend the analysis of boson stars and modify the Einstein-Hilbert action by introducing a nonminimal coupling of the scalar field to gravity via the Ricci curvature scalar. We show that already this minimal extension of general relativity results in configurations that resemble more the dark energy stars then the ordinary boson stars, with compactness significantly larger then that in ordinary boson stars (if matter is not constrained with the energy conditions).

Another field-theoretic model that we investigate in this thesis involves a global monopole and a combined system of a boson star and a global monopole [7]. Global monopoles are extensively studied configurations in the context of cosmology. Namely, they belong to the class of topological defects, whose networks were studied in the 1980s and 1990s as a possible origin of Universe's large scale structure. Modern cosmological observations have ruled out topological defects as the principal seeds for structure formation, albeit a small fraction of cosmic microwave background thermal fluctuations might still originate from topological defects [8]. The simplest field-theoretic realization of the global monopole includes a scalar field theory with an (global) $\mathcal{O}(3)$ - symmetry which is spontaneously broken to $\mathcal{O}(2)$ by the vacuum. Within the framework of classical general relativity, the most prominent feature of the global monopole is the gravitationally repulsive core mass. When gravity is modified by introducing a nonminimal coupling how-

ever, the locally attractive regions of effective force emerge, thus enabling the existence of bound orbits. Due to all these peculiar features of global monopoles, it seemed reasonable to investigate the system consisting of a boson star and a global monopole. Indeed, we show that a repulsive monopole stabilizes an attractive boson star and the resulting configuration exhibits large energy density, large (and negative) principal pressures, large compactness, large effective potential, large local forces, and yet exhibit no event horizon. As such a composite system of a boson star and a global monopole represents a convincing microscopic candidate for a *black hole mimicker*.

1.2   Thesis Overview

The thesis is organized as follows:

Chapter 2 – *Gravitational vacuum stars*

This chapter is divided into two sections. In the first section we perform linear stability analysis of the continuous pressures gravastar following the conventional Chandrasekhar's method. Einstein equations for small radial perturbations around the equilibrium are solved as an eigenvalue problem. A set of parameters leading to a stable fundamental mode is found thus proving radial stability of the continuous pressure gravastar. In the second section the continuous gravastar model is extended by introducing an electrically charged component. The Einstein-Maxwell system with the de Sitter interior and Reissner-Nordström exterior is solved. The effect of the electric charge in terms of the anisotropy and the compactness is considered. This chapter is based on the articles [9, 10].

Chapter 3 – Nonminimal boson stars

A classical general relativity is modified by a rather *minimal* extension of the Einstein-Hilbert action by a nonminimal coupling of the scalar field to the Ricci curvature scalar, yielding configurations that resemble more the dark energy stars then the ordinary boson stars. Restrictions on matter from energy conditions are imposed showing

that the maximally allowed masses are shifted to the lower values due to the violation of the weak and dominant energy conditions. The effective compactness is calculated displaying its maximum value in the region of negative pressures which has been shown to be greater then that in ordinary boson stars. This chapter is based on the article [11].

Chapter 4 – Nonminimal boson D-stars

This chapter is divided into two parts. In the first part a global monopole, modeled by a classical field theory consisting of three interacting real scalar fields, is extended by introducing nonminimal coupling to gravity. Contrary to the minimal case, locally positive core mass functions and bound orbits are found. All other relevant functions (energy density, pressures, effective force, Newtonian force *etc.*) are analyzed depending on the deficit solid angle and the nonminimal coupling strength.

In the second section an analysis of the system consisting of the boson star and the global monopole which are nonminimally coupled to gravity is performed. According to the strength of the nonlinear gravitational effects and the gravitational backreaction, three distinct coupling regimes are featured: weak, mild and strong. In the strong coupling regime a composite object with the maximum compactness of order unity is found and compared to a Schwarzschild black hole.

Chapter 5 – Conclusions

This chapter brings conclusions and summary. Some ideas for future work are also discussed.

CHAPTER 2

GRAVITATIONAL VACUUM STARS

2.1 Radial stability

Since the seminal work of Mazur and Mottola [3] the concept of the **gravitational vacuum star** – the gravastar – as an alternative to a black hole has attracted a plethora of interest. In this version of the gravastar a multilayered structure has been introduced: from the repulsive de Sitter core (where a negative pressure helps balance the collapsing matter) one crosses multiple layers (shells) and without encountering an event horizon one eventually reaches the (pressureless) exterior Schwarzschild space-time. Afterwards some simplifications [4, 12] and modifications [13, 14] have been introduced in the original (multi)layer - onion-like picture.

Important step was done when it was shown that due to anisotropy of matter comprising the gravastar [15] one can eliminate layer(s) and the transition from the interior de Sitter to the exterior Schwarzschild space-time is possible by continuous stress-energy tensor [5] (see also [16]). The gravastar has been confronted with its rivals - black holes [17, 18] and wormholes [19, 20, 21], and investigated with respect to energy conditions (violations) [22]. Almost every research mentioned above to some extent addresses the problem of the gravastar stability, since the stability problem is crucial for any object or situation to be considered as physically viable. In Ref. [3] it was first shown that such an object is thermodynamically stable while axial stability of thin-shells gravastars was

tested in [12, 13]. Stability within the thin shell approach based on the Darmois-Israel formalism was recently reviewed in [23]. In [24] stability analysis of the thin shell gravastar problem is closely related to an attempt to distinguish the gravastar from a black hole by analysis of quasi normal modes produced by axial perturbations. The problem of stability of the rotating thin shell gravastar was addressed in [25]. Stability in (multi)layer version of the gravastar was also considered in [18, 26, 27, 28]. The axial stability of the continuous pressure gravastar was shown to be valid in [5]. This analysis was based on the Ref. [29] where stability of objects with de Sitter center was investigated.

In this section we analyze the radial stability of the continuous pressure gravastars following the conventional Chandrasekhar's method. Originally Chandrasekhar developed the method for testing the radial stability of the isotropic spheres [30] in terms of the radial pulsations. In Ref. [31] Chandrasekhar's method was generalized to anisotropic spheres. Stability of anisotropic stars was investigated before in [32, 33] and radial stability analysis for anisotropic stars using the quasi-local equation of state was given in [34].

The section is organized as follows. In next subsection 2.1.1 the Einstein equations and their linearization is given. The pulsation equation is derived, static solutions are described and an equation of state is calculated. In subsection 2.1.2 the eingenvalue problem is presented and results and discussion are given in last subsection 2.1.3.

Unless stated explicitly in this chapter we shall work in geometrized units for which $G_N = 1 = c$.

2.1.1   Linearization of the Einstein equation

Since we are interested to analyze the response of the gravastar-like objects to small radial perturbations, we assume that the pulsating object retains its spherical symmetry, and introduce the Schwarzschild coordinates:

$$ds^2 = -e^{\nu(r,t)}dt^2 + e^{\lambda(r,t)}dr^2 + r^2 d\theta^2 + r^2 \sin^2\theta d\phi^2, \tag{2.1}$$

where λ and ν are, in this dynamical setting, time-dependent metric functions. The standard anisotropic energy-momentum tensor appropriate to describe gravastar-

like objects is:

$$T_\mu^\nu = (\rho + p_r)u_\mu u^\nu + g_\mu^\nu p_r - l_\mu l^\nu (p_t - p_r) - k_\mu k^\nu (p_t - p_r), \tag{2.2}$$

where u^μ is the fluid 4-velocity, $u^\mu = dx^\mu/ds$, l_μ and k_μ are the unit 4-vectors in the θ and ϕ directions, respectively, $l_\mu = -r\,\delta_\mu^\theta$, $l^\nu = \delta_\theta^\nu/r$, $k_\mu = -r\sin\theta\,\delta_\mu^\phi$, $k^\nu = \delta_\phi^\nu/(r\sin\theta)$.

The velocity of the fluid element in the radial direction $\dot\xi$ is defined by:

$$\dot\xi \equiv \frac{dr}{dt} = \frac{u^r}{u^t}, \tag{2.3}$$

where ξ is the radial displacement of the fluid element, $r \to r + \xi(r,t)$. The components of the 4-velocity are obtained by employing $u_\mu u^\mu = -1$ and Eq. (2.3):

$$u^\mu = (e^{-\nu/2}, \dot\xi e^{-\nu/2}, 0, 0). \tag{2.4}$$

The non-zero components of the energy-momentum tensor (2.2) linear in $\dot\xi$ are:

$$T_t^t = -\rho, \qquad T_r^r = p_r, \qquad T_\theta^\theta = T_\phi^\phi = p_t,$$
$$T_t^r = -\dot\xi(\rho + p_r), \qquad T_r^t = e^{\lambda-\nu}\dot\xi(\rho + p_r). \tag{2.5}$$

The components of the Einstein tensor for the metric (2.1) are given in Appendix A. Following the standard Chandrasekhar method, all matter and metric functions should only slightly deviate from its equilibrium solutions,

$$\lambda(r,t) = \lambda_0(r) + \delta\lambda(r,t), \ \nu(r,t) = \nu_0(r) + \delta\nu(r,t), \tag{2.6}$$

$$\rho(r,t) = \rho_0(r) + \delta\rho(r,t), \ p_r(r,t) = p_{r0}(r) + \delta p_r(r,t), p_t(r,t) = p_{t0}(r) + \delta p_t(r,t). \tag{2.7}$$

The subscript 0 denotes the equilibrium functions and $\delta f(r,t)$ are the so-called Eulerian perturbations, where $f \in \{\lambda, \nu, \rho, p_r, p_t, \}$. The Eulerian perturbations measure a local departure from equilibrium in contrast to the Lagrangian perturbations, denoted as $df(r,t)$, which measure a departure from equilibrium in the co-moving system (fluid rest frame). The Lagrangian perturbations in the linear approximation play a role of a total differential and are linked to the Eulerian

perturbations via the equation (see *e.g.* Ref. [35]):

$$df(r,t) = \delta f(r,t) + f_0'(r)\xi. \tag{2.8}$$

A linearization of the Einstein equations $G_{\mu\nu} = 8\pi T_{\mu\nu}$ leads to the two sets of equations: one for the equilibrium (static) functions and the other for the perturbed functions. The equilibrium functions obey the following set of equations:

$$8\pi\rho_0 = e^{-\lambda_0}\left(\frac{\lambda_0'}{r} - \frac{1}{r^2}\right) + \frac{1}{r^2}, \tag{2.9}$$

$$8\pi p_{r0} = e^{-\lambda_0}\left(\frac{\nu_0'}{r} + \frac{1}{r^2}\right) - \frac{1}{r^2}, \tag{2.10}$$

$$8\pi p_{t0} = \frac{1}{2}e^{-\lambda_0}\left(-\frac{\nu_0'\lambda_0'}{2} - \frac{\lambda_0'}{r} + \frac{\nu_0'}{r} + \frac{\nu_0'^2}{2} + \nu_0''\right), \tag{2.11}$$

In practice, one usually combines these three equations into the Tolman-Oppenheimer-Volkoff (TOV) equation (see Appendix A):

$$p_{r0}' = -\frac{1}{2}\left(\rho_0 + p_{r0}\right)\nu_0' + \frac{2}{r}\Pi_0, \tag{2.12}$$

where Π_0 denotes the anisotropic term $\Pi_0 = p_{t0} - p_{r0}$. The other set of equations emerging from the linearization of the above Einstein equations yields the set of equations for the perturbed functions:

$$\left(re^{-\lambda_0}\delta\lambda\right)' = 8\pi r^2\delta\rho, \tag{2.13}$$

$$\delta\nu' = \left(\nu_0' + \frac{1}{r}\right)\delta\lambda + 8\pi re^{\lambda_0}\delta p_r, \tag{2.14}$$

$$\dot{\delta\lambda}\frac{e^{-\lambda_0}}{r} = -8\pi\dot{\xi}(\rho_0 + p_{r0}), \tag{2.15}$$

$$e^{\lambda_0-\nu_0}(\rho_0 + p_{r0})\ddot{\xi} + \frac{1}{2}(\rho_0 + p_{r0})\delta\nu' + \frac{1}{2}(\delta\rho + \delta p_r)\nu_0' + \delta p_r' - \frac{2}{r}\delta\Pi = 0. \tag{2.16}$$

Equation (2.16) is known as the *pulsation equation* [31] and it serves to probe the radial stability of the system of interest. It is actually the TOV equation for the perturbed functions which is obtained – analogously as the non-perturbed TOV – by combining Eqs. (2.13)–(2.15).

In order to solve the pulsation equation (2.16) for gravastar-like objects all

perturbed functions should be expressed in terms of the radial displacement ξ (and its derivatives) and the equilibrium functions. In performing this, one first integrates Eq. (2.15) yielding:

$$\delta\lambda = -8\pi r e^{\lambda_0}\xi(\rho_0 + p_{r0}). \tag{2.17}$$

Using this expression in Eq. (2.13) one obtains:

$$\delta\rho = -\frac{1}{r^2}\left[r^2(\rho_0 + p_{r0})\xi\right]'. \tag{2.18}$$

After inserting $\delta\lambda$ in Eq. (2.14) a dependence on δp_r remains which should be expressed in terms of the displacement function (and its derivatives) and the equilibrium functions. To accomplish this, one ought to explore the system at hand in more detail.

One of the possibilities, as suggested firstly by Chandrasekhar for isotropic structures [30] and more recently by Dev and Gleiser for anisotropic objects [31], is to make use of the baryon density conservation to express the radial pressure perturbation in terms of the displacement function and the static solutions. In this approach the adiabatic index appears as a free parameter. Chandrasekhar used this method to establish limiting values of the adiabatic index leading to an (un)stable isotropic object of a constant energy density. He showed that there were no stable stars of this kind if the adiabatic index was less than $4/3 + \kappa M/R$ (κ is a constant depending on the structure of the star, M and R are the star's mass and radius). In Ref. [31] the Chandrasekhar method was extended to various anisotropic star models and showed that the limiting value of the adiabatic index is shifted to lower values, *i.e.* anisotropic stars can approach stability region with smaller adiabatic index than in Chandrasekhar's case.

In this section our primary concern is to probe the radial stability of one particular anisotropic object – gravastar. Due to the peculiar character of the gravastar (especially its radial pressure – see below) one cannot expect the adiabatic index to be constant along the whole object. In fact the adiabatic index is a function of the energy density and pressure(s). This is the main reason why here we shall not test stability by fixing the appropriate values of the adiabatic index that guarantee stability. The required information will rather be extracted from a given static solution by constructing the equation of state.

Static solution

The procedure discussed so far is applicable to all spherically symmetric structures. To apply it to gravastar configurations one has to recall the basic characteristics of gravastars in the continuous pressure picture [5]. The energy density $\rho_0(r)$ is positive and monotonically decreases from the center to the surface. Gravastar has a de Sitter interior, $p_{r0}(0) = -\rho_0(0)$, and a Schwarzschild exterior. Furthermore, the atmosphere of the gravastar is defined as an outer region, near to the surface, where "normal" physics is valid [15], *i.e.* where both the energy density and the radial pressure are positive and monotonically decreasing functions of the radial coordinate. In the gravastar's atmosphere the sound velocity v_s, defined by

$$v_s^2 = \frac{dp_{r0}}{d\rho_0}, \tag{2.19}$$

is real $(v_s^2 > 0)$ and subluminal $(v_s < 1)$.

From the peculiar shape of the gravastar's (radial) pressure one can immediately infer that the sound velocity ought to be real only in the gravastar's atmosphere, whilst in the gravastar's interior it is imaginary, $v_s^2 < 0$. This is the main reason why, in probing the radial stability, we shall be primarily concerned with the physical processes occurring in the gravastar's atmosphere.

To construct a static gravastar, we adopt the energy density profile and the anisotropic term from the previous work [5]:

$$\rho_0(r) = \rho_c(1 - (r/R)^n), \tag{2.20}$$

$$\Pi_0(r) = \beta\rho_0(r)^m\mu_0(r). \tag{2.21}$$

Here n, m are (free) parameters and $\rho_c = \rho_0(0)$ is the central energy density. β is the anisotropy-strength measure and R is the radius of the gravastar for which $p_{r0}(R) = 0$. $\mu_0(r)$ is the compactness function defined by $\mu_0(r) = 2m_0(r)/r$, where $m_0(r)$ is the mass function $m_0(r) = 4\pi \int \rho_0(r)r^2 dr$. The radial pressure p_{r0} is a solution of the TOV (2.12) and the tangential pressure is readily obtained from the anisotropy and the radial pressure by employing the identity $p_{t0} = p_{r0} + \Pi_0$.

One such solution for fixed $(R, n, m) = (1, 2, 3)$ is shown in Fig. 2.1 for three different values of the central energy density ρ_c corresponding to three different values of the anisotropy strengths β. Since the radius R is fixed there is
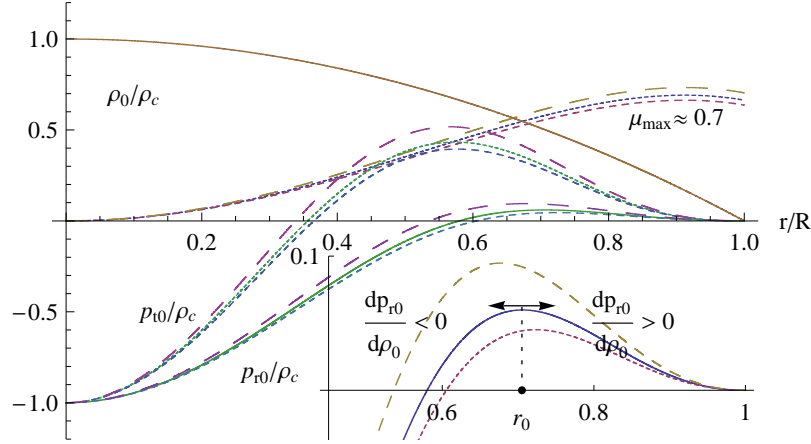
Figure 2.1. *The energy density ρ_0/ρ_c, radial pressure p_{r0}/ρ_c, tangential pressure p_{t0}/ρ_c and compactness μ_0 as a function of radius r/R for $\{R, n, m\} = \{1, 2, 3\}$. Three different values of the central energy density $\rho_c = \{0.19, 0.20, 0.21\}$ and their anisotropy strengths $\beta = \{92.90, 84.77, 76.11\}$ correspond to the lower, middle and upper curve, respectively. r_0 denotes the radius at which the sound velocity (2.19) vanishes (for the central curve).*

an interplay between the central energy density ρ_c and anisotropy strength β – higher central energy density ρ_c requires smaller anisotropy strength β. In subsection 2.1.2 where the radial stability of these three gravastar configurations will be tested it will be elaborated on this particular choice of parameters.

In the inset of Fig. 2.1 the radial pressure close to the surface is extracted in order to show important features of the gravastar's atmosphere. At the radius r_0 the sound velocity of the fluid vanishes $(dp_{r0}/d\rho_0|_{r=r_0} = 0)$ and hence r_0 serves as a division point of propagating (or physically reasonable) $(r > r_0, v_s^2 > 0)$ and non-propagating regions $(r < r_0, v_s^2 < 0)$ when probing radial pulsations of the gravastar.

The dominant energy condition (see Appendix B) is obeyed by both radial and tangential pressure throughout the gravastar. The compactness function has been shown in Fig. 2.1 also with approximately $\mu_{\max} \approx 0.7$ for all three configurations. Such huge values of the compactness function are hardly obtained in configurations with positive pressures and as such can be attributed to the violation of the strong energy condition, clearly present in the gravastar (de Sitter) interior.
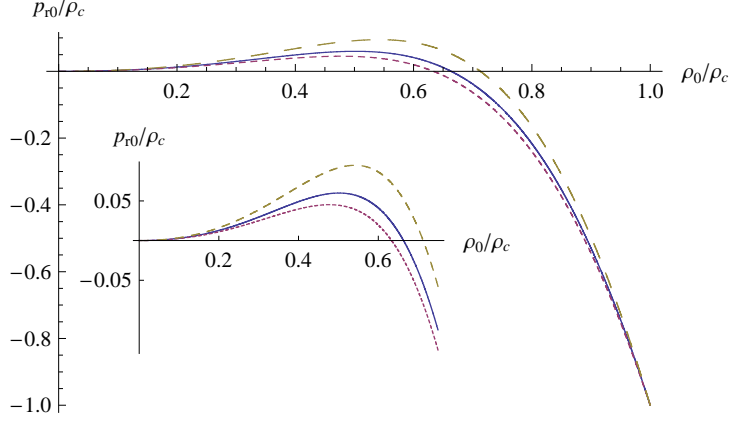
Figure 2.2. *The radial pressure p_{r0}/ρ_c against the energy density ρ_0/ρ_c (EoS) for $\{R, n, m\} = \{1, 2, 3\}$. Three different values of the central energy density $\rho_c = \{0.19, 0.20, 0.21\}$ and their anisotropy strengths $\beta = \{92.90, 84.77, 76.11\}$ correspond to the lower, middle and upper curve, respectively.*

Equation of state

Here we show that the equation of state (EoS) appropriate to describe the gravastar (inferred from (2.20) and (2.21)) is actually a function of the energy density (only) parameterized by the anisotropy strength β. Next this result is used to compute the Eulerian perturbation of the radial pressure δp_r from the EoS, by perturbing the energy density only. Ultimately this completes the task to express all perturbed functions in terms of the displacement (and its derivatives) and the static solutions.

Generally, for isotropic structures, before solving the TOV, one assumes that the pressure p and the energy density ρ are functions of the specific entropy s and the baryon density n. If the system is described by the one-fluid model than in static and dynamic settings it exhibits isentropic behavior (constant s), in which case one can set $s = 0$. Thus it is possible to eliminate the baryon density n and express the pressure in terms of the energy density only, leading to a barotropic equation of state $p = p(\rho)$. It is a rather simple task now to perturb this EoS and express the perturbed pressure in terms of the perturbed energy density.

For anisotropic objects the EoS is highly dependent on the anisotropic term model (see *e.g.* the TOV (2.12)). The anisotropic term used here (2.21) is a func-

tion (or a quasi-local variable [1]) of the energy density. This means that for a fixed anisotropy strength β there is a two parameter family of values $\{\rho_c, R\}$ belonging to the same EoS (see Fig. 2.2). As a consequence, one can obtain perturbed (radial) pressure by perturbing energy density only, and keeping anisotropy strength β fixed.

To illustrate this in more detail, an analytic form of the EoS is introduced which, to a good approximation, describes the gravastar defined by (2.20) and (2.21): [2]

$$p_{r0}(\rho_0) = -\rho_0^2 \left(\frac{1}{\rho_c} - \alpha \, \mu_0(\rho_0) \right). \tag{2.22}$$

Here α is closely related to the anisotropy strength β, $\mu_0(\rho_0)$ is the compactness function which is a function of the energy density. Now it is clear that for a fixed α the (radial) pressure is fully determined by the energy density.

In the linear approximation the Eulerian perturbation for the radial pressure expressed in terms of derivatives of the radial displacement and the static solutions is:

$$\delta p_r = -p'_{r0}\xi + \frac{dp_{r0}(\rho_0)}{d\rho_0}(\delta\rho + \rho'_0\xi). \tag{2.23}$$

Here $dp_{ro}(\rho_0)/d\rho_0$ denotes the derivative of the radial pressure with respect to the energy density. This is equal to $\frac{dp_{ro}/dr}{d\rho_0/dr}$ as both the radial pressure and the energy density are functions of radius r only.

Similarly, the Eulerian perturbation of the anisotropy $\delta\Pi$ assumes the form:

$$\delta\Pi = -\Pi'_0\xi + \frac{d\Pi_0[\rho_0]}{d\rho_0}(\delta\rho + \rho'_0\xi). \tag{2.24}$$

With the above two expressions the pulsation equation (2.16) is fully determined. However, before we proceed to solve the pulsation equation it is useful to rewrite Eq. (2.23) in a slightly different form in order to compare the result here with that of Chandrasekhar's for isotropic and Dev and Gleiser's for anisotropic stars.

---

[1] By the quasi-local variable we mean a function which is an integral in space of some local function – for example, the mass function $m_0(r)$ is a quasi-local variable of the energy density (which is a local function) as it is the volume integral of the energy density (the same holds for the compactness function). For a discussion of quasi-local variables and quasi-local EoS see *e.g.* Refs. [36, 37] and Ref. [34].

[2] It is worth noting that the analytic form of the EoS (2.22) is not restricted to the chosen energy density (2.20). For example, it is also appropriate to describe a gravastar with the energy density of the form $\rho_0(r) = \rho_c \, e^{-\eta \, r^2}$.

By means of the TOV (2.12) the perturbed energy density (2.18) can be written as

$$\delta\rho = -\rho_0'\xi - (\rho_0 + p_{r0})\frac{e^{\nu_0/2}}{r^2}\left(r^2 e^{-\nu_0/2}\xi\right)' - \frac{2}{r}\Pi_0\xi. \qquad (2.25)$$

Inserting this result in Eq. (2.23) the radial pressure perturbation becomes

$$\delta p_r = -p_{r0}'\xi - (\rho_0 + p_{r0})\frac{dp_{r0}[\rho_0]}{d\rho_0}\frac{e^{\nu_0/2}}{r^2}\left(r^2 e^{-\nu_0/2}\xi\right)' - \frac{2}{r}\Pi_0\frac{dp_{r0}[\rho_0]}{d\rho_0}\xi. \qquad (2.26)$$

If one now identifies the adiabatic "index" as

$$\gamma = \frac{\rho_0 + p_{r0}}{p_{r0}}\frac{dp_{r0}[\rho_0]}{d\rho_0}, \qquad (2.27)$$

our result is evidently equal to that of Dev and Gleiser (Ref. [31], Eq. (86)). Moreover, if one turns off anisotropy ($\Pi_0 = 0$) Chandrasekhar's result is obtained.

2.1.2   The pulsation equation as an eigenvalue problem

As in Chandrasekhar's method all matter and metric functions exhibit oscillatory behavior in time, $f(r,t) = e^{i\omega t}f(r)$. Hence the pulsation equation assumes the form:

$$\mathcal{P}_0\xi'' + \mathcal{P}_1\xi' + \mathcal{P}_2\xi = -\omega^2\mathcal{P}_\omega\xi, \qquad (2.28)$$

where $\mathcal{P}_0, \mathcal{P}_1, \mathcal{P}_2$ and $\mathcal{P}_\omega$ are polynomial functions of r and of equilibrium functions only (see Fig. 2.3). Eq. (2.28) represents an eigenvalue equation for the radial displacement ξ (with ω^2 being an eigenvalue). Solutions of this differential equation are obtained by specifying boundary conditions at the center and at the surface of the gravastar:

$$\xi = 0 \quad \text{at} \quad r = 0, \qquad (2.29)$$

$$\Delta p_r = 0 \quad \text{at} \quad r = R. \qquad (2.30)$$

The boundary condition at the center demands that there is no displacement of the fluid at the center of the gravastar. The boundary condition at the surface follows from the requirement that the Lagrangian perturbation of the radial pressure has to vanish at the surface [35, 38, 39]. In the model presented here, where $\Delta p_r = (dp_{r0}(\rho_0)/d\rho_0)\Delta\rho$, the sound velocity vanishes at the surface,

$dp_{r0}/d\rho_0|_{r=R} = 0$. This means that, apart from being finite, there are no further restrictions on $\Delta\rho(R)$. This also implies that it is sufficient to demand that $\xi(R)$ and $\xi'(R)$ are bounded in order to satisfy the boundary condition at the surface [38]. The choice

$$\xi'(R) = 0, \tag{2.31}$$

enables one to compare the results in the gravastar's atmosphere with the radial oscillations of the polytropes. This can be relevant as the EoS of the gravastar's atmosphere close to the surface can be approximated by the polytropic EoS $p_r \propto \rho^{1+1/n_p}$, where n_p is a polytropic index [5].

In order to study radial stability of the system described by Eq. (2.16) subject to the boundary conditions (2.29) and (2.30), it is plausible to recast the pulsation equation into the standard Sturm-Liouville form (see *e.g.* Ref. [35]):

$$(\mathcal{P}\xi')' + \mathcal{Q}\xi = -\omega^2 \mathcal{W}\xi, \tag{2.32}$$

where

$$\mathcal{P} = e^{\int \mathcal{P}_1/\mathcal{P}_0 \, dr} \qquad \text{and} \qquad \mathcal{Q} = \frac{P_2}{P_0}P, \quad \mathcal{W} = \frac{P_\omega}{P_0}\mathcal{P}. \tag{2.33}$$

The leading coefficient in the pulsation equation $\mathcal{P}_0$ has three zeros - two at the ends $\{0, R\}$ and one in the interior region r_0 $(dp_{r0}/d\rho_0|_{r=r_0} = 0)$, hence $\mathcal{P}_1/\mathcal{P}_0$ has three singular points (see Fig. 2.3), though all three are regular singular points or Fuchsian singularities [40] [3].

In order to obtain $\mathcal{P}$ the integral $\int \mathcal{P}_1/\mathcal{P}_0 \, dr$ should be calculated. Since the interior singularity arises at r_0 which is a division point between propagating and non-propagating domains, it is reasonable to divide the whole interval $\mathcal{I} = (0, R)$ into two parts: $\mathcal{I}_1 = (0, r_0)$ and $\mathcal{I}_2 = (r_0, R)$. In performing the integration numerically, infinitesimally small regions around all three singular points $\{0, r_0, R\}$ are excluded, so that both integrals are render convergent and finite. As a consequence, the leading coefficient in the Sturm-Liouville equation $\mathcal{P}$ is a positive function on the (whole) interval $\mathcal{I}$, whilst the weight function $\mathcal{W}$ is negative on the interval $\mathcal{I}_1$ and positive on the interval $\mathcal{I}_2$. As elucidated in the previous subsection, the interesting region is the gravastar's atmosphere, *i.e.* the second

---

[3] A singular point r^* is regular (or Fuchsian) if the function $\mathcal{P}_1/\mathcal{P}_0$ has a pole of at most first order, and the function $\mathcal{P}_2/\mathcal{P}_0$ has a pole of at most second order at the singular point $r = r^*$.
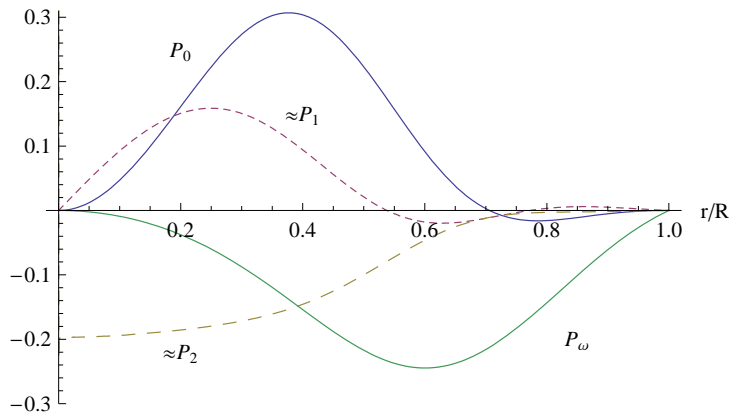
Figure 2.3. *The polynomial functions $\mathcal{P}_0, \mathcal{P}_1/20, \mathcal{P}_2/100$ and $\mathcal{P}_\omega$ from the pulsation equation (2.16) for $(R, n, m) = (1, 2, 3)$ and $(\rho_c, \beta) = (0.2, 84.77)$*

interval, $\mathcal{I}_2$. In this region the standard Sturm-Liouville eigenvalue problem formalism (see *e.g.* [38]) is applied, since $\mathcal{P} > 0$ and $\mathcal{W} > 0$. Therefore if ω^2 is positive, ω itself is real and the solution is oscillatory. If on the other hand ω^2 is negative, ω is imaginary and the solution is exponentially growing or decaying in time, thus signalizing instabilities. The number of nodes of the eigenvector ξ for a given eigenvalue ω^2 is closely related to the stability criteria. To be more precise, if for $\omega^2 = 0$ eigenvector ξ has no nodes, then all higher frequency radial modes are stable. Otherwise, if for $\omega^2 = 0$ eigenvector ξ exhibits nodes, then all radial modes are unstable. Furthermore, if the system is stable, then the following relations hold

$$\omega_0^2 < \omega_1^2 < \cdots < \omega_n^2 < \ldots, \tag{2.34}$$

where n equals the number of nodes.

2.1.3 Results and discussion

In testing stability of certain configurations in general, it seems natural that one attempts to find the critical values of the parameters for which the system is marginally stable. Marginal stability means here that the system exhibits the fundamental mode $(n = 0)$ for $\omega_0^2 = 0$. For example, in the case of neutron stars (described by the polytropic EoS), there exists a critical value of the central energy density for which the stellar mass M as a function of radius R is extremal.
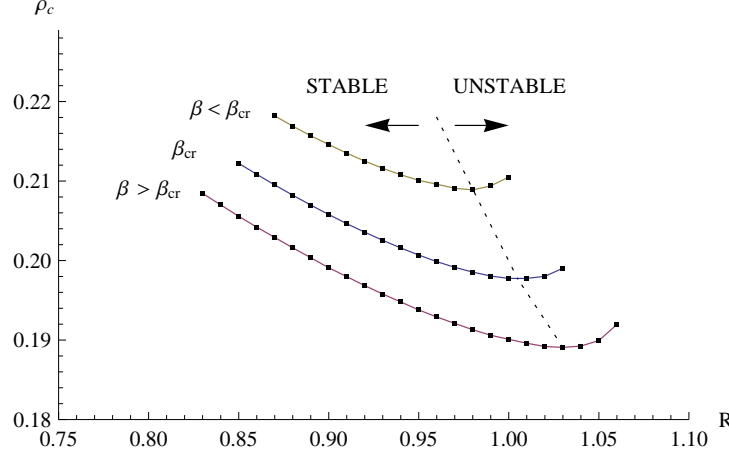
Figure 2.4. *The central energy density ρ_c against the radius R. For $\{R, n, m\} = \{1, 2, 3\}$ the anisotropy-parameter $\beta = \{92.90, 84.77, 76.11\}$ is constant on each curve and fixed by choosing the central energy density to be $\rho_c = \{0.19, 0.20, 0.21\}$ from the lower to the upper curve, respectively. The minimum of each curve represents marginally stable configurations.*

For such a critical value of the central energy density the star exhibits the fundamental mode with $\omega_0^2 = 0$. At the account of the $M(R)$ curve one can then read off which EoS will produce a stable star and which will not.

The gravastar-model described here displays a quite similar behavior. For each EoS (one β) the extremum of the $\rho_c(R)$ curve represents critical values of the central energy density ρ_c^{crit} and radius R^{crit} for which we have a fundamental mode, $\omega_0^2 = 0$ (see Fig. 2.4). Then for smaller radii the system exhibits stability, whereas for larger radii (than the critical one) it reveals instability. In Fig. 2.5 the behavior of the displacement function ξ for these three possible cases is given. If one fixes the radius R then there is an interplay between the central energy density ρ_c and the anisotropy strength β which characterizes a gravastar. Thus each curve represents one EoS. The central (solid) curve in Fig. 2.5 represents the fundamental mode. The upper (short-dashed) curve clearly shows stability of all radial modes as for $\omega_0^2 = 0$ there are no nodes, while the lower (long-dashed) curve represents the EoS which generates instabilities of all radial modes as there is a node in the fundamental mode. The lower, middle and upper curves in Fig. 2.5 correspond to the upper, middle and lower curves in Fig. 2.1 and
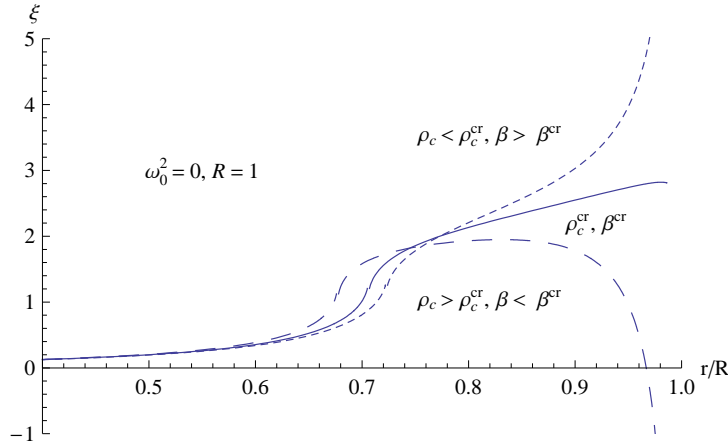
Figure 2.5. *The displacement function $\xi(r)$ for $\{R, n, m\} = \{1, 2, 3\}$ and $\omega^2 = 0$. Three different values of the central energy density $\rho_c = \{0.19, 0.20, 0.21\}$ and their respective anisotropy strengths $\beta = \{92.90, 84.77, 76.11\}$ correspond to the lower (unstable), middle (marginally stable) and upper (stable) curve respectively.*

Fig. 2.2, respectively. Here again one can relate this result to that of Ref. [31]: from Fig. 2.5, according to the values of the anisotropy strengths β, one can conclude that the anisotropy enhances stability.

Albeit from the viewpoint of radial pulsations, the gravastar's inner region does not seem to be physically attractive as the sound velocity is imaginary there, it is important to add a couple of comments on the radial displacement's behavior in that region. It is strongly attenuated in the gravastar's interior (see Fig. 2.5). This holds for all $\omega^2 > 0$. Therefore the radial pulsations of the gravastar as a whole can be seen as occurring prevalently in the gravastar's atmosphere whereas entering the interior region they are highly (but smoothly) attenuated. This is actually what one would intuitively expect from the repulsive gravitation caused by the de Sitter-like interior. [4]

Even though in this section the focus was set on one specific star model – the gravastar – the method used here can be extended to a broader class of anisotropic stars. The method can be actually generalized and applied to all anisotropic stars with the anisotropy being the function of the energy density. In this way the

---

[4]A good example of such a space is an inflationary universe. The electric and magnetic fields of free photons in such an inflationary (quasi-de Sitter) space get (exponentially) damped as $\propto 1/a^2$, while the physical wavelength gets stretched as $\propto a$. Here a denotes the scale factor of the Universe, which during inflation grows nearly exponentially in time.

adiabatic "index" does not have to be set to a constant but calculated from the static configurations. This comprises one of the main results of this section.

The main result of this section is the observation that the continuous pressure gravastar-model presented here exhibits radial stability as illustrated in Fig. 2.4 and Fig. 2.5. This result is important as it, along with the axial stability analysis, suggests that gravastars, albeit at a first sight being bizarre objects, can be viable physical compact object candidates.

2.2 Electrically charged gravastar

Charged anisotropic models were considered in a number of papers [41, 42, 43, 44, 45, 46, 47, 48] with differing contexts including electromagnetic mass models, δ-shell models, models with conformal symmetry or with varying cosmological constant *etc*.

In this section the gravastar picture is extended to include the effect of the electric charge as a natural step in gravastar investigations. Although astrophysical objects are essentially neutral, the problem of the electric charge in the phenomenological context could occur in the (strange) quark stars considerations, or accreting objects. Also, the influence of the electric charge on the space-time curvature and other features of the Einstein–Maxwell system, could be seen in the context of the model of a classical charged massive particle. Therefore the electric charge extension in the gravastar context could be understood as a natural step in investigations. The solutions for the charged gravastar obtained here satisfy the dominant energy condition (DEC) everywhere and possess no horizons. A valid DEC is taken as the principal criterion for the viability of solutions. The interior metric is obtained by solving the Einstein-Maxwell equations in which the matter — anisotropic inhomogeneous charged fluid — through the Gauss law constraint of electrostatics serves as a source for the electric field. Such charged objects induce the Reissner-Nordström (RN) exterior metric which smoothly joins the regular interior solution.

This section is organized into two subsections: in subsection 2.2.1 we present the model and solve the Einstein-Maxwell system; in subsection 2.2.2 we bring out the main results and conclusions.

2.2.1 The Model

From the previous chapter we adopt an essential ingredients of the gravastar with the continuous profiles of the energy density and pressures, and proceed to solving the Einstein–Maxwell system which is governed by the equations

$$R_{\mu\nu} - \frac{1}{2}g_{\mu\nu}R = 8\pi T_{\mu\nu}, \qquad F^{\mu\nu}{}_{;\nu} = 4\pi j^{\mu} , \tag{2.35}$$

where $R_{\mu\nu}$ is the Ricci tensor, $R = R^{\mu}_{\mu}$ is the Ricci scalar, $T_{\mu\nu} = {}^{(f)}T_{\mu\nu} + {}^{(c)}T_{\mu\nu}$ is the total energy-momentum tensor which is a sum of the anisotropic fluid and the electrostatic field. The electromagnetic part of the energy-momentum tensor is given by

$$^{(c)}T^{\nu}_{\mu} = \frac{1}{4\pi}\left(F^{\nu\delta}F_{\mu\delta} - \frac{1}{4}\delta^{\nu}_{\mu}F^{\alpha\beta}F_{\alpha\beta}\right) , \tag{2.36}$$

where $F_{\mu\nu}$ is the electromagnetic field strength tensor given in terms of the electromagnetic four-potential A_{μ}:

$$F_{\mu\nu} = \partial_{\mu}A_{\nu} - \partial_{\nu}A_{\mu} . \tag{2.37}$$

j^{μ} is the source four-current.

Presently we use the general form of the spherically symmetric static metric

$$ds^2 = g_{tt}(r)\,dt^2 + g_{rr}(r)\,dr^2 + r^2 d\Omega^2 . \tag{2.38}$$

Assuming now that the system at hand produces only electric field, the only non-vanishing component of the electromagnetic four-potential is $A_{\mu} = \delta^t_{\mu}A_t(r)$. It then follows that the only non-vanishing component of the field strength tensor is $F_{tr} = -F_{rt} = -\partial_r A_t$, so the locally measured radial electric field is

$$E = \partial_r A_t / \sqrt{-g_{tt}\,g_{rr}}. \tag{2.39}$$

The four-velocity of the static fluid element is $u^{\mu} = \delta^{\mu}_t / \sqrt{-g_{tt}}$, and the four-current of the electric charge with density $\sigma(r)$ is $j^{\mu} = \sigma\,u^{\mu} = \delta^{\mu}_t \sigma / \sqrt{-g_{tt}}$. The Maxwell equation reads $(r^2\,E(r))' = 4\pi\,r^2\,\sigma / \sqrt{g_{rr}}$, where prime denotes the derivative with respect to r. Integrating from the center to some radius r one

obtains the electric field

$$E(r) = \frac{q(r)}{r^2} \, , \qquad \text{where} \qquad q(r) = \int_0^r 4\pi \, r'^2 \, \sigma(r') \, \sqrt{g_{rr}(r')} \, dr' \qquad (2.40)$$

is the amount of the electric charge within the sphere of radius r. Now we can obtain the electromagnetic part of the energy momentum tensor

$$^{(c)}T_\nu^\mu = \frac{q^2(r)}{8\pi \, r^4} \, \text{diag}(-1, -1, 1, 1) \, , \qquad (2.41)$$

and the part due to the anisotropic fluid is

$$^{(f)}T_\nu^\mu = \text{diag}\left(-\rho(r), p_r(r), p_t(r), p_t(r)\right) \, . \qquad (2.42)$$

It is interesting to observe (see Eq. (2.41)) that the electrically charged components within the gravastar creates an anisotropy in principal pressures of the magnitude $E^2/4\pi$ – the radial pressure of the fluid is decreased while the transversal pressures (and the energy density) are increased for the same amount $E^2/4\pi$. Writing the metric components g_{tt} and g_{rr} in terms of two metric functions, $\nu(r)$ and $m(r)$, as

$$g_{tt}(r) = -e^{\nu(r)} \quad , \quad g_{rr}(r) = (1 - 2m(r)/r)^{-1} \, , \qquad (2.43)$$

the Einstein equations yield

$$
\begin{aligned}
m'(r) &= 4\pi \, r^2 \, \rho(r) + \frac{q(r)^2}{2r^2} \, , &(2.44) \\
p_r'(r) &= -(\rho(r) + p_r(r))\frac{\nu'}{2} + \frac{\sigma(r) \, q(r)}{r^2\sqrt{1 - 2m(r)/r}} + \frac{2}{r}\left(p_t(r) - p_r(r)\right), &(2.45) \\
\nu'(r) &= \frac{2m(r)/r^3 + 8\pi p_r - q^2(r)/r}{1 - 2m(r)/r}. &(2.46)
\end{aligned}
$$

Eq. (2.44) defines the 'mass function' $m(r)$ and (2.45) is the well-known Tolman-Oppenheimer-Volkoff (TOV) equation (see Appendix A) for the anisotropic and electrically charged fluid.

For the electrically charged gravastar model, we couple two density profiles in the following way

$$\sigma(r) = \varepsilon \, \rho(r) \, \sqrt{1 - 2m(r)/r} \, , \qquad (2.47)$$

with ε constant [45, 47, 49, 50]. The equations (2.44–2.46) together with the Maxwell equation that can be written as

$$q'(r) = 4\pi \, r^2 \, \sigma(r) \, \frac{1}{\sqrt{1 - 2m(r)/r}} \, , \qquad (2.48)$$

constitute central equations of this section which are solved upon providing boundary conditions

$$m(0) = 0, \quad p_r(0) = -\rho_0, \quad \nu(\infty) = 0, \quad q(0) = 0. \qquad (2.49)$$

2.2.2   Results and conclusions

The interior solution needs to be matched to the exterior segment of the Reissner–Nordström (RN) space-time

$$ds^2 = -\left(1 - \frac{2M}{r} + \frac{Q^2}{r^2}\right) dt^2 + \left(1 - \frac{2M}{r} + \frac{Q^2}{r^2}\right)^{-1} dr^2 + r^2 d\Omega^2 \, . \qquad (2.50)$$

This metric has two horizons: an event horizon and an internal Cauchy horizon. The horizons are obtained for $g_{rr}^{-1} = 0$ yielding

$$r_\pm = M \pm M\sqrt{1 - \kappa^2}, \qquad (2.51)$$

where $\kappa = Q/M$. If the two metrics are now matched at $r = R$, we obtain

$$m(R) = M - \frac{Q^2}{2R} \quad \text{and} \quad q(R) = \varepsilon m_f(R) = Q \, . \qquad (2.52)$$

These conditions set restrictions on the values for ε:

$$\varepsilon_\pm = \frac{2}{\tilde{\mu}\kappa}\left(1 \pm \sqrt{1 - \tilde{\mu}\kappa^2}\right) \quad , \qquad \tilde{\mu} = 4\frac{\tilde{m}_c(R)}{m_f(R)} + \frac{2m_f(R)}{R} \, , \qquad (2.53)$$

where $\tilde{m}_c = m_c/\varepsilon^2$ and were the total interior mass is written as a sum of the two constituents masses:

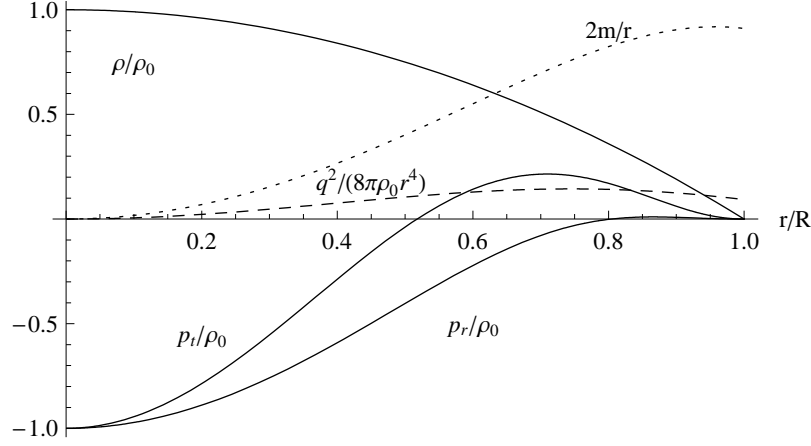$$m(r) = m_f(r) + m_c(r) \, , \qquad (2.54)$$

Figure 2.6. *Continuous profile gravastar solution inducing the ERN ($\kappa = Q/M = 1$) space-time: energy density (2.20) with $n = 2$ and pressure anisotropy (2.21) with $m = 2$, $\rho_0 R^2 = 21/32\pi$ and surface compactness $\mu = 0.91$.*

with

$$m_f(r) = \frac{q(r)}{\varepsilon} = \int_0^r 4\pi\, r'^2\, \rho(r')\, dr' \quad , \quad m_c = \int_0^r \frac{q^2(r')}{2r'^2}\, dr' \,, \tag{2.55}$$

where subscript f stands for the (gravastar) fluid and subscript c stands for the (electrically) charged component of matter.

If the RN horizons become degenerate, that is for $\kappa = 1$, an extremal black hole forms. The horizons will not form only if $\kappa > 1$, but a naked singularity would form in this case, which is not supported by Roger Penrose's cosmic censorship hypothesis (see *e.g.* Ref. [51]). Hence we demand $\kappa \leq 1$. From this condition it follows that the allowed values for ε are:

$$\varepsilon \in [0, \varepsilon_-] \cup [\varepsilon_+, \infty > . \tag{2.56}$$

For $\varepsilon_1 = \varepsilon_2$, or equivalently $\kappa = 1$, we get the upper bound on the central fluid energy density ρ_0. A second interval, $\varepsilon \in [\varepsilon_+, \infty >$ leads to solutions violating the dominant energy condition (see Appendix B).

The solution displayed in Fig. 2.6 corresponds to the maximum allowed (fluid) density $\rho_0 = 21/(32\pi R^2)$, *i.e.* to the extremal Reissner–Nordström (ERN) case. It is evident that the radial and transversal pressures obey the dominant energy condition while the compactness is safely protected from reaching unity.
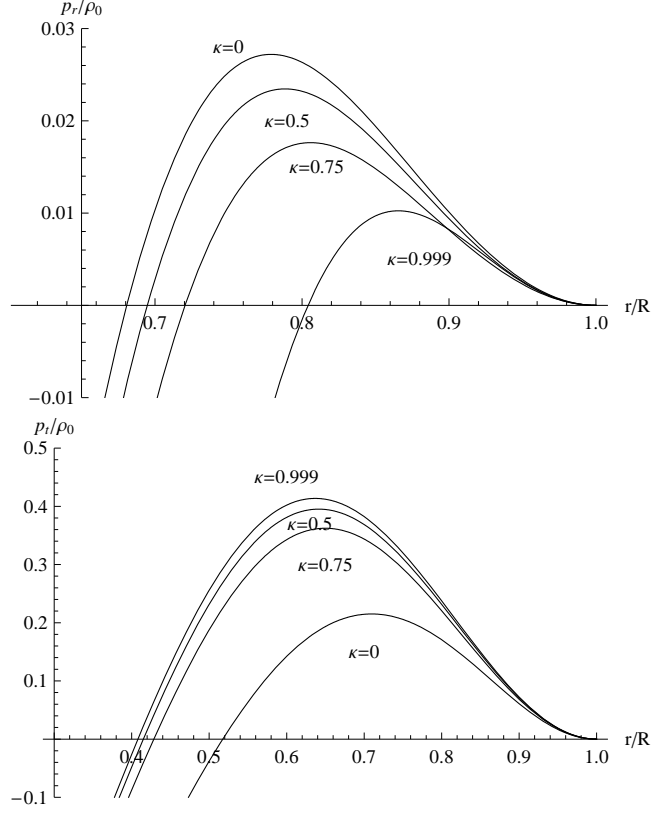
Figure 2.7. *The fluid radial pressure (upper plot) and the fluid transversal pressure (lower plot) in the gravastar atmosphere and crust for the energy density (2.20) with $n = 2$ and the pressure anisotropy (2.21) with $m = 2$, and with $\rho_0 R^2 = 21/32\pi$ for a sequence of solutions $\kappa = Q/M = 0, 0.5, 0.75, 0.999$.*

In Fig. 2.7 we plot the radial (upper plot) and tangential pressures (lower plot) for four different values of κ: $\kappa = 0$, 0.5, 0.75 and $\kappa = 0.999$ (close to the ERN case). It is interesting to observe that the radial pressures are decreased while the transversals are increased with the amount of the electric charge. This trend is actually favorable in the context of compact objects for which we wish large compactness and valid dominant energy condition. Since the total mass is increased by adding a charged component, the maximum compactness is also increased while the radial pressures are decreased and as such protected from violation of the dominant energy condition.
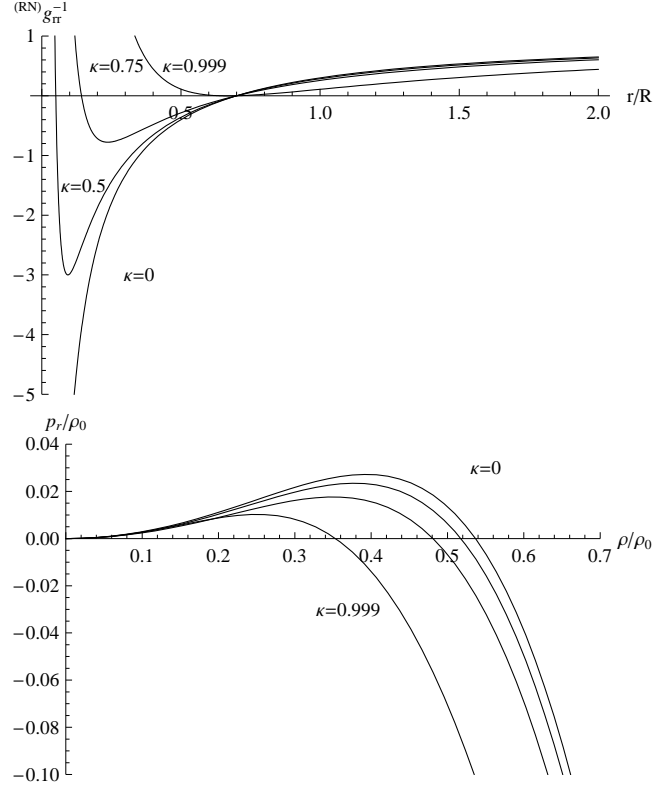
Figure 2.8. *RN metric g_{rr}^{-1} in the upper plot and the fluid equation of state $p_r(\rho)$ in the lower plot for the energy density (2.20) with $n = 2$ and the pressure anisotropy (2.21) with $m = 2$, and with $\rho_0 R^2 = 21/32\pi$ for a sequence of solutions $\kappa = Q/M = 0, 0.5, 0.75, 0.999$.*

Even though from the above analysis we have seen that for the physically acceptable choice $\kappa \leq 1$, the RN space-time possess two horizons, they are placed inside the gravastar since

$$r_+ = M + M\sqrt{1 - \kappa^2} < R, \tag{2.57}$$

which can be seen in the upper plot of Fig. 2.8 – for the given maximal central energy density, all the RN horizons are placed inside the gravastar for $\kappa \in [0, 1]$. It is important to note that in the atmosphere of the gravastar the radial pressure has a negative gradient, so in this region a conventional star-like behavior is expected. This trend is shown in the lower plot of Fig. 2.8 where we plot the equation of state $p_r(\rho)$ for those four different values of κ. All these solutions

exhibit the polytropic pattern in the low density region,

$$p(\rho) = k\rho^\gamma = k\rho^{1+1/n_p}. \tag{2.58}$$

For all solutions the polytropic index is $n_p \simeq 1$ and k decreases with the charge-to-mass ratio κ. The speed of sound calculated from the EoS, $v_s^2 = dp_r/d\rho$, is always subluminal for all solutions in Figs. 2.6 and 2.7, and is less than in the case of the uncharged gravastar.

The obtained results, apart from better understanding of the gravastar concept, also help understanding the effect of the matter anisotropy since it is naturally embedded in the Einstein-Maxwell systems due to the presence of the electrically charged component. In the next chapter we shall see that in the gravitationally bound scalar matter, the anisotropy also arises as a consequence of the *scalar charge*.

CHAPTER 3

NONMINIMAL BOSON STARS

3.1 Introduction

Although gravastar configurations rest upon a very attractive idea, all these models are macroscopic in the sense that their foundation rest on studying Einstein's theory in presence of a matter fluid that obeys some phenomenological equation of state, and as such do not have a proper field-theoretic foundation. Both cases – when the energy density is distributed on thin-shells [4] and when it continuously varies throughout the star [5, 9, 10] – rely on the so-called *Ansätze*–approach. In this approach Einstein's equations are solved in presence of a radially distributed matter fluid, for which an equation of state or some other relation among the thermodynamic functions (the energy density, the radial and tangential pressures) is provided. All these models are essentially toy models, and they are important in the sense that they can be used to provide a better understanding of the main characteristics of black hole mimickers. But, a complete understanding of these objects will be attained only if we can provide theirs faithful microscopic (field-theoretic) description.

A good example of the field-theoretic model exhibiting the anisotropy in principal pressures and relatively large compactness is certainly a boson star. Boson stars are nonsingular asymptotically flat solutions of the Einstein-Klein-Gordon field equations which govern massive complex scalar fields coupled to gravity. The extensive research started by Kaup [6], who has introduced the notion of

the gravitationally bound state of scalar particles. Soon many papers considering various versions of scalar field configurations appeared [52, 53, 54, 55, 56, 57]. The growing importance of boson stars resulted in extensive research which has been reviewed in [58, 59, 60, 61]. On the formation of boson stars an interested reader may find in Ref. [62]. Boson stars were also considered in the context of dark matter (see *e.g.* Refs. [63, 64, 65]). When the boson star configurations are considered, one immediately recognizes that a massive scalar field, even if self-interacting, cannot produce anisotropy which could support an object with (asymptotically) de Sitter interior. Albeit boson stars belong to the realm of very compact objects, it turns out that getting closer to the main black hole features requires modification of general relativity. Even though Einstein's theory has passed all observational tests in the weak field limit, the *true* theory of gravity may differ significantly in the regime of strong gravitational fields. Moreover, large scale cosmological observations and conceptual difficulties in quantizing general relativity call as well for its modifications.

In this chapter we show that even a rather *minimal* extension of the Einstein–Hilbert action by a nonminimal coupling of the scalar field to the Ricci curvature scalar results in configurations that resemble more the dark energy stars then the ordinary boson stars. Even though many of those configurations are endowed by negative principal pressures, the strong energy condition, as a signal of repulsive gravity, is not significantly violated in these configurations. Yet, the maximum effective compactness is attained in the region of negative pressures, and is greater then that in ordinary boson stars. This fact supports an idea that the dark energy stars might present a promising black hole mimicker. While some attempts have been made to study dark energy stars (see for example Refs. [16, 29, 66, 67, 68, 69]), which are loosely speaking in literature taken as objects that contain a negative pressure somewhere in the interior, no systematic study has been so far performed of whether and when boson stars in nonminimal setting violate energy conditions. In this work we fill that gap.

The chapter is organized as follows. In Sec. 3.2 we present the basic Einstein equations for spherically symmetric configurations of a nonminimally coupled complex scalar field. In Sec. 3.3 a brief description of ordinary boson star solutions is presented which leads to a situation in which a necessity of additional mechanism is needed. The nonminimal coupling is introduced in Sec. 3.4, where

we present solutions with required anisotropic behaviour of pressures, *i.e.* dark energy-like stars comprising negative pressures. In that section we also perform analysis of the parameter space for which the weak and dominant energy conditions are violated. Moreover, we investigate the effective compactness. Finally, in Sec. 3.5 we discuss our results.

3.2 A model for the nonminimally coupled boson star

For gravity we take the standard Einstein-Hilbert action:

$$S_{EH} = \int d^4x \sqrt{-g} \frac{R}{16\pi G_N}, \tag{3.1}$$

where G_N is the Newton constant, R is the Ricci scalar, and g is the determinant of the metric tensor $g_{\mu\nu}$, which is given by

$$g_{\mu\nu} = \text{diag}(-e^{\nu(r)}, e^{\lambda(r)}, r^2, r^2 \sin^2\theta). \tag{3.2}$$

The space-time metric is static and spherically symmetric as we are interested only in spherically symmetric equilibrium configurations. For matter we take an action of a complex scalar field with a mass m_ϕ and a quartic self-interaction λ_ϕ coupled nonminimally to gravity:

$$S_\phi = \int d^4x \sqrt{-g} \left(-g^{\mu\nu} \partial_\mu \phi^* \partial_\nu \phi - m_\phi^2 \phi^* \phi - \frac{\lambda_\phi}{2}(\phi^*\phi)^2 + \xi R \phi^* \phi \right), \tag{3.3}$$

where ξ measures the strength of the coupling between scalar field ϕ and gravity *via* the Ricci scalar R and ϕ^* is the complex conjugate of ϕ. It is worth noting here that in order to produce stable configurations, the scalar field must be complex. According to the *Derrick's theorem* [70] regular, static, nontopological, localized scalar field solutions cannot be created by real scalar fields (see [71] and *e.g.* [58]). The energy-momentum tensor of a complex scalar field is obtained by varying its

action with respect to the metric tensor $g^{\mu\nu}$:

$$
\begin{aligned}
T_{\mu\nu}^{\phi} &= 2\delta_{(\mu}^{\alpha}\delta_{\nu)}^{\beta}\partial_{\alpha}\phi^{*}\partial_{\beta}\phi - g_{\mu\nu}\left[g^{\alpha\beta}\partial_{\alpha}\phi^{*}\partial_{\beta}\phi + m_{\phi}^{2}\phi^{*}\phi + \frac{1}{2}\lambda_{\phi}(\phi^{*}\phi)^{2}\right] \\
&\quad - 2\xi\phi^{*}\phi G_{\mu\nu} + 2\xi\nabla_{\mu}\nabla_{\nu}(\phi^{*}\phi) - 2\xi g_{\mu\nu}\Box(\phi^{*}\phi).
\end{aligned}
\tag{3.4}
$$

By varying now the full action

$$
S = S_{EH} + S_{\phi},
\tag{3.5}
$$

with respect to the metric tensor $g^{\mu\nu}$ we obtain the Einstein equations:

$$
R_{\mu\nu} - \frac{1}{2}g_{\mu\nu}R = 8\pi G_{N}T_{\mu\nu}.
\tag{3.6}
$$

The Klein-Gordon equation, the equation of motion for the scalar field ϕ (or ϕ^{*}), is obtained from Bianchi identities or by varying (3.5) with respect to ϕ^{*} (or ϕ), resulting in:

$$
\left[\Box - m_{\phi}^{2} - \lambda_{\phi}\phi^{*}\phi + \xi R\right]\phi = 0,
\tag{3.7}
$$

where $\Box = g^{\alpha\beta}\nabla_{\alpha}\nabla_{\beta}$ is the scalar d'Alemebertian operator in the curved space-time. In order to proceed we choose a harmonic time-dependence for the scalar field

$$
\phi(r,t) = \phi_{0}(r)e^{-\imath\omega t}, \qquad \phi_{0}(r) \in \mathbb{R}.
\tag{3.8}
$$

Even though the scalar field that induces the metric is time-dependent, the energy momentum tensor created by this field is time-independent and thus leads to time-independent metric functions. Hence, the condition (3.8) does not contradict the Birkhoff theorem. Furthermore, the same *Ansatz* for the classical field was also used in Ref. [72] bearing the name *coherent state*, presumably alluding to their resemblance to quantum coherent states. [1] Highly excited field configurations were used to explain flat rotation curves inside galactic halos in Ref. [73]. Furthermore, in Ref. [74] it was shown that it is possible to construct a stable multistate boson star, with coexisting ground and first excited states. In Ref. [75] dynamical evolution of the boson stars in the excited states was investigated.

---

[1]One should keep in mind however that, a scalar field written as in (3.8), apart from the ground state, can also represent excited states with higher energy, and a particular combination of these states can indeed form coherent states. In general, these states contain 'coherent' radial oscillations, but do not in the usual sense constitute quantum coherent states.

Upon inserting the *Ansätze* (3.8) and (3.2) into (3.4) one gets for non-vanishing components of the stress energy tensor:

$$
\begin{aligned}
T^t_t &= \left(-m^2_\phi - \omega^2 e^{-\nu} - \frac{\lambda_\phi}{2}\phi^2_0 \right)\phi^2_0 - e^{-\lambda}(1+4\xi)\phi'^2_0 - 2\xi\phi^2_0 G^t_t \\
&\quad -4\xi e^{-\lambda}\left[\phi''_0 + \left(\frac{\nu' - \lambda'}{2} + \frac{2}{r} \right)\phi'_0 \right]\phi_0 + 2\xi e^{-\lambda}\nu'\phi_0\phi'_0 , \quad\quad (3.9)
\end{aligned}
$$

$$
\begin{aligned}
T^r_r &= \left(-m^2_\phi + \omega^2 e^{-\nu} - \frac{\lambda_\phi}{2}\phi^2_0 \right)\phi^2_0 + e^{-\lambda}\phi'^2_0 - 2\xi\phi^2_0 G^r_r \\
&\quad -2\xi e^{-\lambda}\left(\nu' + \frac{4}{r} \right)\phi_0\phi'_0, \quad\quad (3.10)
\end{aligned}
$$

$$
\begin{aligned}
T^\theta_\theta &= \left(-m^2_\phi + \omega^2 e^{-\nu} - \frac{\lambda_\phi}{2}\phi^2_0 \right)\phi^2_0 - e^{-\lambda}\phi'^2_0 - 2\xi\phi^2_0 G^\theta_\theta \\
&\quad -4\xi e^{-\lambda}\left[\phi''_0 + \left(\frac{\nu' - \lambda'}{2} + \frac{2}{r} \right)\phi'_0 \right]\phi_0 - 4\xi\frac{e^{-\lambda}}{r}\phi_0\phi'_0, \quad\quad (3.11)
\end{aligned}
$$

$$
T^\phi_\phi = T^\theta_\theta. \quad\quad (3.12)
$$

Similarly, the scalar field equation of motion (3.7) becomes:

$$
\phi''_0 + \left(\frac{2}{r} + \frac{\nu' - \lambda'}{2} \right)\phi'_0 - e^{\lambda}\left(m^2_\phi + \lambda_\phi\phi^2_0 - \omega^2 e^{-\nu} - \xi R \right)\phi_0 = 0. \quad\quad (3.13)
$$

By virtue of (3.13) it is possible to eliminate the second derivative of the scalar field ϕ''_0 in the components of the energy-momentum tensor (3.9-3.12), leading to the following form for the first two Einstein equations ($G^\nu_\mu = 8\pi G_N T^\nu_\mu$):

$$
\begin{aligned}
\left[1 + 2\xi(8\pi G_N)\phi^2_0 \right] G^t_t &= 8\pi G_N\bigg\{ \left(-m^2_\phi - \omega^2 e^{-\nu} - \frac{\lambda_\phi}{2}\phi^2_0 \right)\phi^2_0 - e^{-\lambda}(1+4\xi)\phi'^2_0 \\
&\quad -4\xi\left[m^2_\phi + \lambda_\phi\phi^2_0 - \omega^2 e^{-\nu} - \xi R \right]\phi^2_0 \\
&\quad +2\xi e^{-\lambda}\nu'\phi_0\phi'_0 \bigg\}, \quad\quad (3.14)
\end{aligned}
$$

$$
\begin{aligned}
\left[1 + 2\xi(8\pi G_N)\phi^2_0 \right] G^r_r &= 8\pi G_N\bigg\{ \left(-m^2_\phi + \omega^2 e^{-\nu} - \frac{\lambda_\phi}{2}\phi^2_0 \right)\phi^2_0 + e^{-\lambda}\phi'^2_0 \\
&\quad -2\xi e^{-\lambda}\left(\nu' + \frac{4}{r} \right)\phi_0\phi'_0 \bigg\}, \quad\quad (3.15)
\end{aligned}
$$

where the Einstein tensors G^t_t and G^r_r are given in Appendix A. There is one more independent equation. Instead of using the $(\theta\theta)$ Einstein equation (or the equivalent $(\varphi\varphi)$ equation), it is in fact more convenient to use the trace equation,

$G^\mu_\mu = -R = 8\pi G_N T^\mu_\mu$, leading to:

$$R = \frac{8\pi G_N \left\{ 2m_\phi^2 \phi_0^2 + 2(1+6\xi)\left[e^{-\lambda}\phi_0'^2 + (m_\phi^2 - \omega^2 e^{-\nu} + \lambda_\phi \phi_0^2)\right]\phi_0^2 \right\}}{1 + 2\xi(1+6\xi)8\pi G_N \phi_0^2}. \quad (3.16)$$

It is instructive to add a couple of remarks on this equation. For the conformal coupling $\xi = -1/6$, the only non-vanishing term in the Ricci curvature scalar is the scalar field mass. Hence in limit of a vanishing scalar field mass, for which the Ricci scalar is zero, one obtains a conformal gravity limit, as expected. Nevertheless, for $\xi \neq -1/6$, as we shall see in the subsequent sections, a variety of configurations is possible.

Equations (3.14–3.15) and (3.16) constitute the central equations in this chapter.

Dimensionless variables

Before we proceed to solving Eqs. (3.14–3.15) and (3.16), for the purpose of numerical studies, it is convenient to work with dimensionless variables/functions. Hence we perform the following rescaling:

$$\frac{r}{\sqrt{8\pi G_N}} \to x, \qquad 8\pi G_N \phi_0(r)^2 \to \sigma(r)^2,$$

$$8\pi G_N R \to \tilde{R}, \qquad 8\pi G_N m_\phi^2 \to \tilde{m}_\phi^2, \qquad 8\pi G_N \omega^2 \to \tilde{\omega}^2. \quad (3.17)$$

Upon these transformations all variables/functions get expressed in terms of the reduced Planck units:

$$\bar{m}_P = \sqrt{\frac{\hbar c}{8\pi G_N}} = 0.2435 \times 10^{19} \frac{\text{GeV}}{c^2} = 0.4341 \times 10^{-8} \text{ kg},$$

$$\bar{l}_P = \sqrt{\frac{\hbar 8\pi G_N}{c^3}} = 8.1024 \times 10^{-35} \text{ m}. \quad (3.18)$$

The rescaled (dimensionless) differential equations to be solved are then:

$$\lambda' = \frac{1 - e^\lambda}{x} + x\frac{e^\lambda(\tilde{m}_\phi^2 + \tilde{\omega}^2 e^{-\nu} + \frac{\lambda_\phi}{2}\sigma^2)\sigma^2 + (1+4\xi)\sigma'^2 - 2\xi\nu'\sigma\sigma'}{1 + 2\xi\sigma^2}$$

$$+ \frac{4x\xi e^\lambda(\tilde{m}_\phi^2 - \tilde{\omega}^2 e^{-\nu} + \lambda_\phi \sigma^2 - \xi\tilde{R})\sigma^2}{1 + 2\xi\sigma^2}, \quad (3.19)$$

$$\nu' = \frac{(e^\lambda - 1)(1 + 2\xi\sigma^2)/x + xe^\lambda(-\tilde{m}_\phi^2 + \tilde{\omega}^2 e^{-\nu} - \frac{\lambda_\phi}{2}\sigma^2)\sigma^2 + x\sigma'^2 - 8\xi\sigma\sigma'}{1 + 2\xi\sigma^2 + 2\xi x\sigma\sigma'},$$

$$\text{(3.20)}$$

$$\sigma'' = -\left(\frac{2}{x} + \frac{\nu' - \lambda'}{2}\right)\sigma' + e^\lambda(\tilde{m}_\phi^2 + \lambda_\phi\sigma^2 - \tilde{\omega}^2 e^{-\nu} - \xi\tilde{R})\sigma, \qquad \text{(3.21)}$$

with the dimensionless Ricci scalar

$$\tilde{R} = \frac{2\tilde{m}_\phi^2\sigma^2 + 2(1 + 6\xi)\left[(\tilde{m}_\phi^2 - \tilde{\omega}^2 e^{-\nu} + \lambda_\phi\sigma^2)\sigma^2 + e^{-\lambda}\sigma'^2\right]}{1 + 2\xi(1 + 6\xi)\sigma^2}, \qquad \text{(3.22)}$$

where now the *primes* denote derivatives with respect to x.

Equations (3.19–3.21) (with Eq. (3.22)) yield a unique solution (that depends of course on σ_0) when subject to the boundary conditions:

$$(1) \quad \lambda(0) = 0, \qquad (2) \quad \nu(\infty) = 0, \qquad (3) \quad \sigma(0) = \sigma_0, \qquad (4) \quad \sigma(\infty) = 0.$$

$$\text{(3.23)}$$

The first boundary condition ensures that the *mass function $m(r)$* defined in terms of the metric function as

$$e^{-\lambda} = 1 - \frac{2G_N m(r)}{r} = 1 - \frac{2\tilde{m}(x)}{x} \qquad \text{(3.24)}$$

is zero at $r = 0$ (or equivalently at $x = 0$). The second boundary condition in (3.23) ensures asymptotic flatness at large distances,

$$e^{\nu(r)}|_{r\to\infty} = \left(1 - \frac{2G_N m(r)}{r}\right)\Big|_{r\to\infty} \to 1. \qquad \text{(3.25)}$$

The third and fourth boundary conditions in (3.23) are typical for boson stars with a positive scalar mass term ($m_\phi^2 > 0$). Equations (3.19–3.21) together with the boundary conditions (3.23) constitute an eigenvalue problem for ω – that is, for each central field value σ_0 there is an unique ω that satisfies the given boundary conditions. The ground state is characterized by zero nodes in the field $\sigma(x)$ (defined as the points x where $\sigma(x) = 0$), while the n-th excited state has n-nodes in $\sigma(x)$. In this chapter, if not explicitly stated otherwise, boson stars in their ground state will be studied.

We solve these nonlinear, mutually coupled, differential equations numerically

by using the software package COLSYS [76].

Universality

In order to solve the problem numerically we need to specify the set of parameters $\{\lambda_\phi, \tilde{m}^2, \tilde{\omega}^2, \xi\}$. However, for a successful numerical integration these parameters cannot be very different from unity. On the other hand, in physically interesting situations these parameters may wildly differ from unity. For example, compact stars have radial size that is measured in kilometers, while numerical solutions give objects whose size is of the order of the Planck length, $l_P \sim 10^{-38}$ km, obviously not very useful. In order to overcome this impasse, we observe that the dimensionless equations (3.19–3.22) possess a 'conformal' symmetry. Indeed, Eqs. (3.19–3.22) are invariant under the following conformal transformations

$$x \to \beta x, \quad \lambda \to \frac{\lambda}{\beta^2}, \quad \tilde{R} \to \frac{\tilde{R}}{\beta^2}, \quad \tilde{m}^2 \to \frac{\tilde{m}^2}{\beta^2}, \quad \tilde{\omega}^2 \to \frac{\tilde{\omega}^2}{\beta^2}, \quad \sigma \to \sigma, \quad \xi \to \xi.$$
(3.26)

How the mass of the whole boson star changes due to these rescalings can be estimated from the identity

$$M \sim \rho R^3,$$
(3.27)

where ρ is the density which can be approximated by the value of the potential at a scalar field maximum

$$\rho \sim V(\sigma_0) \sim \tilde{m}_\phi^2 \sigma_0^2 + \lambda_\phi \sigma_0^4.$$
(3.28)

On the other hand, from the virial theorem, according to which star's *gradient energy* $\sim$ *potential energy*, the radius of the star, *i.e.* its core in which most of its energy is contained, can be estimated from

$$
\begin{aligned}
(\nabla \phi)^2 &\sim V(\phi), \\
\frac{\sigma^2}{\tilde{R}^2} &\sim \tilde{m}_\phi^2 \sigma^2 + \lambda_\phi \sigma^4.
\end{aligned}
$$
(3.29)

This then implies that the mass of a boson star scales as the radius, $\tilde{M} \propto \tilde{R}$, leading to

$$M \overset{\sim}{\to} \beta M.$$
(3.30)

For example, for a compact object whose radial size is $R \sim 10$ km $= \beta \, \bar{l}_P$, we obtain that β is of the order of $\beta \sim 10^{38}$. It then follows that the mass of the scalar field changes from $m_\phi \sim \bar{m}_P$ to $m_\phi \sim 10^{-38} \bar{m}_P$ and the coupling constant from $\lambda_\phi \sim 1$ to $\lambda_\phi \sim 10^{-76}$. In light of Eq. (3.18), the total mass from $M \sim \bar{m}_P$ changes to $M \sim 0.2 \, M_\odot$, where $M_\odot = 2 \times 10^{30}$ kg is the solar mass.

On the other hand, one can start by setting the scalar field mass m_ϕ and estimate the resulting star radius and its total mass. This allows one to build models that can account for astrophysical objects of vastly different sizes, namely from dark compact objects [77, 78] to galactic dark matter halos [72, 73, 79].

3.3 Ordinary boson stars: Case of minimal coupling

Since the properties of the boson stars with quartic self-interaction are quite extensively studied in Ref. [52], here we shall only briefly discuss their main characteristics. Perhaps the most peculiar feature of these configurations is the anisotropy in their principal pressures. Whereby in the (usual) fluid approach to the physics of neutron stars, anisotropy is treated as a rather dubious and speculative concept, it appears as a fairly natural property of boson stars. One can verify this by inspecting Eqs. (3.10-3.11), which for $\xi = 0$ yield:

$$\Pi = p_t - p_r = -2e^{-\lambda} \phi_0'^2. \tag{3.31}$$

Here we have identified the components of the energy-momentum tensor as

$$T_\mu^\nu = \text{diag}(-\rho, p_r, p_t, p_t), \tag{3.32}$$

where ρ is the energy density, p_r the radial pressure and p_t is the tangential pressure ($p_t = p_\theta = p_\phi$).

From Eq. (3.31) we see that anisotropy is strictly a negative function of the radial coordinate. This fact entails that, regardless of the coupling strength, for minimal coupling, one can only create configurations with $p_r \geq p_t$. In the next section we elaborate more on the consequences of this fact.
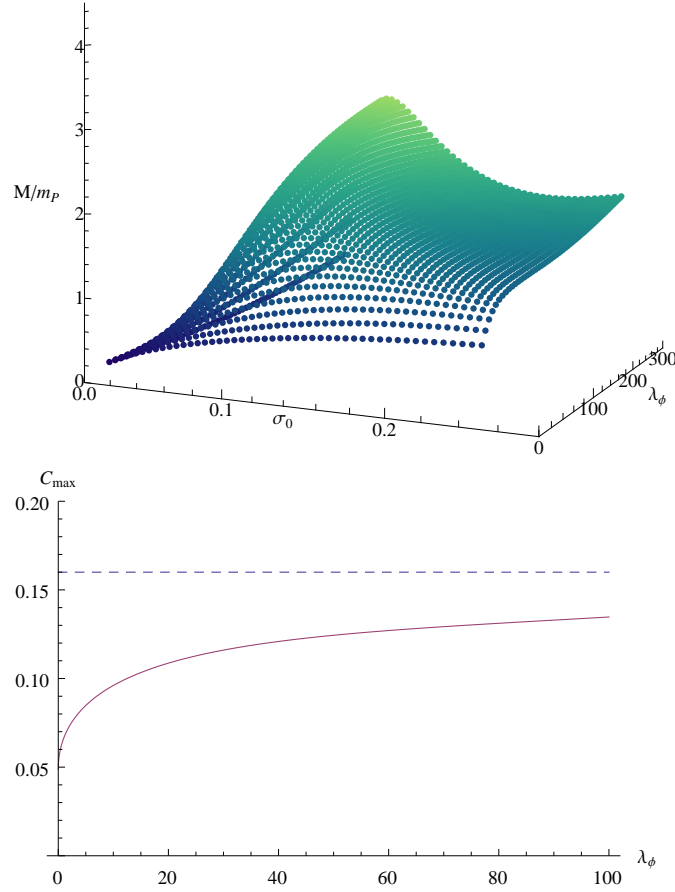
Figure 3.1. *The star mass as a function of the central field value σ_0 and λ_ϕ for $\xi = 0$ in the upper plot and the maximal effective compactness as a function of λ_ϕ in the lower plot. Also $m_\phi^2 = \bar{m}_P^2$.*

In order to build a viable astrophysical object, its stability is clearly a basic requirement. Stability of boson stars has been extensively studied in the literature both analytically [80, 81, 82] and numerically [83, 84, 85] [2]. Numerical methods include dynamical evolution of the system at hand, whilst the analytical one rely on the standard Chandrasekhar methods, *i.e.* studying the response to a linear perturbation of *static* equilibrium configurations, whereby the total particle number is conserved [3]. Both avenues, however, lead to the same conclusion that can be summarized as follows: there exists a critical value of the central field σ_c

---

[2]The catastrophe theory is another interesting method that can be found in Ref. [86].

[3]Since the action (3.3) is invariant under the $U(1)$ symmetry, according to the Noether theorem, there is a conserved (scalar) charge density.

for which the ground state of boson star (nodeless in $\sigma(x)$) will be marginally stable upon small radial perturbations. For this critical field value, the total mass of the star exhibits turnaround in $M(\sigma_0)$-curve (see *e.g.* [35]). Then the configurations left from the peak are stable and those right from the peak are unstable leading to the collapse to a black hole or a dispersion at infinity. An interested reader may find a discussion in Ref. [87] on what is the likely fate of the boson star for the right-from-the-peak configurations in the $M(\sigma_0)$-curve.
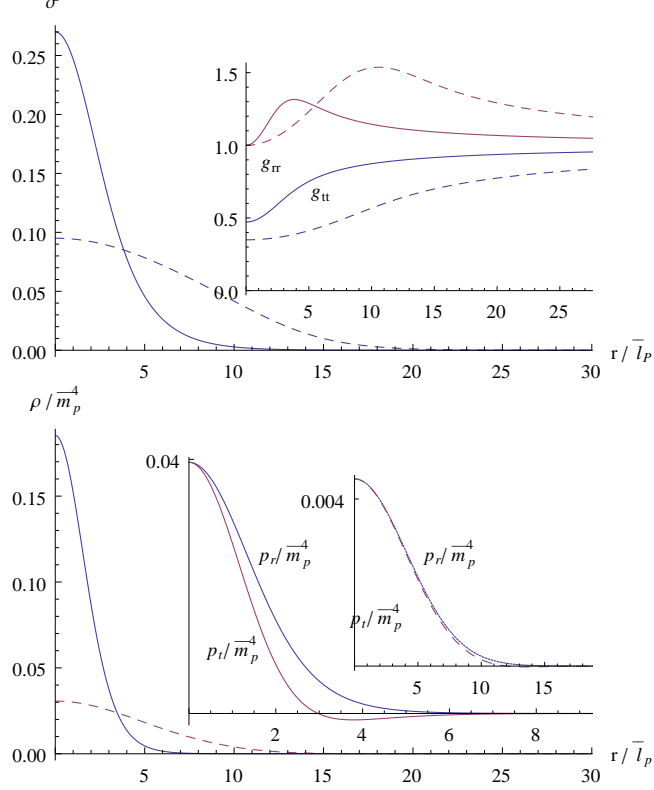

Figure 3.2. *Upper plot: the scalar field as a function of the radial coordinate and in the inset the metric functions g_{tt} and g_{rr}. Lower plot: the energy densities and the principal pressures in the inset. The solid curves are plotted for $\lambda_\phi = 0$ ($\{\sigma_c, M_{\max}\} = \{0.27, 0.633\,\bar{m}_P\}$) and the dashed curves are plotted for $\lambda_\phi = 100$ ($\{\sigma_c, M_{\max}\} = \{0.095, 2.257\,\bar{m}_P\}$). Also $m_\phi^2 = \bar{m}_P^2$ and $\xi = 0$.*

In the absence of the self-interaction it was found that the maximally allowed mass is $M_{\max} = 0.633\,m_{\text{Planck}}^2/m_\phi$, and by switching on the self-interaction it increases as $M_{\max} = 0.22\sqrt{\Lambda}\,m_{\text{Planck}}/m_\phi$, where $\Lambda = \lambda_\phi/(4\pi G_N m_\phi^2)$. In the upper plot of Fig. 3.1 we show the star mass as a function of the central field value σ_0

and λ_ϕ. As the amplitude σ_0 increases its mass also increases (while its radius decreases). For increasing λ_ϕ the maximum mass also increases while the critical central field value σ_c decreases. For any given value of the coupling constant there is only one configuration that meets those of the maximally allowed mass.

In Fig. 3.2 we show two such configurations for $\lambda_\phi = 0$ and $\lambda_\phi = 100$. In the upper plot, the profiles of the scalar field and the metric functions (inset) are shown, while in the lower plot we show the behaviour of the energy densities and the corresponding pressures (inset). Two main criteria can be read off from these graphs. The first is the interplay among the central field value and the radius: while one is increasing, the other one is decreasing and *vice versa*. An important consequence of this trend is equivalence between the $M(\sigma_0)$ and the $M(R)$-curve. That is, both curves exhibit turnaround behaviour for equal maximally allowed masses, and hence either can be used for stability analysis.

Second, the anisotropy in the principal pressures becomes less prominent due to the inclusion of self-interaction. This behaviour implies that boson stars built from strongly self-interacting fields tend to be isotropic. This property is very interesting as it may serve to relate the strongly self-interacting boson stars with the isotropic fermion systems [88]. Indeed, in this regime, boson stars behave like a polytrope with the equation of state $p_t \approx p_r \propto \rho^{1+1/n}$, where n is the polytropic index.

It is also worth noting here that the negative anisotropy (3.31) cannot rise to more exotic structures with negative principal pressures, found in dark energy stars (*e.g.* gravastars). For the latter, one needs anisotropy to be a positive function of the radial coordinate (see *e.g.* Refs. [5, 15]). This is the main reason why we extend this analysis to include nonminimal coupling.

3.4 Dark energy-like stars: Effects of nonminimal coupling

Spherically symmetric static configurations of a nonminimally coupled scalar field modeled by the action (3.3) in the absence of the quartic self-interaction were studied by Bij and Gleiser in Ref. [89]. Adopting the $M(\sigma_0)$ stability criterion, the authors calculated the critical (maximally allowed) mass and the critical particle number for a variety of values of the coupling constant ξ. The analysis is

performed for boson stars both in the ground state (no nodes in the scalar field) as well as in excited states (higher nodes in the scalar field). However, the authors did not analyze the behaviour of the thermodynamic functions, namely of the energy density and pressures.

In the case of nonminimal coupling, the anisotropy becomes rather convoluted function of matter *and* geometry

$$\begin{aligned} \Pi &= -2e^{-\lambda}\phi_0'^2 - 2\xi(G_\theta^\theta - G_r^r)\phi_0^2 + 2\xi e^{-\lambda}\left(\nu' + \frac{4}{r}\right)\phi_0\phi_0' \\ &\quad - 4\xi\left(m_\phi^2 + \lambda_\phi\phi_0^2 - \omega^2 e^{-\nu} - \xi R\right)\phi_0^2. \end{aligned} \tag{3.33}$$

As mentioned in the previous section, it is likely that Π may become positive for some radii, which is an important ingredient of building microscopic configurations with negative pressures.

However, when dealing with spherically symmetric, localized, configurations of matter it seems reasonable to invoke the energy conditions as important criteria for physically acceptable matter.

3.4.1 Constraints from the energy conditions

Various energy conditions have been proposed as reasonable physical restrictions on matter fields (see Appendix B). With or without self-interaction it turns out that the weak energy condition (WEC) is obeyed for nonminimal couplings only *if* greater than a certain (negative) critical value $\xi > \xi_{\mathrm{crit}}^{\mathrm{WEC}}$, whereby $\xi_{\mathrm{crit}}^{\mathrm{WEC}}$ decreases very slowly as λ_ϕ increases. As an example of the indicated transition, we plot the energy density in Fig 3.3 where it is shown that violation of the WEC is more prominent as the value of the nonminimal coupling decreases. One example of a space-time that violates the WEC is that of a wormhole (see *e.g.* Refs. [90, 91, 92, 93]). Some other examples would include a more exotic matter. Although this energy condition is also violated by certain quantum fields, a positive energy density is an essential feature of the classical forms of matter. A consequence of the requirement that the WEC is satisfied is a shift in the "maximally" allowed masses to lower values as depicted in Fig. 3.4 for $\xi < \xi_{\mathrm{crit}}^{\mathrm{WEC}}$.
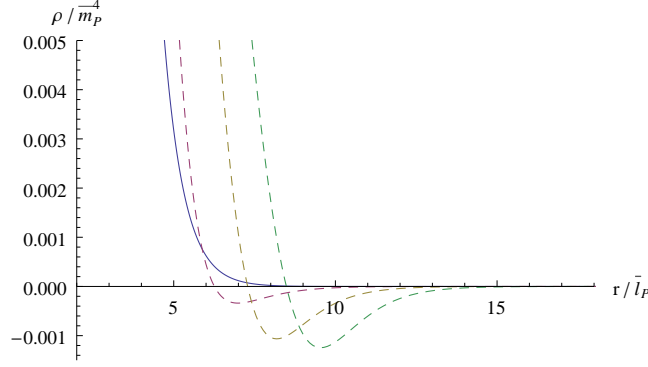
Figure 3.3. *The energy density as a function of the radial coordinate. The solid curve stands for $\xi = \xi_{\mathrm{crit}}^{\mathrm{WEC}} = -1$, the dashed curves are for $\xi = -2, -4, -6$ from left to right, respectively. Also $\lambda_\phi = 0$ and $m_\phi^2 = \bar{m}_P^2$.*
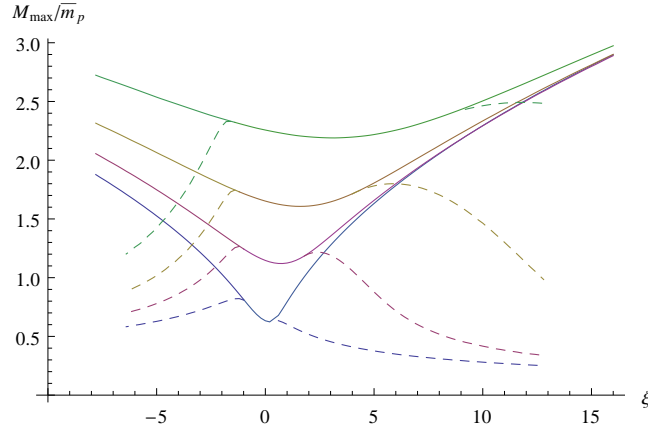

Figure 3.4. *The maximum mass as a function of the coupling ξ for $\lambda_\phi = \{0, 20, 50, 100\}$ from bottom to top. Also $m_\phi^2 = \bar{m}_P^2$. For $\xi < 0$ the dashed curves describe configurations that obey the weak energy condition and for $\xi > 0$ configurations that obey the dominant energy condition. The solid curves describe configurations that are not constrained by energy conditions.*

In addition, we also require that the energy is not transported faster than light, and hence the dominant energy condition (DEC) should be satisfied. Another constraint on parameter space emerges from the requirement $\xi > \xi_{\mathrm{crit}}^{\mathrm{DEC}}$ as shown in Fig. 3.4. The dashed curves represent the maximally allowed masses for the by-the-WEC-and-DEC modified configurations, while the solid curves correspond to

the old (non-modified) configurations. As such Fig. 3.4 represents an important result of this chapter due to the fact that it establishes new configurations for stars that satisfy the WEC and DEC.

The strong energy condition is also violated for certain nonminimal couplings, $\xi > \xi_{\mathrm{crit}}^{\mathrm{SEC}}$. As opposed to the problem of violating the WEC and DEC, a violation of the SEC is actually favorable in building highly compact objects. Namely, a region of a compact object that violates the SEC exhibits repulsive gravity, which is desirable. Violation of the SEC plays an important role in the early universe cosmology, where it is used to explain the origin of Universe's large scale structure generated through matter and gravitational perturbations amplified during a hypothetical inflationary epoch in which the SEC is violated. It is also an essential component of gravastars, which in their interior, where $p_r(0) = p_t(0) = -\rho(0)$, strongly violate the SEC. In the case of gravastars, violation of the SEC is crucial for large values of compactness. Unfortunately, here the SEC is significantly violated only if the DEC is violated. Nevertheless we shall explore some effects of violating the SEC in the next subsection.

3.4.2   Energy density and pressures profiles

It is now of interest to explore thermodynamic functions, namely the energy density and the principal pressures.

Depending on the strength of the self-interaction, configurations with negative principal pressures emerge, that can be approximated by the equation of state $p_r \propto -\rho^\gamma$. This particular equation of state (EoS) has been used to describe *dark energy stars*. Even though these configurations exhibit negative principal pressures, the strong energy condition is not violated thus excluding regions with repulsive gravity. One such configuration is shown in the upper plot of Fig. 3.5. As a matter of fact, in the absence of self-interaction, for $\xi < \xi_{\mathrm{crit}}^{\mathrm{WEC}}$ all configurations lying on the $M_{\mathrm{max}}(\xi)$-curve can be described by the EoS of a dark energy star, $p_r \propto -\rho^\gamma$.
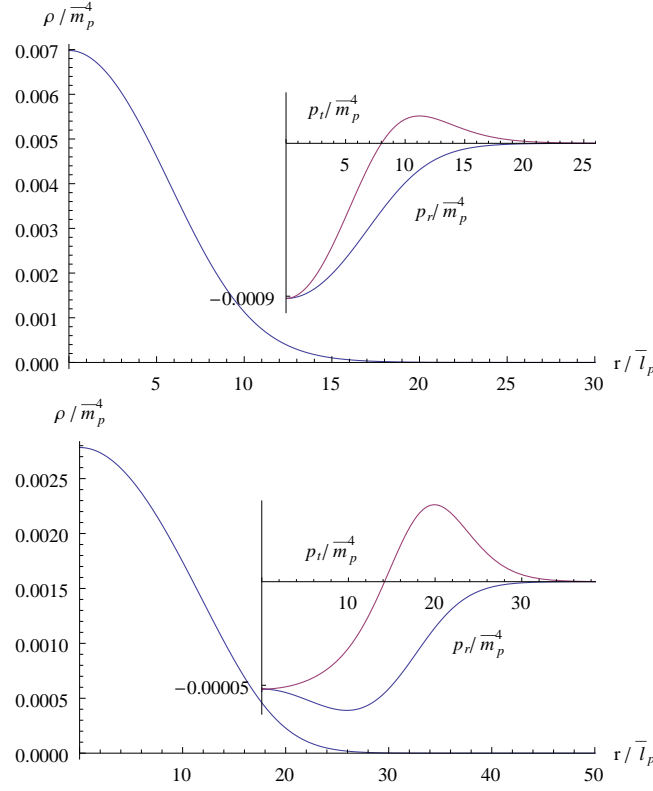
Figure 3.5. *The energy density and the principal pressures (insets) for $m_\phi^2 = \bar{m}_P^2$, $\xi = -4$ and for a) $\{\lambda_\phi, \sigma_c\} = \{0, 0.050\}$ in the upper plot and b) $\{\lambda_\phi, \sigma_c\} = \{100, 0.034\}$ in the lower plot.*

When the self-interaction increases, the pressures increase as well, as can be seen in the lower plot of Fig. 3.5. Nevertheless, no matter how large the self-interaction is, the dark energy star-like configurations are obtained by choosing an appropriate (*i.e.* negative enough) nonminimal coupling. This effect is clearly shown by comparing Fig. 3.6 with Fig. 3.5. It is also of interest to observe that the transversal pressures of these configurations, as positive near surface, are like those of gravastars. This fact brings us to the idea that the gravastars, as not yet formulated within the field theories and as such still of interest to explore, might be produced in modified gravity that includes higher order terms in the Ricci scalar, Ricci tensor and/or Riemann curvature tensor. However, proper dark energy stars, *i.e.* with negative pressures and violating SEC, can be obtained for $\lambda_\phi < 0$.
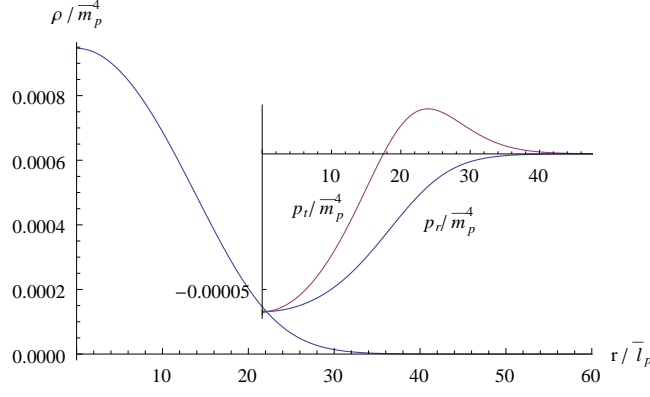
Figure 3.6. *The energy density and the principal pressures (inset) for $\xi = -8$, $\lambda_\phi = 100$, $\sigma_c = 0.02$. Also $m_\phi^2 = \bar{m}_P^2$.*
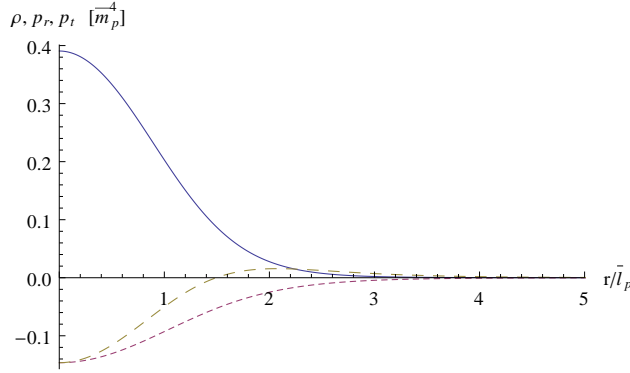

Figure 3.7. *The energy density (solid curve), radial (short-dashed curve) and transversal pressure (long-dashed curve) for $\xi = -0.9$, $\lambda_\phi = -30$, $\sigma_0 = 0.26$. Also $m_\phi^2 = \bar{m}_P^2$.*

We present one such solution in Fig. 3.7. It is interesting that this solution violates only the strong energy condition while the weak and dominant energy conditions are obeyed. Nevertheless, the theories with negative potentials yield Hamiltonians that are unbounded from below, and are at best quasi-stable, *i.e.* field configurations will eventually 'decay' into large fields and roll down to infinity, where energy is minus infinity (see *e.g.* [73]). When excited states of these configurations are considered, the energy density and pressures oscillate in space. Both pressures are now positive functions of coordinate in the region near the surface thus resembling gravastars solutions. We show one such configuration in

Fig. 3.8. However, even though stability might not be questionable in this set-
ting, the weak and dominant energy conditions are violated. Yet, it was argued
in Ref. [73] that a galactic halo consisting of highly excited states of ordinary
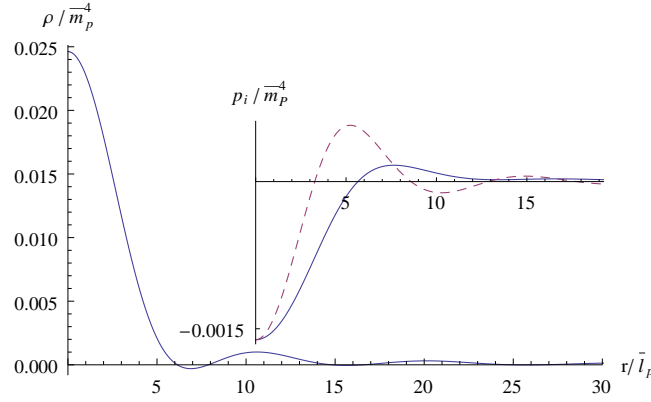boson stars could explain the rotation of low-luminosity spiral galaxies.

Figure 3.8. *The energy density, radial (solid curve in the inset) and transversal pres-
sure (dashed curve in the inset) for $\xi = -0.7$, $\lambda_\phi = 0$, $\sigma_0 = 0.1$ and $m_\phi^2 = 0.9\,\bar{m}_P^2$.*

Configurations obtained for positive values of the nonminimal coupling exhibit
positive pressures and hence are quite similar to the ordinary boson stars. In
Fig. 3.9 we plot the energy density, the radial and the transversal pressure for
$\lambda_\phi = 0$ in the upper plot and $\lambda_\phi = 100$ in the lower plot. For each λ_ϕ two
configurations are presented, one for $\xi_{\text{crit}}^{\text{DEC}}$ and the other one for a nonminimal
coupling that is much larger then the critical one. For each λ_ϕ the effect of
increasing ξ is only to decrease mass and increase radius (thus decreasing the
compactness) without any drastic changes in the behaviour of energy density and
pressures. However, the profiles of the energy density and pressures qualitatively
do change considerably for different λ_ϕ. In the lower plot of Fig. 3.9 the hump
in the energy density occurs as ξ increases. This hump is actually followed by
a violation of the strong energy condition which is more significant for larger ξ.
Hence the hump in the inset of Fig. 3.9 is more prominent. In order to justify this
statement in Fig. 3.10 we plot the energy density and pressures for a configuration
that strongly violates the SEC (in the region of negative transversal pressure -
see inset of Fig. 3.10).

In this subsection, apart from qualitative behaviour of the energy density and
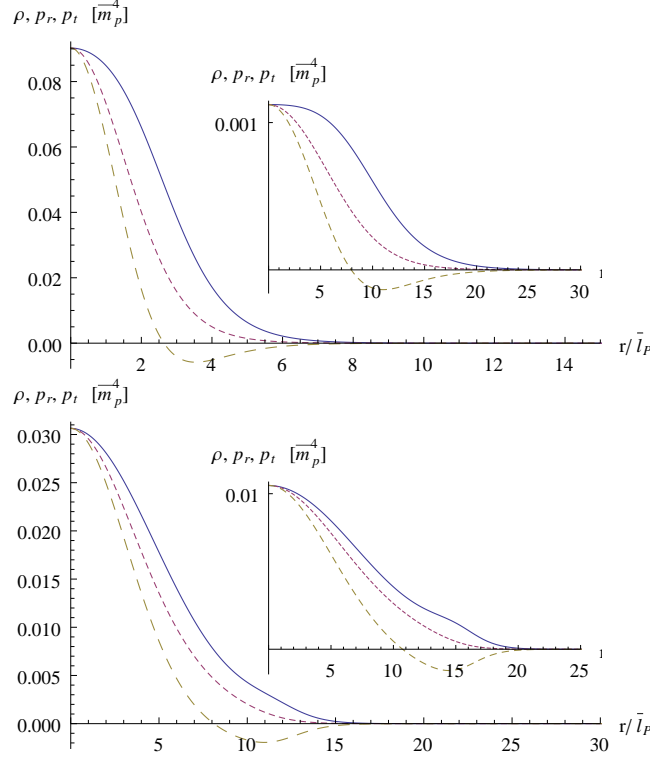
Figure 3.9. *The energy density (solid), the radial pressure (short-dashed) and the transversal pressure (long-dashed) for a) upper plot: $\lambda_\phi = 0$ and $\{\xi, \sigma_c\} = \{0.6, 0.2635\}$ and in the inset $\{6.4, 0.0364\}$ and b) lower plot: $\lambda_\phi = 100$ and $\{\xi, \sigma_c\} = \{7.8, 0.1194\}$ and in the inset $\{12.8, 0.0845\}$. Also $m_\phi^2 = \bar{m}_P^2$.*

.

pressures, one could also infer subtle relations among the total masses and radii. In particular, increasing the central field value is followed by a decreasing radius up to the maximally allowed mass. This interplay among the mass and the radius is best explored by analyzing the effective compactness.

3.4.3 Effective compactness for the nonminimal case

Following Ref. [94], we define the *effective compactness* as

$$C(\sigma_0, \lambda_\phi) = \frac{M_{99}(\sigma_0, \lambda_\phi)}{R_{99}}, \qquad (3.34)$$

where R_{99} is the radius at which the mass, defined in terms of the metric function $e^{-\lambda} = 1 - 2G_N m/r$, equals 99% of the total mass $M = m(\infty)$. The effective radius owes this sort of definition as the scalar field is (exponentially) infinitely extended
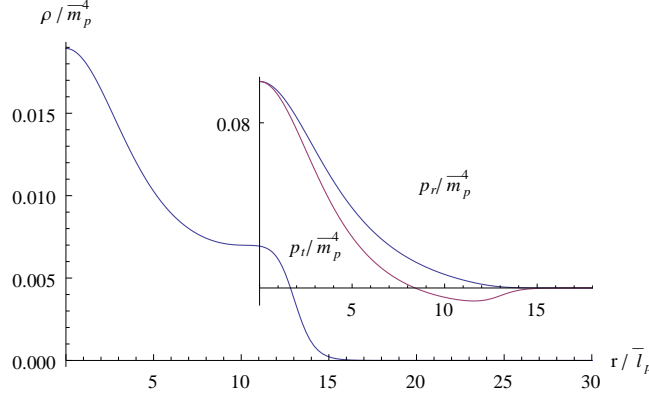
Figure 3.10. *The energy density and the principal pressures (insets) for $m_\phi^2 = \bar{m}_P^2$, $\xi = 16$, $\{\lambda_\phi, \sigma_c\} = \{0, 0.145\}$.*

and thus always with zero compactness. Note that the effective compactness $C(\sigma_0, \lambda_\phi)$ is related to the surface compactness $\mu(R)$ as $\mu(R) = 2C(\sigma_0, \lambda_\phi)$. As shown in Ref. [94] the effective compactness in a minimal setting increases with the self-coupling λ_ϕ and as $\lambda_\phi \to \infty$ the maximal effective compactness approaches $C_{\max} \approx 0.16$ as shown in the lower plot of Fig. 3.1. For each λ_ϕ, the maximal compactness corresponds to the parameters matching the critical field value σ_c. That is the maximally allowed mass and its radius.

If $M_{\max}$ is not constrained by the weak and dominant energy conditions, the effective compactness for $\xi > 0$ is largest for large ξ and $\lambda_\phi = 0$ as shown in Fig. 3.11 and approaches $C_{\max} \approx 0.20$. This value is only slightly larger then the maximal effective compactness obtained in the minimal setting and can be related to a SEC violation. Why this value is not larger, probably can be explained with the fact that the SEC is violated only near the surface where the transversal pressures become negative.

However, for $\xi < 0$ the compactness is much greater and reaches its maximum value for large negative values of the nonminimal coupling and also in the case when $\lambda_\phi = 0$, which approximately equals $C_{\max} \gtrsim 0.25$. Even though the strong energy condition is not violated in this region, an increased effective compactness can be attributed to negative pressures that weaken gravity, thus enabling more matter to be accommodated in a fixed volume. This result is also very important as it suggests that, in order to build a highly compact object, we ought to have configurations with negative principal pressures *and* a violation of the SEC.
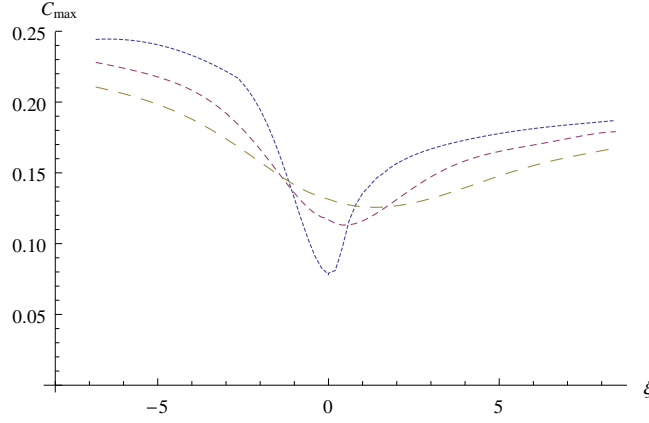
Figure 3.11. *The effective compactness as a function of the ξ-coupling for $\lambda_\phi = 0$ (dotted curve), $\lambda_\phi = 20$ (short dashed curve) and $\lambda_\phi = 50$ (long dashed curve). Also $m_\phi^2 = \bar{m}_P^2$.*

When restrictions from the weak and dominant energy conditions are included, the effective compactness behaves as shown in Fig. 3.12. The maximal values for each λ_ϕ are obtained for $\xi_{\text{crit}}^{\text{WEC,DEC}}$ and then abruptly decrease with increasing/decreasing nonminimal coupling. This brings us to the conclusion that the most compact objects are produced in the domain of negative pressures and large self-couplings, with the maximum effective compactness only slightly larger then in the minimal case $C_{\text{max}} \gtrsim 0.16$.

Nevertheless, figures 3.11 and 3.12 are very useful, as one can easily relate the mass to the radius. If we want to create a compact object with, for example, a radius of $R = 15\,\text{km}$, then from C_{max} one can easily read off its mass. The range of effective compactness $C_{\text{max}} = 0.05 - 0.25$ correspond to the masses $M = (0.5 - 2.5)\,M_\odot$.

However, in order to obtain scalar's masses and self-couplings, one needs to employ the universality described in Sec. 3.2. By fixing the radius to, *e.g.*, $R = 15\,\text{km}$ one can calculate β for any configuration with differing radii (in the reduced Planck units). Then, the scalar's mass and self-coupling are easily obtained by applying the rescaling conditions $m_\phi^2 \to m_\phi^2/\beta^2$ and $\lambda_\phi \to \lambda_\phi/\beta^2$. By inspection of all above diagrams depicting the energy density and pressures (in previous subsection) it can be inferred that the radii of all given configurations roughly fall within the range $r = (10 - 40)\,\bar{l}_P$. Hence, if we want to create a star of $R = 15\,\text{km}$ the corresponding βs are $\beta = (18.6 - 4.6) \times 10^{36}$ leading to the scalar's
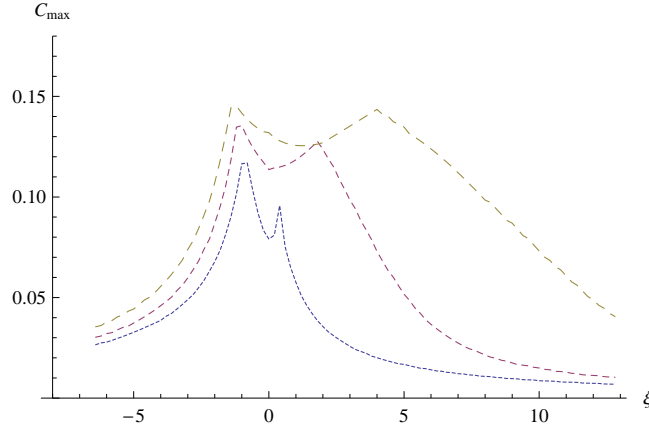
Figure 3.12. *The effective compactness as a function of ξ for configurations that obey the WEC and DEC. $\lambda_\phi = 0$ (dotted curve), $\lambda_\phi = 20$ (short dashed curve) and $\lambda_\phi = 50$ (long dashed curve). Also $m_\phi^2 = \bar{m}_P^2$.*

masses $m_\phi = (0.27 - 1.08) \times 10^{-8}$ eV, which could be in the range of the neutrino masses. To calculate the rescaled self-coupling, let us, for convenience take its starting value $\lambda_\phi = 50$. After the rescaling we obtain $\lambda_\phi = (14 - 0.24) \times 10^{-73}$. But of course, if one considers a case when the coupling has reached saturation, one could increase the value of the un-rescaled λ_ϕ arbitrarily, which would then yield more reasonable (*i.e.* larger) values of the rescaled λ_ϕ.

3.5   Conclusions

In this chapter we have examined spherically symmetric configurations made of a scalar field nonminimally coupled to gravity.

We have showed that already a *minimal* extension of Einstein's theory to the nonminimal coupling results in radically different configurations from standard boson stars, *i.e.* dark energy-like stars which are characterized by negative principal pressures. Upon investigating the energy conditions in more detail, it turned out that the strong energy condition, which should be violated in the interior of dark energy stars, and whose violation signals repulsive gravity, is satisfied in the interior of these configurations. However, we presented an example of a *proper* dark energy star, *i.e.* with negative pressures and a violating SEC, which is obtained for a negative self-interaction. Even though the configuration presented

here does not suffer from violation of the weak and dominant energy condition, configurations with negative potentials, in general, are not that appealing due to their stability issues. We also presented one higher mode solution that led to gravastar-like principal pressures. That is, both principal pressures reveal positive atmosphere (region near surface). But, the strong energy condition is obeyed while the weak and dominant conditions are violated, thus again without space-time regions with repulsive gravity.

When imposing restrictions on classical matter by energy conditions we found regions of parameter space for which both the weak and dominant energy conditions are violated. In particular, the weak energy condition is violated for all negative values of the nonminimal coupling, if it is less then a critical value $\xi < \xi_{\mathrm{crit}}^{\mathrm{WEC}}$. The dominant energy condition is violated for all positive values of the nonminimal coupling if greater then a critical value $\xi > \xi_{\mathrm{crit}}^{\mathrm{DEC}}$. The consequences of a violation of the WEC and DEC are encoded in the maximally allowed masses that are now shifted to lower values. The strong energy condition is violated in the region of a positive nonminimal coupling and is followed by humps in the energy density. Even though violation of the energy conditions does not support the view of classical matter, it would be of interest to explore in more details the imprint of a test particle moving in such a background.

Furthermore, we analyzed the effective compactness for configurations that do or do not satisfy the WEC and DEC, and found that the maximum effective compactness is attained in the regimes of negative pressures for non-self-interacting configurations and equals $C_{\mathrm{max}} \gtrsim 0.25$ for configurations that violate the WEC and $C_{\mathrm{max}} \gtrsim 0.16$ for those configurations that obey the WEC and DEC. This result sets limits on the boson star mass. For example, when $R = 15\,\mathrm{km}$ the maximum mass is $M = (2 - 2.5)\, M_\odot$ which belongs in the domain of neutron stars. Even though the strong energy condition is not violated, an increased maximum effective compactness could be related to the existence of negative pressures.

In addition, we developed a universality condition based upon which one can calculate scalar's masses and self-couplings for all given configurations. Even though in this chapter we focused on parameters that yield compact objects, with the universality condition it is possible to extend this analysis to larger structures that match galactic sizes, such as, for example, dark matter halos.

Although theories with a nonminimally coupled scalar field represent a simple

and quite benign extension of general relativity, they provide a plethora of different interesting astrophysical structures, ranging from isotropic polytropes to highly anisotropic dark energy-like stars. Nevertheless, within this model it is, in fact, not possible to create a *highly* compact, nonsingular object whose characteristics are arbitrarily close to those of the Schwarzschild black hole. Yet, from this chapter one can infer that the real black hole mimicker might be produced in the context of modified theories of gravity.

CHAPTER 4

NONMINIMAL BOSON D-STARS

4.1 Nonminimal global monopole

Topological defects – monopoles, cosmic strings, domain walls and cosmic textures – can be created by spontaneous symmetry breaking during phase transitions in the early Universe. If the broken symmetry is independent of space-time coordinates then the defects are called *global*. The standard example of a global monopole is a field theory consisting of three real scalar fields, whose action is $\mathcal{O}(3)$ - symmetric which during a thermally induced phase transition breaks down to $\mathcal{O}(2)$. A typical Lagrangian of the model contains a negative mass term and a positive quartic coupling. Together with other topological defects, global monopoles were studied in cosmology in the hope to provide the explanation for the origin of the large scale structure of the Universe. However, modern cosmic microwave background observatories (such as the WMAP satellite and the South Pole Telescope) have ruled out topological defects as the chief contributor to the origin of large scale structure, albeit there is still the possibility that a small fraction of large scale structure originates from topological defects [8]. Furthermore, it was suggested that the galactic dark matter in spiral galaxies could be explained by global monopoles as its energy density is decreasing with the distance as $1/r^2$ [95] due to the Goldstone boson term in the energy-momentum tensor (which is a fundamental property of global symmetry violation). Correspondingly, the total monopole mass grows linearly with distance, *i.e.* it diverges. Neverthe-

less, if the monopole self-gravity is included, the divergence problem ceases to exist. There has been a large amount of papers discussing the gravitational field of the global monopole (see *e.g.* [96, 97, 98, 99]) starting with the seminal work of Barriola and Vilenkin [7], who showed that the gravitational field outside the monopole has an effect analogous to that of a tiny mass at the monopole origin and a deficit solid angle (which is proportional to the energy of spontaneous symmetry breaking scale). Lousto *et al.* [100] showed that this small core mass of the monopoles produces a repulsive potential. This feature of global monopoles, apart from large scale configurations, is also very important in the context of compact objects. Liebling *et al.* found quantitative range of the deficit solid angle for which regular solutions with or without an event horizon can exist [101, 102]. The idea of the so called topological inflation was also considered in the context of global monopoles due to the existence of de Sitter cores [103].

Nucamendi *et al.* [104] extended the gravitating global monopole by introducing nonminimal coupling. The main result of their analysis is the existence of bound orbits which are not present in the minimally coupled global monopole. Though, an in-depth analysis of nonminimally coupled global monopoles as compact objects (in terms of energy density, pressures, compactness *etc.*), is still lacking. In this section we bridge that gap.

This section is organized as follows: in the subsection 4.1.1 we bring out an analytical derivation of a model for the nonminimally coupled global monopole. In the subsection 4.1.2 the results for the global monopole which is minimally coupled to gravity is briefly demonstrated, while the main results for the nonminimally coupled global monopole are presented in subsection 4.1.3 including metric functions, energy densities, pressures, compactnesses, effective forces, Newtonian forces and Newtonian forces produces by core masses.

4.1.1 A model for the nonminimally coupled global monopole

The action for the nonminimally coupled global monopole is

$$S_\phi = \int d^4x \sqrt{-g} \left(-\frac{1}{2} g^{\mu\nu} (\partial_\mu \phi^a)(\partial_\nu \phi^a) - V(\phi^a) + \frac{1}{2} \xi R(\phi^a \phi^a) \right), \qquad (4.1)$$

where ϕ^a ($a = 1, 2, 3$) is a scalar field triplet with global $\mathcal{O}(3)$ symmetry which is spontaneously broken to $\mathcal{O}(2)$. Hence we choose the simplest symmetry breaking potential

$$V(\phi^a) = \frac{\mu^2}{2} \phi^a \phi^a + \frac{\lambda_\phi}{4} (\phi^a \phi^a)^2 + \frac{\mu^4}{4\lambda_\phi} , \tag{4.2}$$

where μ is the monopole mass term and λ_ϕ is the self-interacting strength. The quantity ξ measures the strength of the coupling between the scalar field and gravity via Ricci scalar R. The energy-momentum tensor of the global monopole is obtained by varying its action with respect to the metric tensor $g^{\mu\nu}$ yielding:

$$\begin{aligned} T^\phi_{\mu\nu} &= (\partial_\mu \phi^a)(\partial_\nu \phi^a) - g_{\mu\nu} \left[\frac{1}{2} g^{\alpha\beta} (\partial_\alpha \phi^a)(\partial_\beta \phi^a) + \frac{\mu^2}{2} \phi^a \phi^a + \frac{\lambda_\phi}{4} (\phi^a \phi^a)^2 + \frac{\mu^4}{4\lambda_\phi} \right] \\ &\quad - \xi \left(G_{\mu\nu} + g_{\mu\nu} \Box - \nabla_\mu \nabla_\nu \right) (\phi^a \phi^a) . \end{aligned} \tag{4.3}$$

The equation of motion for the scalar field is obtained by varying the full action $S = S_{EH} + S_{GM}$ with respect to ϕ^a resulting in:

$$\Box \phi^a - \frac{\partial V}{\partial \phi^a} + \xi R \phi^a = 0 . \tag{4.4}$$

For the global monopole we take the so-called hedgehog *Ansatz*

$$\vec{\phi}(\vec{r}, t) = \phi(r) \left(\sin\theta \, \cos\varphi, \sin\theta \, \sin\varphi, \cos\theta \right) , \tag{4.5}$$

where we recognize a spherical harmonic function $Y_{lm}(\theta, \varphi)$ of degree $l = 1$ and of order m:

$$Y_{1m} = \left(\sin\theta \, \cos\varphi, \sin\theta \, \sin\varphi, \cos\theta \right) . \tag{4.6}$$

In the given metric the d'Alembertian operator is

$$\begin{aligned} \Box &= \frac{1}{\sqrt{-g}} \partial_\mu g^{\mu\nu} \sqrt{-g} \partial_\nu \\ &= -e^{-\nu} \partial_t^2 + \frac{e^{-\frac{\nu+\lambda}{2}}}{r^2} \partial_r \left(e^{\frac{\nu-\lambda}{2}} r^2 \right) \partial_r \\ &\quad + \frac{1}{r^2} \left(\frac{1}{\sin\theta} \partial_\theta \sin\theta \, \partial_\theta + \frac{1}{\sin^2\theta} \partial_\varphi^2 \right) . \end{aligned} \tag{4.7}$$

The second part of this operator is the angular momentum operator

$$\hat{L}^2 = -\frac{1}{\sin\theta}\,\partial_\theta\,\sin\theta\,\partial_\theta - \frac{1}{\sin^2\theta}\,\partial_\varphi^2\,, \tag{4.8}$$

whose eigenfunctions are the spherical harmonics

$$\hat{L}^2\,Y_{lm}(\theta,\varphi) = l(l+1)\,Y_{lm}(\theta,\varphi)\,. \tag{4.9}$$

Thus we have

$$\hat{L}^2\,\vec{\phi}(\vec{r},t) = 2\,\vec{\phi}(\vec{r},t). \tag{4.10}$$

With the given *Ansatz* (4.5) the potential (4.2) can be written as

$$V(\phi) = \frac{\lambda_\phi}{4}\left(\phi^2 - \phi_0^2\right)^2\,, \tag{4.11}$$

where $\phi_0^2 = -\mu^2/\lambda_\phi$ (with $\mu^2 < 0$).

Upon inserting (4.5) and (3.2) into (4.3) one gets for non-vanishing components of the stress energy tensor:

$$
\begin{aligned}
T_t^t &= -\frac{1}{2}e^{-\lambda}(1+4\xi)\phi'^2 - \frac{\phi^2}{r^2} - \frac{\lambda_\phi}{4}(\phi_0^2 - \phi^2)^2 \\
&\quad -\xi G_t^t\phi^2 + \xi e^{-\lambda}\nu'\phi\phi' - 2\xi\left(\lambda_\phi(\phi^2 - \phi_0^2) + \frac{2}{r^2} - \xi R\right)\phi^2\,, \tag{4.12}
\end{aligned}
$$

$$
\begin{aligned}
T_r^r &= \frac{1}{2}e^{-\lambda}\phi'^2 - \frac{\phi^2}{r^2} - \frac{\lambda_\phi}{4}(\phi_0^2 - \phi^2)^2 \\
&\quad -\xi G_r^r\phi^2 - \xi e^{-\lambda}\left(\nu' + \frac{4}{r}\right)\phi\phi'\,, \tag{4.13}
\end{aligned}
$$

$$
\begin{aligned}
T_\theta^\theta &= -\frac{1}{2}e^{-\lambda}(1+4\xi)\phi'^2 - \frac{\lambda_\phi}{4}(\phi_0^2 - \phi^2)^2 \\
&\quad -\xi G_\theta^\theta\phi^2 + 2\xi\frac{e^{-\lambda}}{r}\phi\phi' - 2\xi\left(\lambda_\phi(\phi^2 - \phi_0^2) + \frac{2}{r^2} - \xi R\right)\phi^2\,. \tag{4.14}
\end{aligned}
$$

Similarly, the scalar field equation of motion (4.4) becomes:

$$\phi'' + \left(\frac{\nu' - \lambda'}{2} + \frac{2}{r}\right)\phi' - e^\lambda\left(\mu^2 + \lambda_\phi\phi^2 + \frac{2}{r^2} - \xi R\right)\phi = 0\,, \tag{4.15}$$

where prime denotes derivatives with respect to the radial coordinate r.

The first two Einstein equations ($G^\nu_\mu = 8\pi G_N T^\nu_\mu$) are:

$$\left[1 + \xi(8\pi G_N)\phi^2\right] G^t_t = 8\pi G_N \left\{ -\frac{1}{2}e^{-\lambda}(1 + 4\xi)\phi'^2 - \frac{\phi^2}{r^2} - \frac{\lambda_\phi}{4}(\phi_0^2 - \phi^2)^2 \right.$$
$$\left. + \xi e^{-\lambda}\nu'\phi\phi' - 2\xi\left(\lambda_\phi(\phi^2 - \phi_0^2) + \frac{2}{r^2} - \xi R\right)\phi^2 \right\}, \tag{4.16}$$

$$\left[1 + \xi(8\pi G_N)\phi^2\right] G^r_r = 8\pi G_N \left\{ \frac{1}{2}e^{-\lambda}\phi'^2 - \frac{\phi^2}{r^2} - \frac{\lambda_\phi}{4}(\phi_0^2 - \phi^2)^2 \right.$$
$$\left. - \xi e^{-\lambda}\left(\nu' + \frac{4}{r}\right)\phi\phi' \right\}, \tag{4.17}$$

and, as in the previous chapter, instead of using the $(\theta\theta)$ Einstein equation (or the equivalent $(\varphi\varphi)$ equation), we use the trace equation, $G^\mu_\mu = -R = 8\pi G_N T^\mu_\mu$, leading to:

$$R = 8\pi G_N \frac{(1 + 6\xi)\left[e^{-\lambda}\phi'^2 + \frac{2\phi^2}{r^2} - \lambda_\phi\phi^2(\phi_0^2 - \phi^2)\right] + \lambda_\phi\phi_0^2(\phi_0^2 - \phi^2)}{1 + \xi(1 + 6\xi)8\pi G_N\phi^2}. \tag{4.18}$$

For the case of conformal coupling, $\xi = -1/6$, the only non-vanishing term in the Ricci curvature scalar is the term related to the potential. Analogous to the case of boson stars, the conformal gravity is obtained in the limit of zero global monopole mass term μ^2 since $\phi_0^2 = -\mu^2/\lambda_\phi$.

Equations(4.16–4.17) and (4.18) constitute the central equations in this section.

A simplified version for $\xi = 0$

Let us first demonstrate basic monopole characteristics through an extremely simplified model in which we choose a step function for the monopole field profile [100], *i.e.*

$$\phi(r) = \left\{ \begin{array}{ll} 0 & \text{if } r < \delta \\ \phi_0 & \text{if } r > \delta, \end{array} \right. \tag{4.19}$$

where δ is the so called monopole core radius. This choice of the monopole field corresponds to the pure false vacuum inside the core and an exactly true vacuum at the exterior.

For $r < \delta$ the components of the metric tensor are

$$T_t^t = T_r^r = T_\theta^\theta = T_\varphi^\varphi = -\frac{1}{4}\lambda_\phi \phi_0^4. \tag{4.20}$$

Upon solving Einstein's equations, for the interior solution we obtain the de Sitter metric

$$e^{-\lambda} = e^\nu = 1 - H^2 r^2, \tag{4.21}$$

with $H^2 = 2\pi G_N \lambda_\phi \phi_0^4 / 3$.

Similarly, for $r > \delta$, the metric outside the monopole core is obtained by solving Einstein's equations for the components of the energy-momentum tensor

$$T_t^t = T_r^r = -\frac{\phi_0^2}{r^2}, \quad T_\theta^\theta = T_\varphi^\varphi = 0, \tag{4.22}$$

yielding

$$e^{-\lambda} = e^\nu = 1 - \Delta - \frac{2G_N M}{r}, \tag{4.23}$$

where M is an integration constant and

$$\Delta \equiv 8\pi G_N \phi_0^2 \tag{4.24}$$

is the energy scale of the symmetry breaking in the reduced Planck units. The quantity Δ has a meaning of the deficit solid angle.

Both constants, δ and M, are determined by continuously matching interior and exterior metrics yielding

$$\delta = \frac{2}{\sqrt{\lambda_\phi}\phi_0}, \qquad M = -\frac{16\pi}{3}\frac{\phi_0}{\sqrt{\lambda_\phi}}. \tag{4.25}$$

This result is very interesting as it shows that the effective mass of the monopole core is negative. However, the energy density $\rho = -T_t^t$ is positive definite and thus the total mass is also positive

$$M_{tot}(r) = 4\pi \int_0^r \rho r^2 dr = 4\pi\phi_0^2 r - \frac{16\pi}{3}\frac{\phi_0}{\sqrt{\lambda_\phi}}, \tag{4.26}$$

where the second term is obtained as an integration constant $M_{tot}(r = 0) = -16\pi\phi_0/(3\sqrt{\lambda_\phi})$.

Now we see that this (total) mass is linearly divergent (due to the long range Goldstone field) as mentioned in the introduction of this section. Nevertheless, the term that causes divergence – the deficit solid angle – does not contribute to the Newtonian force. In other words, particles moving in the global monopole field will experience only repulsive force due to the monopole negative core mass, as we shall see from the results of this section.

A simplified version for $\xi \neq 0$

In this subsection we introduce the nonminimal coupling and perform the same analysis as in the previous subsection. In this case the field cannot be approximated simply by the step function owing to the ϕ-dependent term in the equation of motion (4.15). That is, for $r > \delta$, the term that multiplies ϕ will vanish only if we assume the following *Ansatz*:

$$\phi(r) = \begin{cases} 0 & \text{if} \quad r < \delta \\ \phi_0 - \gamma/r^2 & \text{if} \quad r > \delta, \end{cases} \tag{4.27}$$

where $\gamma = \text{const}$. For $r < \delta$ the components of the metric tensor are

$$T_t^t = T_r^r = T_\theta^\theta = T_\varphi^\varphi = -\frac{1}{4}\lambda_\phi \phi_0^4. \tag{4.28}$$

The solution to the Einstein equations for the interior part again yield the de Sitter metric

$$e^{-\lambda} = e^\nu = 1 - H^2 r^2, \tag{4.29}$$

with $H^2 = 2\pi G_N \lambda_\phi \phi_0^4 / 3$.

For $r > \delta$ the metric outside the monopole core is obtained by solving Einstein equations for the components of the energy-momentum tensor

$$T_t^t = T_r^r = -\frac{\phi_0^2}{r^2}\frac{1}{1 + \xi\Delta}, \quad T_\theta^\theta = T_\varphi^\varphi = 0, \tag{4.30}$$

yielding

$$e^{-\lambda} = e^\nu = 1 - \frac{\Delta}{1 + \xi\Delta} - \frac{2G_N M}{r}, \tag{4.31}$$

where M is again an arbitrary integration constant which is, along with the core size δ, fixed by continuously matching interior and exterior metrics yielding

$$\delta = \frac{2}{\sqrt{\lambda_\phi}\phi_0}\frac{1}{\sqrt{1+\xi\Delta}}, \qquad M = -\frac{16\pi}{3}\frac{\phi_0}{\sqrt{\lambda_\phi}}\frac{1}{(1+\xi\Delta)^{3/2}}. \qquad (4.32)$$

The total mass is

$$M_{tot}(r) = 4\pi\int_0^r \rho r^2 dr = \frac{4\pi\phi_0^2}{1+\xi\Delta}r - \frac{16\pi}{3}\frac{\phi_0}{\sqrt{\lambda_\phi}}\frac{1}{(1+\xi\Delta)^{3/2}}. \qquad (4.33)$$

Dimensionless variables - Reduced Planck units

Before we proceed to solving Eqs. (4.16–4.17) and (4.18), for the purpose of numerical studies, we perform the following rescaling:

$$\frac{r}{\sqrt{8\pi G_N}} \to x, \qquad 8\pi G_N\left(\frac{\phi}{\phi_0}\right)^2 \to \tilde{\phi}^2, \qquad 8\pi G_N\phi_0^2 \to \Delta, \qquad 8\pi G_N R \to \tilde{R}. \qquad (4.34)$$

It also follows that the energy density, pressures and core mass scale as

$$(8\pi G_N)^2\rho \to \tilde{\rho}, \qquad (8\pi G_N)^2 p_{r,t} \to \tilde{p}_{r,t}, \qquad \sqrt{G_N/8\pi}M \to \tilde{M} \qquad (4.35)$$

The rescaled (dimensionless) differential equations to be solved are then:

$$\frac{d\lambda}{dx} = \frac{1-e^\lambda}{x} + \Delta\frac{x}{1+\xi\Delta\tilde{\phi}^2}\left\{\frac{1}{2}(1+4\xi)\tilde{\phi}'^2 + e^\lambda\frac{\tilde{\phi}^2}{x^2} + e^\lambda\Delta\frac{\lambda_\phi}{4}(1-\tilde{\phi}^2)^2\right.$$

$$\left. -\xi\nu'\tilde{\phi}\tilde{\phi}' + 2\xi e^\lambda\left(\Delta\lambda_\phi(\tilde{\phi}^2-1) + \frac{2}{x^2} - \xi\tilde{R}\right)\tilde{\phi}^2\right\}, \qquad (4.36)$$

$$\frac{d\nu}{dx} = \frac{e^\lambda-1}{x}\frac{1+\xi\Delta\tilde{\phi}^2}{1+\xi\Delta\tilde{\phi}^2+\xi\Delta x\tilde{\phi}\tilde{\phi}'}$$

$$-\Delta\frac{x}{1+\xi\Delta\tilde{\phi}^2+\xi\Delta x\tilde{\phi}\tilde{\phi}'}\left\{-\frac{1}{2}\tilde{\phi}'^2 + 4\xi\frac{\tilde{\phi}\tilde{\phi}'}{x} + e^\lambda\left(\frac{\tilde{\phi}^2}{x^2} + \Delta\frac{\lambda_\phi}{4}(1-\tilde{\phi}^2)^2\right)\right\}, \qquad (4.37)$$

$$\frac{d^2\tilde{\phi}}{dx^2} = -\frac{1}{2}\left(\frac{d\nu}{dx} - \frac{d\lambda}{dx} + \frac{4}{x}\right)\tilde{\phi}' + e^\lambda\left[\Delta\lambda_\phi(\tilde{\phi}^2-1) + \frac{2}{x^2} - \xi\tilde{R}\right]\tilde{\phi}, \qquad (4.38)$$

with the dimensionless Ricci scalar obeying

$$\tilde{R} = \Delta \frac{(1 + 6\xi)\left[e^{-\lambda}\tilde{\phi}'^2 + 2\frac{\tilde{\phi}^2}{x^2} - \Delta\lambda_\phi\tilde{\phi}^2(1 - \tilde{\phi}^2)\right] + \Delta\lambda_\phi(1 - \tilde{\phi}^2)}{1 + \xi(1 + 6\xi)\Delta\tilde{\phi}^2}. \tag{4.39}$$

In the limit $x \to \infty$ ($\tilde{\phi} \to 1$) Eqs. (4.36) and (4.37) can be formally integrated yielding

$$e^{-\lambda(x)} = e^{\nu(x)} = 1 - \frac{\Delta}{1 + \xi\Delta} - \frac{2M}{x}. \tag{4.40}$$

where M is an integration constant. In analogy with the space-times without deficit solid angle for which the metric function is written in terms of the mass function $g_{rr}^{-1} = 1 - 2m(x)/x$, for $x < \infty$ we have $M = M(x)$, and so we shall name $M(x)$ the *core mass function*. Besides, the deficit solid angle is modified due to the presence of nonminimal coupling:

$$\tilde{\Delta} = \frac{\Delta}{1 + \xi\Delta}. \tag{4.41}$$

The boundary conditions for Eqs. (4.36–4.38) are:

$$(1)\ e^{\lambda(0)} = 1, \quad (2)\ e^{\nu(\infty)} = 1 - \tilde{\Delta}, \quad (3)\ \tilde{\phi}(0) = 0, \quad (4)\ \tilde{\phi}(\infty) = 1. \tag{4.42}$$

We solve these nonlinear, mutually coupled, differential equations numerically by using the software code COLSYS [76]. For this purpose we map an infinite space $r \in [0, \infty >$ to the interval $x \in [0, 1]$ by virtue of the transformation $r = x/(1-x)$.

Just like in the previous chapter for the case of nonminimal boson stars, all physical quantities involved to describe nonminimal global monopole are given in the reduced Planck units. Hence, following the same rationale, we observe that Eqs. (4.36–4.39) are invariant under the following conformal transformations

$$x \to \beta x, \quad \lambda_\phi \to \frac{\lambda_\phi}{\beta^2}, \quad \tilde{R} \to \frac{\tilde{R}}{\beta^2}, \quad \tilde{\phi} \to \tilde{\phi}, \quad \xi \to \xi. \tag{4.43}$$

The core mass scales as

$$M \to \beta M. \tag{4.44}$$

Core mass Newtonian force, compactness, metric transformation and deficit solid angle

From the asymptotic form of the metric

$$ds^2 = -\left(1 - \tilde\Delta - \frac{2G_N M}{r}\right) dt^2 + \frac{dr^2}{1 - \tilde\Delta - \frac{2G_N M}{r}} + r^2 d\Omega^2 \,, \tag{4.45}$$

which is valid only for large r, we can assume that the g_{rr} component for smaller r can be written in terms of the core mass function $M(r)$

$$g_{rr}^{-1} = 1 - \tilde\Delta - \frac{2G_N M(r)}{r} \,, \tag{4.46}$$

from which the Newtonian potential generated by the core mass function is

$$\phi_M(r) = -\frac{G_N M(r)}{r}. \tag{4.47}$$

If a test particle has an angular momentum (per unit mass) L, then the Newtonian force generated by the core mass function, felt by the test particle, is

$$F_M(r) = -\nabla\phi_M(r) + \frac{L^2}{r^3}. \tag{4.48}$$

If we now rewrite g_{rr}^{-1} in slightly different form

$$g_{rr}^{-1} = (1 - \tilde\Delta)\left(1 - \frac{1}{1 - \tilde\Delta}\frac{2G_N M(r)}{r}\right) \,, \tag{4.49}$$

we can read off the compactness function

$$\mu(r) = \frac{1}{1 - \tilde\Delta}\frac{2G_N M(r)}{r} \,, \tag{4.50}$$

from which it follows that, in order to avoid an event horizon formation, the compactness function must be less then unity.

If we now transform the asymptotic metric (4.40) by virtue of *new* coordinates

$$\tilde r^2 = \frac{r^2}{1 - \tilde\Delta}, \quad \tilde t^2 = (1 - \tilde\Delta)t^2 \,, \tag{4.51}$$

to the following form

$$ds^2 = -\left(1 - \frac{2\tilde{G}_N \tilde{M}}{\tilde{r}}\right) d\tilde{t}^2 + \frac{d\tilde{r}^2}{1 - \frac{2\tilde{G}_N \tilde{M}}{\tilde{r}}} + (1 - \tilde{\Delta})\tilde{r}^2 d\Omega^2 , \qquad (4.52)$$

the meaning of the deficit solid angle is now transparent: the surface area of the sphere with a radius r is now $4\pi(1 - \tilde{\Delta})r^2$.
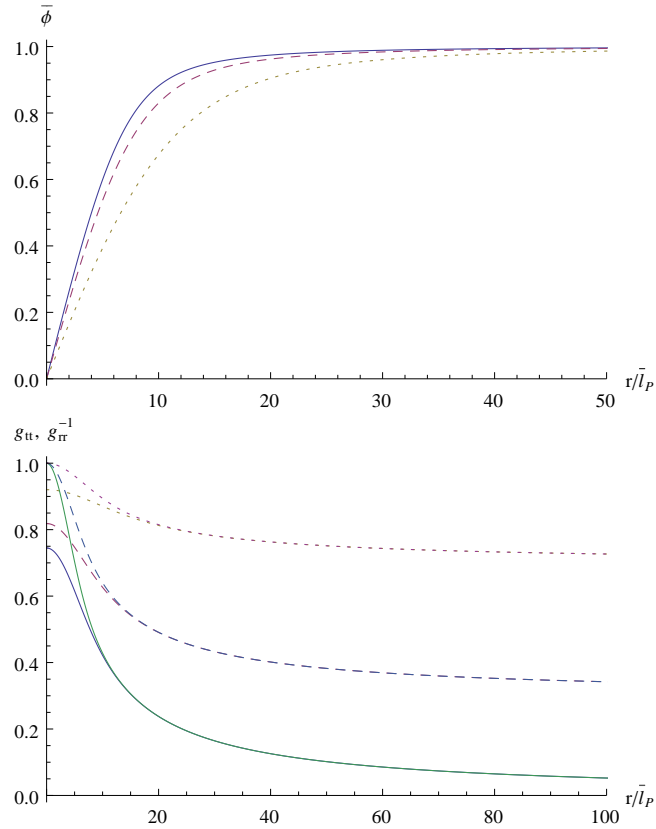
4.1.2   Results for $\xi = 0$

Figure 4.1. *Monopole field $\bar{\phi}$ (upper plot) and metric functions g_{tt} and g_{rr}^{-1} (lower plot) as a function of $x = r/\bar{l}_P$ for $\lambda_\phi = 0.1$, $\xi = 0$, $\Delta = 0.999$ for solid, $\Delta = 0.7$ for dashed and $\Delta = 0.3$ for dotted curves.*

In the case of minimal coupling it has been shown [101, 102] that for monotonically increasing scalar field, the regular solutions without horizon exist only for $\Delta < 1$. For $1 < \Delta < 3$ there are regular solutions with the horizon. However, for

$\Delta > 3$ there are no regular solutions which has been shown to be in accord with topological inflation (see *e.g.* [101]). The existence of the horizon can be seen from the asymptotic behaviour of the metric functions: in the limit $r \to \infty$ the metric functions g_{tt} and g_{rr}^{-1} approach zero for $\Delta \to 1$. In this work we are interested in the regular monopole solutions without horizon.

First, it is instructive to explore the effect of different symmetry-breaking scales Δ on the monopole configuration in the minimal coupling case. Hence in figures 4.1-4.4 we plot all relevant functions of the monopole configurations for three different values of Δ: $\Delta = 0.3$ for dotted, $\Delta = 0.7$ for dashed and $\Delta = 0.999$ for solid curves. In the upper plot of Fig. 4.1 we see that the change of Δ only slightly influences the shape of the monopole field - the fields remain monotonic. However, the metric functions shown in the lower plot of Fig. 4.1 do change significantly as Δ increases – as expected, for $\Delta \to 1$ we have $g_{tt}, g_{rr}^{-1} \to 0$.
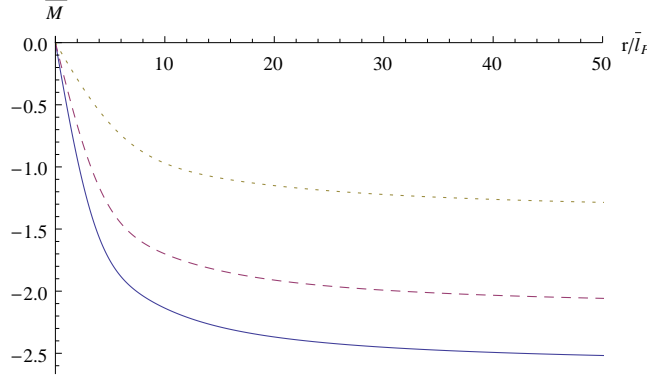

Figure 4.2. *Core mass functions $\bar{M}$ as a function of $x = r/\bar{l}_P$ for $\lambda_\phi = 0.1$, $\xi = 0$, $\Delta = 0.999$ for solid, $\Delta = 0.7$ for dashed and $\Delta = 0.3$ for dotted curves.*

The core mass function is more negative for larger Δ as seen in Fig. 4.2 which is also in agreement with Eq. (4.32). Correspondingly, the Newtonian forces produced by the core masses (4.48) (dashed curves), the Newtonian force (C.12) (dotted curves) and also the effective forces (D.12) (solid curves) are more repulsive for larger Δ as shown in Fig. 4.3. For small Δ the Newtonian force is in agreement with the effective force as seen in the upper plot of Fig. 4.3. Since the effective force does not cross zero, there exist no bound orbits for the minimally coupled monopole. This result is very interesting and in a way represents a signature of the global monopole configuration in the minimal setting – even though

the energy density is positive and decreasing as $1/r^2$ the particle moving in the monopole field feels a repulsive force.
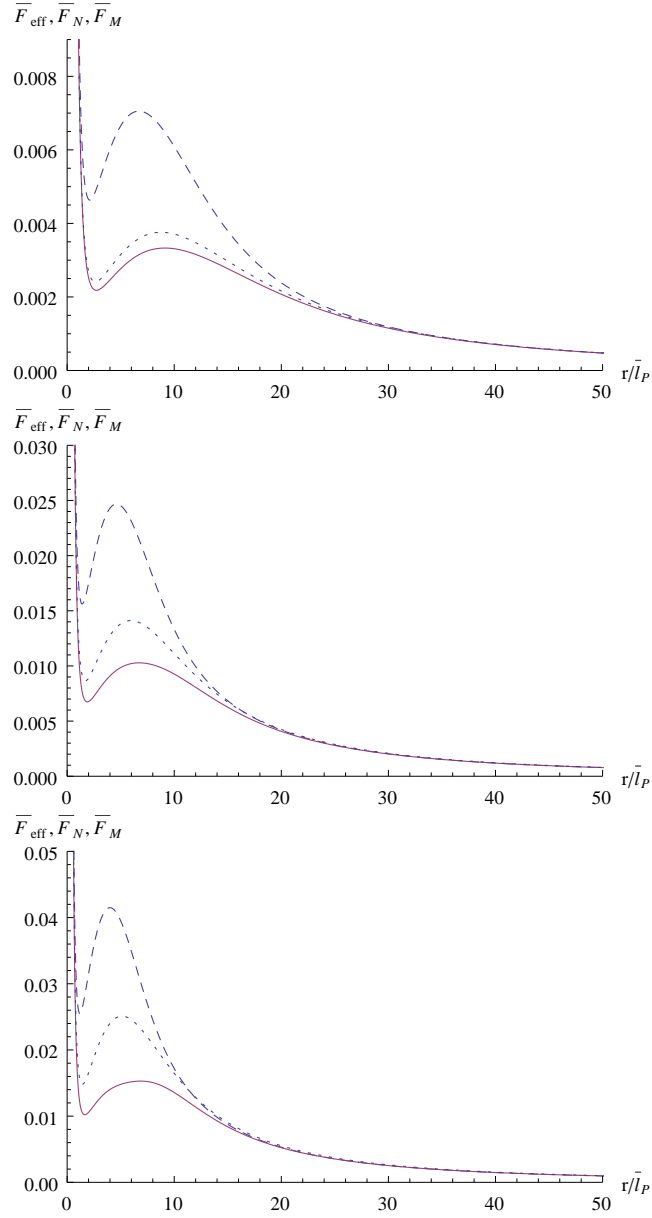

Figure 4.3. *$\bar{F}_M$ (4.48) (dashed), Newtonian $\bar{F}_N$ (C.12) (dotted) and the effective $\bar{F}_{\text{eff}}$ forces (D.12) (solid) for $\Delta = 0.3$ (upper plot), $\Delta = 0.7$ (middle plot) and $\Delta = 0.999$ (lower plot). Also the angular momentum and the energy per unit mass are $\bar{L} = 0.1$ and $\bar{E} = 1$.*

This is due to the fact that the total mass, which is obtained as the volume

integral of the energy density, can be written as a sum of two parts: one part comes from the core mass function and the other part comes from the deficit solid angle. Only the core mass function contributes to the Newtonian force as the second part is linear in r, thus yielding a constant Newtonian potential which produces no Newtonian force. In all three cases both Newtonian forces are in qualitative agreement with the effective forces for small r while for large r all forces agree very well both qualitatively and quantitatively, as expected. The differences between the Newtonian and the effective forces can be traced back to the nonlinear effects and the *gravitational slip* which is defined as the difference between the two Newtonian potentials (the one corresponds to g_{tt} and the other to g_{rr}) and which is known to be different from zero in the presence of matter. Independently on the value of Δ, the energy density is always positive-definite while the pressures are negative-definite functions of the radial coordinate in the minimal coupling case. Also the magnitude of all three thermodynamic functions are larger for larger Δ as shown in Fig. 4.4. In all these cases the strong energy condition is violated and this trend is more prominent for larger Δ.
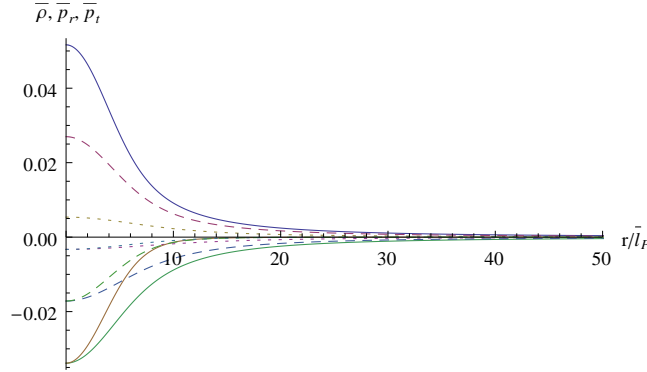

Figure 4.4. *Energy density $\bar{\rho}$ and principal pressures $\bar{p}_r, \bar{p}_t$ as a function of $x = r/\bar{l}_P$ for $\lambda_\phi = 0.1$, $\xi = 0$, $\Delta = 0.999$ for solid, $\Delta = 0.7$ for dashed and $\Delta = 0.3$ for dotted curves. The energy density is positive-definite and pressures are negative; transversal pressure is larger then the radial in all three cases.*

The monopole radius which can be roughly estimated as a radius where the central energy density drops to its 1% value, does not significantly depend on the symmetry breaking scale. Nevertheless, according to Eq.(4.32) the size of the core for $\xi = 0$ decreases as $1/\sqrt{\Delta}$, meaning that larger Δ produces a smaller

monopole core.

4.1.3 Results for $\xi \neq 0$

In this subsection we show how nonminimal coupling of the monopole field to gravity affects the behaviour of minimally coupled global monopole studied in the previous section. This analysis was firstly obtained by Nucamendi *et al.* [104] and our results are in agreement with theirs. Just like in the case of boson stars, nonminimal coupling drastically changes the monopole configuration.

Firstly, from the asymptotic behaviour of the metric function (4.40) we observe that an event horizon forms if $1 - \tilde{\Delta} - 2G_N M(r)/r = 0$ for a finite r. In this thesis we shall not consider configurations with an event horizon and hence we shall demand that $2G_N M(r)/r < 1 - \tilde{\Delta}$ for all finite r. When $r \to \infty$, $G_N M(r)/r \to 0$ and the above condition reduces to $\tilde{\Delta} < 1$. In Fig. 4.5 we show how ξ depends on Δ if we demand that $\tilde{\Delta} < 1$.
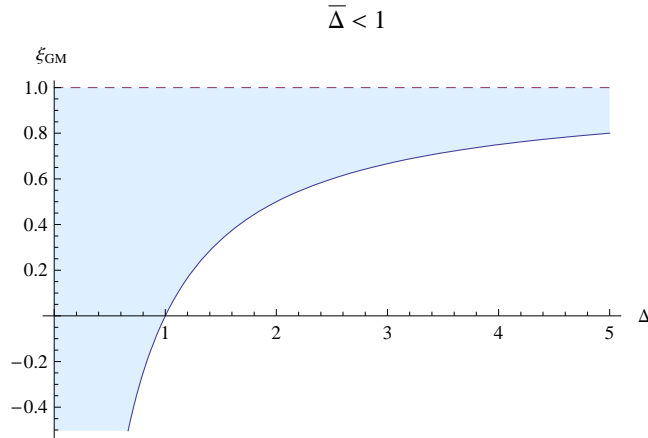

Figure 4.5. *Nonminimal coupling ξ as a function of the symmetry-breaking scale Δ for $\tilde{\Delta} = 1$. Shaded region shows allowed values of ξ for a given Δ.*

Shaded region shows allowed values of ξ for a given Δ. Here, for example, we have the situation that the horizon will not form for $\Delta = 1$ if ξ is only slightly greater then zero. Besides, there are no restrictions on Δ if $\xi \geq 1$. Hence, in the nonminimal case there are much more allowed values for Δ that lead to regular solutions without horizons.

The most important feature of nonminimal global monopoles is the existence

of bound orbits which can be traced back to the minima of the effective potential. In this section we present all relevant functions for three different values of ξ: $\xi = -1$ for solid, $\xi = 1$ for dashed and $\xi = 2$ for dotted curves. Here the energy of the symmetry-breaking scale is fixed and equals $\Delta = 0.1$. The self-coupling is also fixed $\lambda_\phi = 0.1$. Even though the effect of nonminimal coupling is large, the monopole field still retains its monotonic behaviour as seen in the upper plot of Fig. 4.6. The same can be said for the metric functions shown in the lower plot of Fig. 4.6. This graph is useful as one may, in particular, read off the radial coordinate $x = r/\bar{l}_P$ for which the asymptotic form of the metric (4.40) is valid.

Nevertheless, the core mass function is not so immune to the ξ-parameter as shown in Fig. 4.7. For positive ξ, in particular for $\xi > 1$, the core mass function as a function of the radial coordinate exhibits locally positive values.
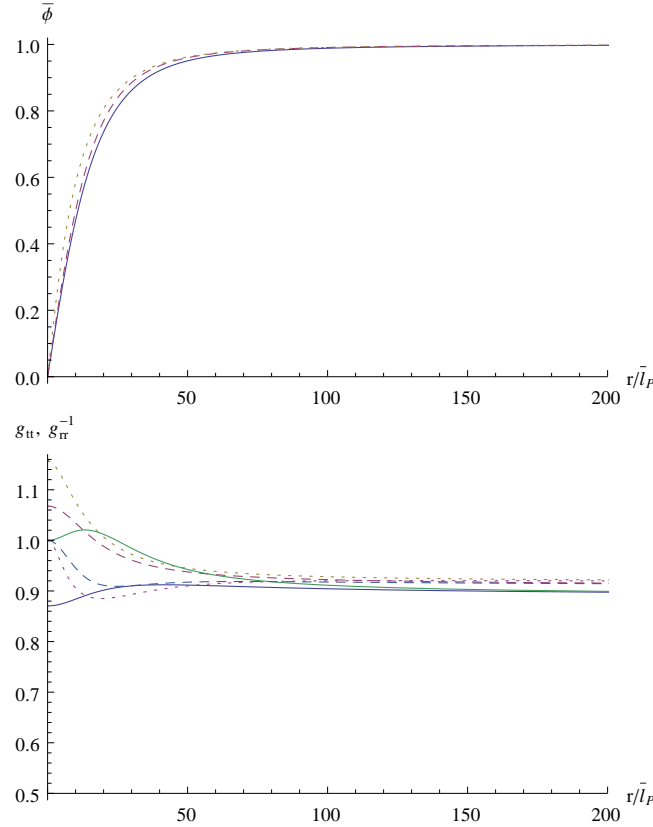

Figure 4.6. *The monopole field $\bar{\phi}$ in the upper plot and metric functions g_{tt} and g_{rr}^{-1} in the lower plot for $\lambda_\phi = 0.1$, $\Delta = 0.1$, $\xi = -1$ for solid, $\xi = 1$ for dashed and $\xi = 2$ for dotted curves.*
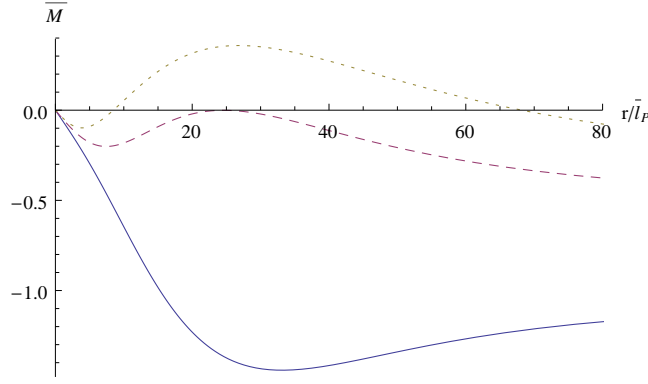
Figure 4.7. *Core mass functions for $\lambda_\phi = 0.1$, $\Delta = 0.1$, $\xi = -1$ for solid, $\xi = 1$ for dashed and $\xi = 2$ for dotted curves.*

This trend is accompanied by the attractive force implied by the core mass function (4.48) as shown in the middle and lower plots of Fig. 4.8 (dashed curves). One could naively conclude that the locally positive values of the core mass functions are responsible for the existence of bound orbits. However, this is not the case as the effective forces (D.12) (solid curves) are repulsive and they are responsible for the existence of bound orbits. While for large r all three forces agree, they show significant disagreements for small r inside the monopole core.

This is an interesting result as it allows to investigate the effects of the backreaction of geometry on matter as well as how matter affects geometry through gravitational slip. While F_N includes the backreaction of geometry on matter, it does not contain nonlinear effects of matter on geometry, F_{eff} includes both the backreaction of geometry on matter as well as nonlinear gravitational effects. Finally, F_M includes nonlinear effects of geometry, but it is insensitive to the effects of gravitational slip. From Fig. 4.8 we see that F_N and F_{eff} agree in all three cases considered, which means that the nonlinear geometrical effects are weak. In all cases F_M shows qualitative disagreement with F_{eff} which implies that in all cases the effects of gravitational slip are significant. From the above analysis it follows that while the effective and the Newtonian force contain information of bound orbits, the force produced by the core mass function does not. This then implies that the core mass function cannot be used to study bound orbits, while the *active* gravitational mass (obtained by integrating $\rho + \sum p_i$ over volume up to some radius r) can be used to study bound orbits.
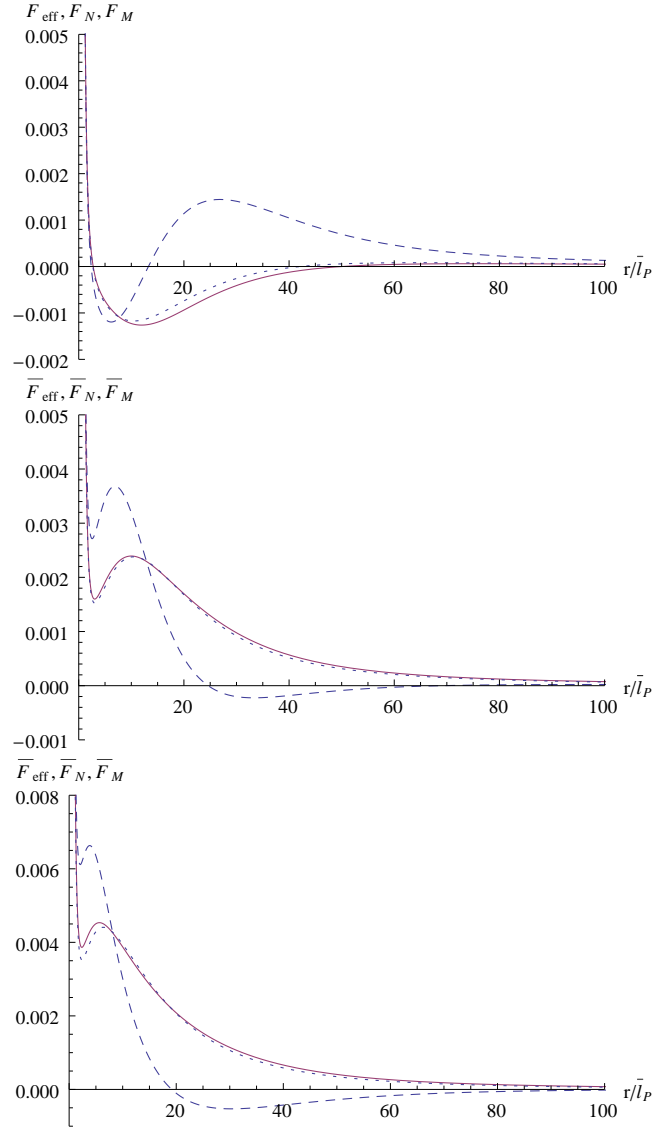
Figure 4.8. *The effective $\bar{F}_{\text{eff}}$ forces (D.12) (solid curves), the Newtonian forces $\bar{F}_N$ (C.12) (dotted curves) and the Newtonian forces produces by the core mass functions (4.48) (dashed curves) for $\xi = -1$ on the upper, $\xi = 1$ on the middle and $\xi = 2$ in the lower plot. The other parameters are $\lambda_\phi = 0.1$, $\Delta = 0.1$. Also the angular momentum and energy (of the particle) per unit mass are $\bar{L} = 0.1$ and $\bar{E} = 1$.*

It is also interesting to show how the thermodynamic functions behave for these three values of ξ. In the upper plot of Fig. 4.9 we see that for positive ξ the energy density is positive-definite while the pressures are negative-definite functions of the radial coordinate. However, for negative ξ the energy density

evolves from the negative center, crosses zero and asymptotically converge to zero from positive values while the pressures exhibit the opposite trend. Locally negative regions of the energy density obviously violate the null energy condition.
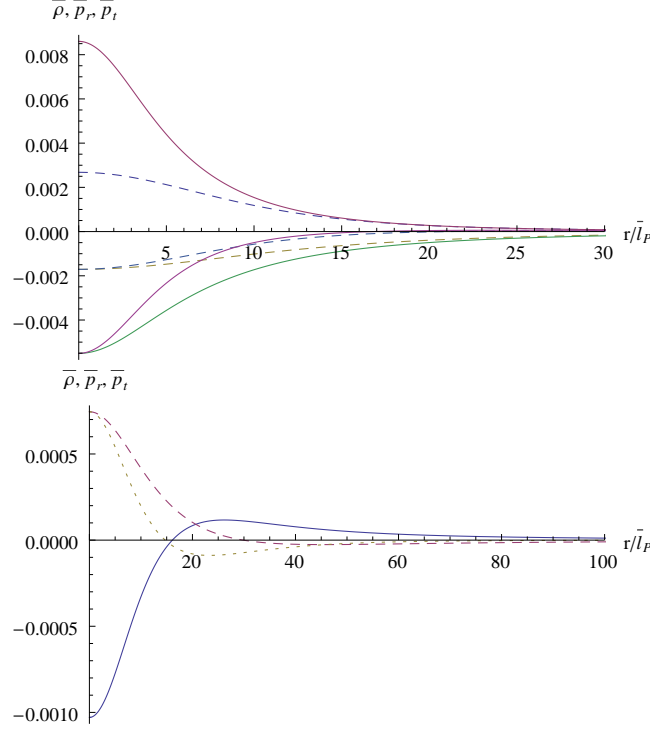

Figure 4.9. *The energy density $\bar{\rho}$ and principal pressures $\bar{p}_r, \bar{p}_t$ as a function of $x = r/\bar{l}_P$ for $\lambda_\phi = 0.1$, $\Delta = 0.1$ and $\xi = 2$ (solid curves) and $\xi = 1$ (dashed curves) in the upper plot and $\xi = -1$ in the lower plot (solid curve for the energy density, dashed for the radial and dotted for the transversal pressure).*

4.2 A nonminimal boson star and a global monopole

D-stars or topological defect stars are *"compact objects with a solid angular deficit, which generalize Q-stars by including a complex scalar field (or a fermion field), the Goldstone field and classical Einstein gravity."* [105]. In Ref. [106] a fermion D-star is investigated while in Ref. [107] an analysis of a boson D-star is performed. While fermion D-stars showed yet unresolved issues on the stability, boson D-stars have revealed an attractive features in the context of compact ob-

jects. Even though the authors presented an approximate solutions to the gravitational field outside D-stars, their analysis motivates the existence of black holes with deficit solid angle. Furthermore, in Ref. [108] the motion around D-stars is investigated while in Ref. [105] D-stars as gravitational lenses were considered.

In this section we perform detailed analysis of the system consisting of a boson star and a global monopole. Both fields are nonminimally coupled to gravity and interact only through the gravitational field.

This section is organized as follows: in subsection 4.2.1 we present a derivation of the Einstein equations for a composite system of a boson star and a global monopole – both fields are nonminimally coupled to gravity. In subsection 4.2.2 we show the results for weakly coupled boson star and a global monopole, for which both fields are only slightly affected in the combined system. In 4.2.3 the results for mild coupling are presented while in 4.2.4 we show the solutions for the composite system produced as a result of the strong (to extremal) coupling between a boson star and a global monopole field. In this regime we find a set of parameters for which a good black hole mimicker with the deficit solid angle may form.

4.2.1   The model

For matter we take a sum of the actions for the nonminimal boson star (Eq. 3.3) and the nonminimal global monopole (Eq. 4.1)

$$S = S_{BS} + S_{GM}. \tag{4.53}$$

The energy momentum tensor of this system is:

$$T_{\mu\nu} = T_{\mu\nu}^{\mathrm{BS}} + T_{\mu\nu}^{\mathrm{GM}} \tag{4.54}$$

where $T_{\mu\nu}^{\mathrm{BS}}$ is given with the Eq. (3.4) and $T_{\mu\nu}^{\mathrm{GM}}$ with Eq. (4.3). As in the previous chapter we make the following rescaling:

$$r = \sqrt{8\pi G_N}x, \qquad 8\pi G_N \phi_1^2 = \sigma^2, \qquad 8\pi G_N \phi_2^2 = \phi_0^2\tilde{\phi}^2, \qquad 8\pi G_N R = \tilde{R}, \tag{4.55}$$

where subscripts 1 and 2 denote the boson star field (and parameters) and the global monopole field (and parameters), respectively.

The deficit solid angle is the same as in the previous chapter $\Delta = 8\pi G_N \phi_0^2$ and $\tilde{\Delta} = \Delta/(1 + \xi_2 \Delta)$.

The equation of motion for the boson star field is obtained by varying the total action with respect to ϕ_1^* leading to

$$\sigma'' = -\left(\frac{2}{x} + \frac{\nu' - \lambda'}{2}\right)\sigma' + e^\lambda(\tilde{m}_1^2 + \lambda_1\sigma^2 - \tilde{\omega}^2 e^{-\nu} - \xi_1\tilde{R})\sigma. \quad (4.56)$$

The equation of motion for the global monopole field is obtained by varying the total action with respect to ϕ_2 leading to

$$\tilde{\phi}'' = -\left(\frac{2}{x} + \frac{\nu' - \lambda'}{2}\right)\tilde{\phi}' + e^\lambda\left(\lambda_2\Delta(\tilde{\phi}^2 - 1) + \frac{2}{x^2} - \xi_2\tilde{R}\right)\tilde{\phi}. \quad (4.57)$$

From the first two Einstein equations $G_{\mu\nu} = 8\pi G_N T_{\mu\nu}$ we obtain the differential equations for the metric functions

$$
\begin{aligned}
\lambda' = {} & \frac{1 - e^\lambda}{x} + \frac{x}{1 + 2\xi_1 + \xi_2\tilde{\phi}^2}\Bigg\{e^\lambda\left((\tilde{m}_1^2 + \tilde{\omega}^2 e^{-\nu} + \lambda_1/2)\sigma^2 + \frac{\tilde{\phi}^2}{x^2} + \frac{\tilde{\lambda}_2}{4}\Delta^2(1 - \tilde{\phi}^2)^2\right) \\
& + (1 + 4\xi_1)\sigma'^2 + \frac{1}{2}(1 + 4\xi_2)\tilde{\phi}'^2 - 2\xi_1\nu'\sigma\sigma' - \xi_2\nu'\tilde{\phi}\tilde{\phi}' \\
& + 4\xi_1 e^\lambda\left[\tilde{m}_1^2 - \tilde{\omega}^2 e^{-\nu} + \lambda_1\sigma^2 - \xi_1\tilde{R}\right]\sigma^2 \\
& + 2\xi_2 e^\lambda\left[\lambda_2\Delta(\tilde{\phi}^2 - 1) + \frac{2}{x^2} - \xi_2\tilde{R}\right]\tilde{\phi}^2\Bigg\}, \quad (4.58)
\end{aligned}
$$

$$
\begin{aligned}
\nu' = {} & \frac{x}{1 + 2\xi_1\sigma^2 + 2\xi_1 x\sigma\sigma' + \xi_2\tilde{\phi}^2 + \xi_2 x\tilde{\phi}\tilde{\phi}'}\Bigg\{\frac{-1 + e^\lambda}{x^2}(1 + 2\xi_1\sigma^2 + \xi_2\tilde{\phi}^2) \\
& + \sigma'^2 - e^\lambda(\tilde{m}_1^2 - \tilde{\omega}^2 e^{-\nu} + \frac{\lambda_1}{2}\sigma^2)\sigma^2 - \frac{8\xi_1\sigma\sigma'}{x} + \frac{\tilde{\phi}'^2}{2} - \frac{4\xi_2\tilde{\phi}\tilde{\phi}'}{x} \\
& - e^\lambda\left[\frac{\tilde{\phi}^2}{x^2} + \frac{\lambda_2}{4}\Delta^2(1 - \tilde{\phi}^2)^2\right]\Bigg\}. \quad (4.59)
\end{aligned}
$$

The rescaled Ricci scalar is

$$
\begin{aligned}
\tilde{R} = {} & \frac{2\tilde{m}_1^2\sigma^2 + 2(1 + 6\xi_1)\left[(\tilde{m}_1^2 - \tilde{\omega}^2 e^{-\nu} + \lambda_1\sigma^2)\sigma^2 + e^{-\lambda}\sigma'^2\right]}{1 + 2\xi_1(1 + 6\xi_1)\sigma^2 + \xi_2(1 + 6\xi_2)\tilde{\phi}^2} \\
& + \frac{\lambda_2\Delta^2(1 - \tilde{\phi}^2) + (1 + 6\xi_2)\left[e^{-\lambda}\tilde{\phi}'^2 + \frac{2\tilde{\phi}^2}{x^2} - \lambda_2\Delta(1 - \tilde{\phi}^2)\tilde{\phi}^2\right]}{1 + 2\xi_1(1 + 6\xi_1)\sigma^2 + \xi_2(1 + 6\xi_2)\tilde{\phi}^2}. \quad (4.60)
\end{aligned}
$$

The set of nonlinear differential equations (4.58-4.60) is solved upon providing the boundary conditions

$$\lambda(0) = 0, \qquad \nu(\infty) = 1 - \tilde{\Delta},$$
$$\sigma(0) = \sigma_0, \qquad \sigma(\infty) = 0,$$
$$\tilde{\phi}(0) = 0, \qquad \tilde{\phi}(\infty) = 1. \tag{4.61}$$

To easily distinguish among the boson star and the global monopole parameters, we shall also use the following abbrevations

$$\xi_{\text{BS}} = \xi_1, \qquad \xi_{\text{GM}} = \xi_2. \tag{4.62}$$

Now we proceed to solving the system that consists of a boson star and a global monopole which interact only gravitationally. So far we have witnessed monotonic behaviour of both fields, the boson star and the global monopole field, for all choices of parameters. In the combined system this is not the case anymore: both fields reconfigure themselves depending on the parameters. Therefore, we distinguish three regimes according to the qualitative behaviour of the fields configurations:

- Weak coupling regime: in this regime both, the boson star and the global monopole fields configurations retain theirs monotonicity.

- Mild coupling regime: in this regime the boson star field is slightly non-monotonic while the monopole field is still monotonic.

- Strong coupling regime: in this regime both, the boson star field and the monopole field are significantly reconfigured into non-monotonic fields. This regime is particularly interesting since the boson star gets very compressed by the monopole and a whole system can reach large compactness suggesting that this object can provide a good black hole mimicker.

In the previous chapter we have seen that boson stars exhibit largest compactness for negative values of nonminimal coupling ξ_{BS}. Here we want to analyze how the presence of a global monopole affects the boson star configuration. Therefore, we take the boson star parameters from the previous chapter with $\tilde{m} = 1$,

$\sigma_0 = 0.05$, $\lambda_{\mathrm{BS}} = 0$ and $\xi_{\mathrm{BS}} = -4$ that produces an attractive effective force and combine it with the global monopole with varying parameters.
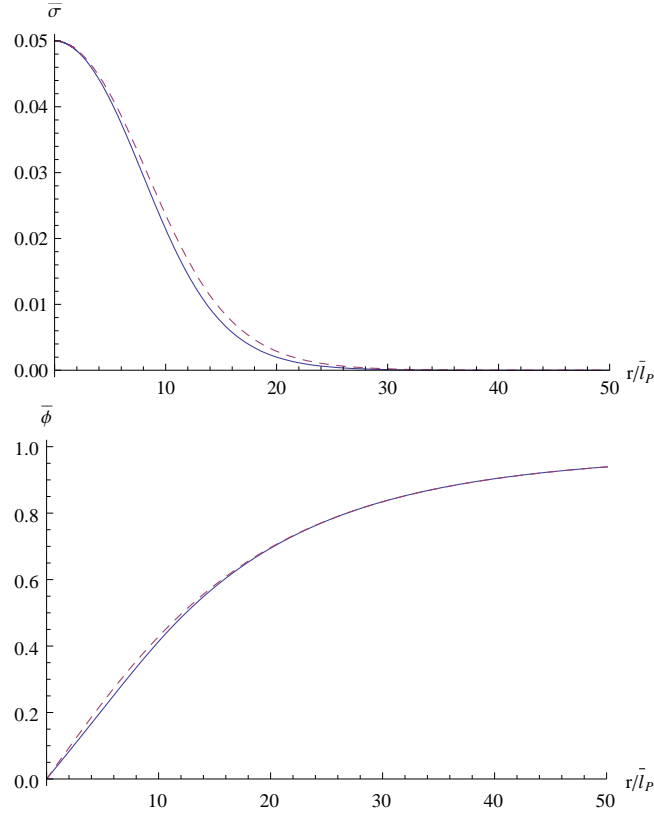

Figure 4.10. *Upper plot: the boson star field in the presence of the global monopole (solid) and the boson star field alone (dashed). Lower plot: the global monopole field in the presence of the boson star (solid) and the global monopole field alone (dashed). The parameters are: $\sigma_0 = 0.05$, $\lambda_{\mathrm{BS}} = 0$, $\xi_{\mathrm{BS}} = -4$, $\lambda_{\mathrm{GM}} = 0.1$, $\Delta = 0.08$, $\xi_{\mathrm{GM}} = -1$.*

4.2.2 Weak coupling regime

In this regime we take a global monopole configuration that produces an attractive effective potential, for example $\Delta = 0.08$, $\lambda_{\mathrm{GM}} = 0.1$ and $\xi_{\mathrm{GM}} = -1$. As seen in Fig. 4.10 both fields, the boson star (dashed curve in the upper plot) and the monopole field (dashed curve in the lower plot) are only slightly affected in the combined system (solid curves). Nevertheless, it is important to point out that both fields in the combined system are reconfigured to slightly lower magnitudes, which is not the case with the combined system with the monopole that produces a repulsive effective potential.
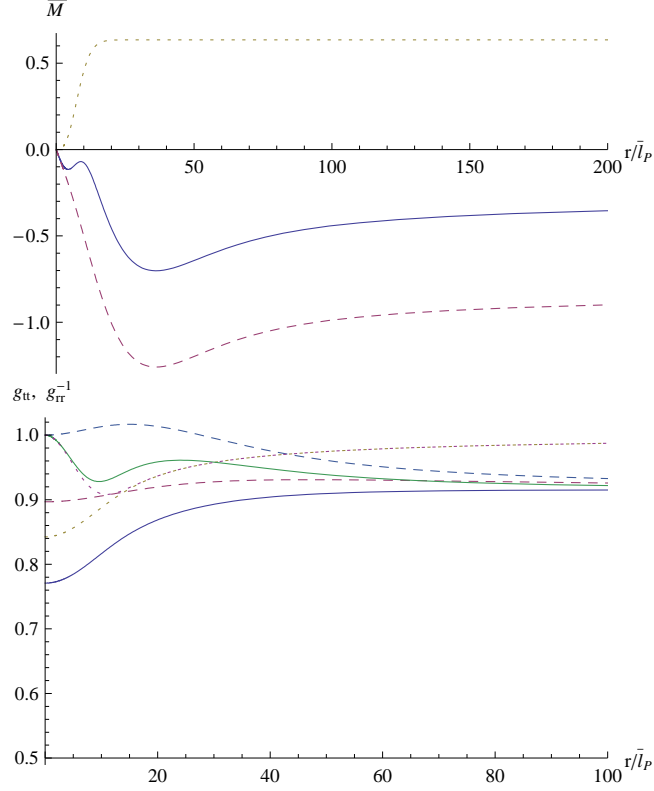
Figure 4.11. *Upper plot: the mass function for the boson star alone (dotted curve), the core mass function for the global monopole alone (dashed curve) and the core mass function for the combined system of the boson star and the global monopole (solid curve). Lower plot: the metric functions g_{tt} and g_{rr}^{-1} for the boson star alone (dotted curves), the global monopole alone (dashed curves) and the combined system of the boson star and the global monopole (solid curves). The parameters are: $\sigma_0 = 0.05$, $\lambda_{\mathrm{BS}} = 0$, $\xi_{\mathrm{BS}} = -4$, $\lambda_{\mathrm{GM}} = 0.1$, $\Delta = 0.08$, $\xi_{\mathrm{GM}} = -1$.*

The core mass function of the combined system is roughly equal to the sum of the constituent masses as seen in the upper plot of Fig. 4.11. Furthermore, the energy density, the pressures, the compactness (as seen in Fig. 4.12) in the combined system also sum up approximately linearly. Due to this fact, one can actually obtain gravastar-like pressures in the combined object: both pressures evolve from a negative center and exhibit a locally positive maximum, just like the gravastar pressures in their atmosphere.
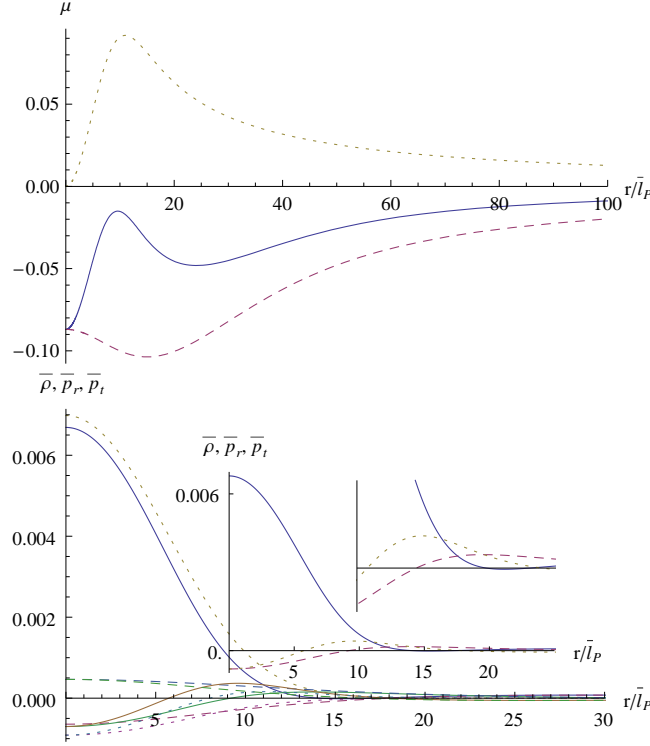
Figure 4.12. *Upper plot: the compactness function for the boson star alone (dotted curve), the global monopole alone (dashed curve) and the combined system (solid curve). Lower plot: the energy density and the pressures for the boson star alone (dotted curves), the global monopole alone (dashed curves) and the combined system (solid curves). The parameters are: $\sigma_0 = 0.05$, $\lambda_{\mathrm{BS}} = 0$, $\xi_{\mathrm{BS}} = -4$, $\lambda_{\mathrm{GM}} = 0.1$, $\Delta = 0.08$, $\xi_{\mathrm{GM}} = -1$.*
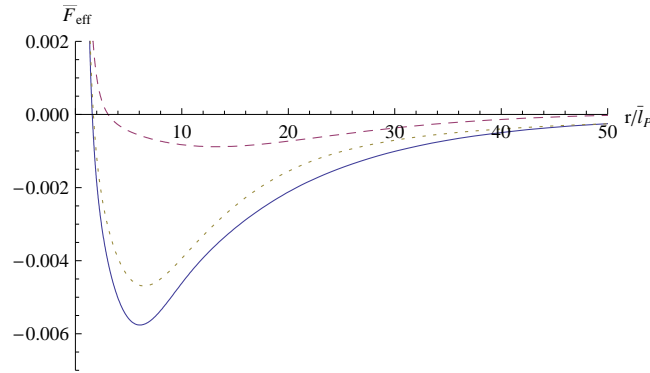

Figure 4.13. *The effective force (D.12) for the boson star alone (dotted curve), the global monopole (dashed curve) and the combined system (solid curve). The parameters are: $\sigma_0 = 0.05$, $\lambda_{\mathrm{BS}} = 0$, $\xi_{\mathrm{BS}} = -4$, $\lambda_{\mathrm{GM}} = 0.1$, $\Delta = 0.08$, $\xi_{\mathrm{GM}} = -1$. Also the angular momentum and the energy per unit mass are $\bar{L} = 0.1$ and $\bar{E} = 1$.*

However, the dominant energy condition is clearly violated in the combined system for the chosen set of parameters. In Fig. 4.13 we see that the effective force of the combined system (solid curve) is also approximately equal to the sum of the effective forces produced by the boson star (dotted curve) and the global monopole (dashed curve).
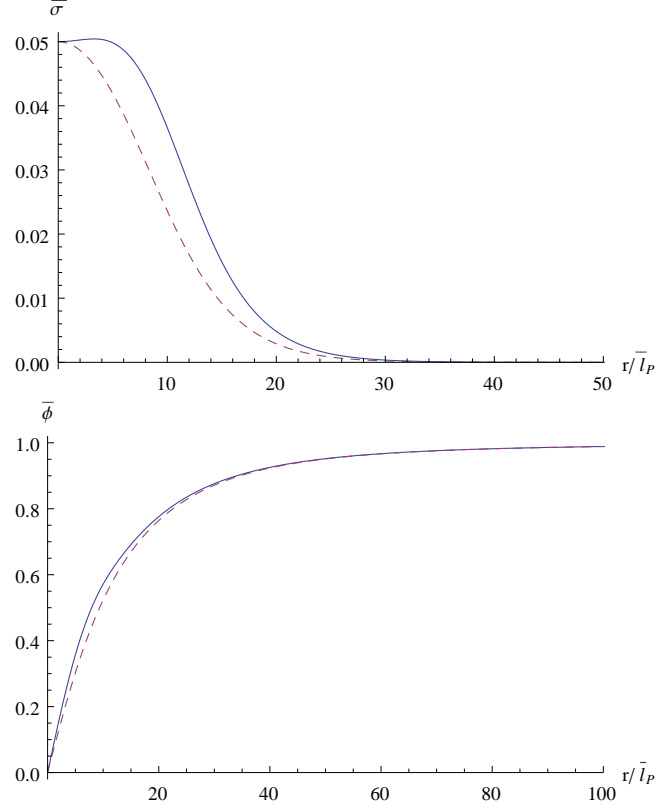

Figure 4.14. *Upper plot: the boson star field in the presence of the global monopole (solid) and the boson star field in the absence of the monopole (dashed). Lower plot: the global monopole field in the presence of the boson star (solid) and the global monopole field in the absence of the boson star (dashed). The parameters are: $\sigma_0 = 0.05$, $\lambda_{BS} = 0$, $\xi_{BS} = -4$, $\lambda_{GM} = 0.1$, $\Delta = 0.08$, $\xi_{GM} = 2$.*

4.2.3   Mild coupling regime

In this subsection we take the global monopole with $\Delta = 0.08$, $\lambda_{GM} = 0.1$, $\xi_{GM} = 2$ that produces repulsive effective force. In Fig. 4.14 we show *i)* in the upper plot how the boson star field (dashed curve) is affected by the presence of the global monopole (solid curve) and *ii)* in the lower plot how the global

monopole field (dashed curve) is affected by the presence of the boson star field (solid curve). For the given set of parameters the boson star field is more sensitive to the presence of the global monopole field then vice versa: the boson star field reconfigures significantly by loosing its monotonicity while the monopole field remains monotonous.
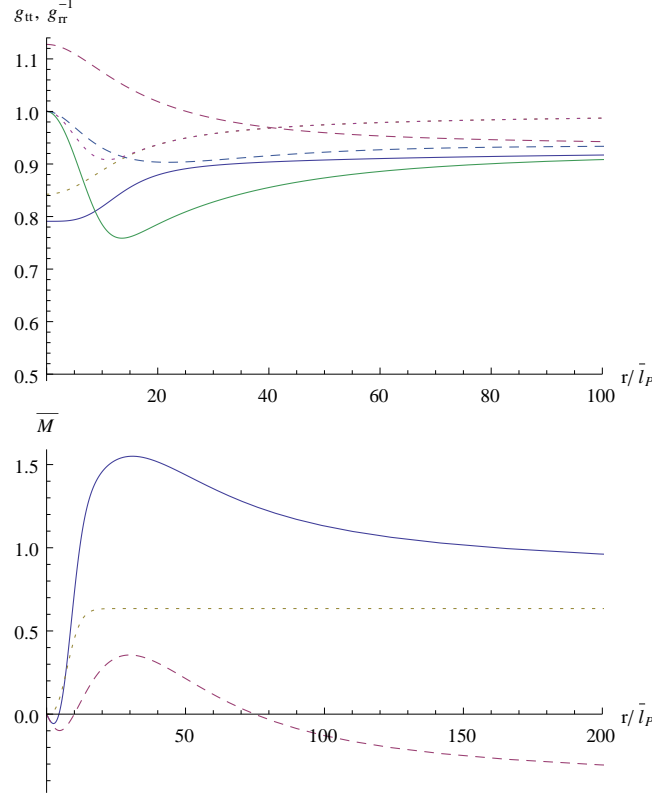

Figure 4.15. *Upper plot: the metric functions g_{tt} and g_{rr}^{-1} for the boson star alone (dotted curves), the global monopole alone (dashed curves) and the combined system of the boson star and the global monopole (solid curves). Lower plot: the mass function for the boson star alone (dotted curve), core mass function for the global monopole alone (dashed curve) and the mass function for the combined system of the boson star and the global monopole (solid curve). The parameters are: $\sigma_0 = 0.05$, $\lambda_{\mathrm{BS}} = 0$, $\xi_{\mathrm{BS}} = -4$, $\lambda_{\mathrm{GM}} = 0.1$, $\Delta = 0.08$, $\xi_{\mathrm{GM}} = 2$.*

In the upper plot of Fig. 4.15 we illustrate how the metric functions g_{tt} and g_{rr}^{-1} are affected by combining the boson star and the global monopole into one system. The approximate value of the radial coordinate for which $g_{tt} \approx g_{rr}^{-1}$ gives us a rough estimate of r where the asymptotic behaviour of the metric (4.40) becomes

valid. In the lower plot of Fig. 4.15 we show a rather unexpected behaviour of the core mass function of the combined system (solid curve), which is clearly greater then the sum of the constituents (core) masses of the boson star (dotted curve) and the global monopole (dashed curve).
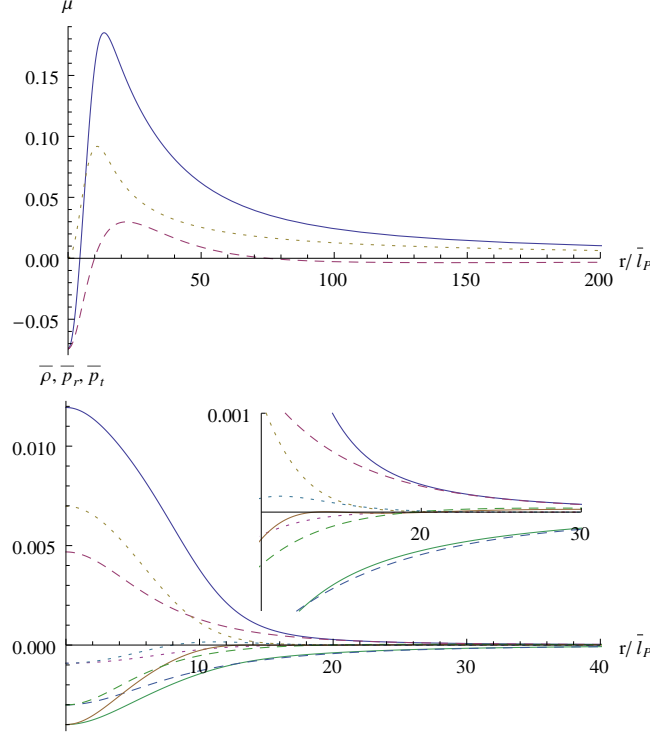

Figure 4.16. *Upper plot: compactness for the boson star alone (dotted curve), the global monopole alone (dashed curve) and the combined system of the boson star and the global monopole (solid curve). Lower plot: energy density and pressures for the boson star alone (dotted curves), the global monopole alone (dashed curves) and the combined system of the boson star and the global monopole (solid curves). The parameters are: $\sigma_0 = 0.05$, $\lambda_{\mathrm{BS}} = 0$, $\xi_{\mathrm{BS}} = -4$, $\lambda_{\mathrm{GM}} = 0.1$, $\Delta = 0.08$, $\xi_{\mathrm{GM}} = 2$.*

This trend is important for the compactness, a function that measures how much mass can be accommodated in a certain radius. It turns out that the compactness is significantly greater in the combined system (solid curve in the upper plot of Fig. 4.16) then in the boson star alone (dotted curve in the the upper plot of Fig. 4.16) or the global monopole alone (dashed curve in the upper plot of Fig. 4.16), or even larger than the sum of the two. From the lower plot of Fig. 4.16 we can trace the change in the behaviour of the energy density and

pressures. In all three cases the energy density is positive while the pressures are negative functions of the radial coordinate. Observe that size of the combined system is approximately the same as the size of the global monopole (the boson star is a bit smaller).
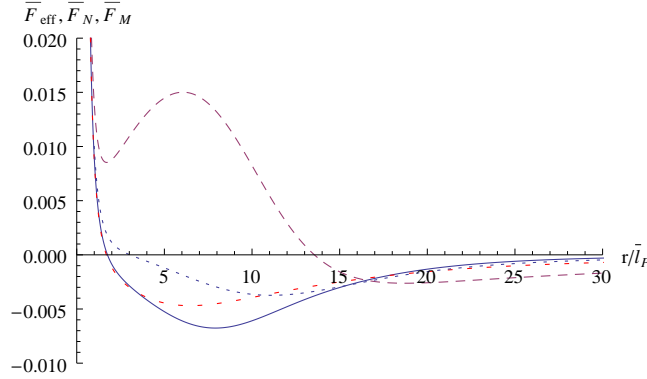

Figure 4.17. *The effective force (D.12) (solid curve), the Newtonian force (C.12) (dotted curve) and the Newtonian force produced by the core mass function (4.48) (dashed curve) for the combined system of the boson star and the global monopole; and the effective force of the boson star alone (sparse dashed red curve). The parameters are: $\sigma_0 = 0.05$, $\lambda_{BS} = 0$, $\xi_{BS} = -4$, $\lambda_{GM} = 0.1$, $\Delta = 0.08$, $\xi_{GM} = 2$. Also the angular momentum and the energy per unit mass are $\bar{L} = 0.1$ and $\bar{E} = 1$.*

Thus, even though the central energy density of the boson star dominates the energy density of the global monopole, while the size of the boson star is smaller, the combined system is approximately of the same size as the global monopole (see inset of the lower plot of Fig. 4.16). In Fig. 4.17 we depict the effective force (D.12) (solid curve), the Newtonian (C.12) (dotted curve) and the Newtonian force produced by the core mass function (4.48) (dashed curve) for the combined system. We also show the effective force of the boson star alone (sparse dashed red curve). Even though, the global monopole produces a repulsive effective force (while the boson star produces an attractive effective force) the effective force produced by the combined system is more attractive than in the case of the boson star alone. Note that the radius of the stable bound orbit (where $F_{\text{eff}} = 0$) is almost the same for the boson star and the combined object, while the global monopole alone has no such orbits. Although there is a qualitative agreement between $\bar{F}_{\text{eff}}$ and $\bar{F}_N$ in that they both exhibit stable bound orbits, quantitatively they differ. Since $\bar{F}_N$ and $\bar{F}_M$ significantly differ

from the $\bar{F}_{\text{eff}}$ of the combined system, the nonlinear effects and the effects of the gravitational slip are present.
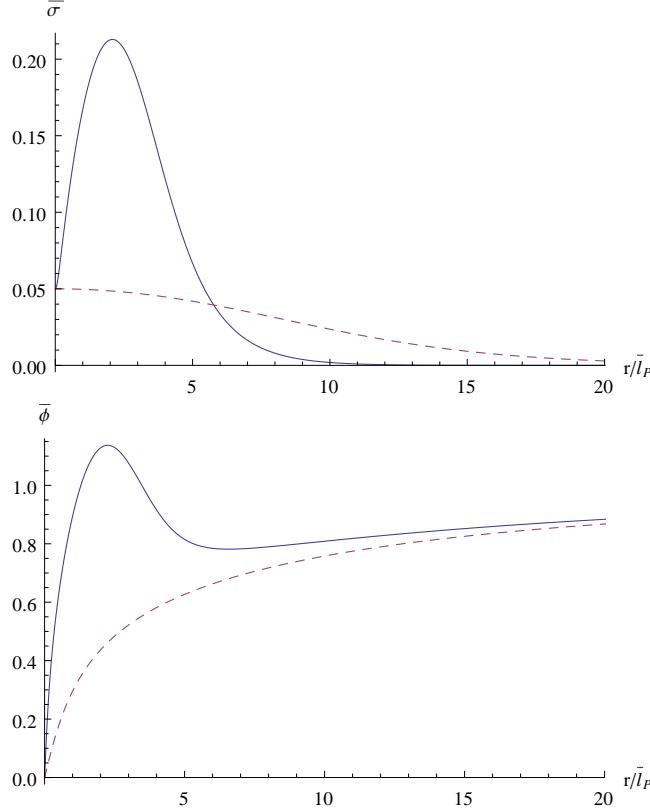

Figure 4.18. *Upper plot: the boson star field alone (dashed curve) and the boson star field in presence of the global monopole (solid curve). Lower plot: the global monopole field alone (dashed curve) and the global monopole field in presence of the boson star (solid). The parameters are: $\sigma_0 = 0.05$, $\lambda_{\text{BS}} = 0$, $\xi_{\text{BS}} = -4$, $\lambda_{\text{GM}} = 0.1$, $\Delta = 0.08$, $\xi_{\text{GM}} = 5$.*

4.2.4   Strong coupling regime

In this subsection we examine the combined system of the boson star and the global monopole when the repulsive monopole effects are strong. As we have seen in the previous section, this is the case for large positive ξ_{GM}. Here we show the examples with $\xi_{\text{GM}} = 5$ and $\xi_{\text{GM}} = 8$, while the other parameters are the same as in the previous subsection. As we shall see in what follows, the effects of strong gravitational fields increase dramatically with increasing ξ_{GM}, reaching compactness close to unity in the latter case. Increasing ξ_{GM} even further leads to

numerically unstable solutions which we interpret as a signature of event horizon formation and therefore black hole - like objects form.
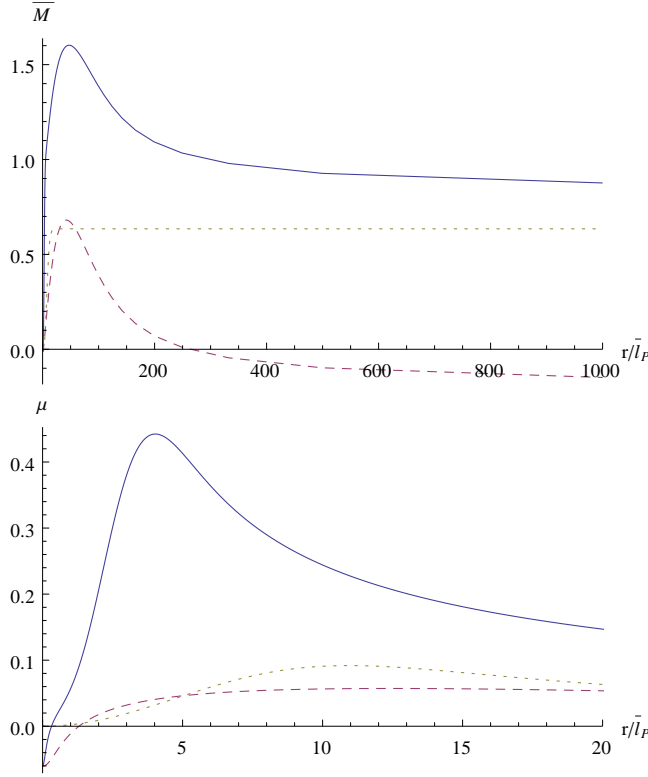

Figure 4.19. *Upper plot: mass function for the boson star alone (dotted curve), core mass function for the global monopole alone (dashed curve) and core mass function for the combined system of the boson star and the global monopole (solid curve). Lower plot: compactness for the boson star alone (dotted curve), the global monopole alone (dashed curve) and the combined system (solid curve). The parameters are: $\sigma_0 = 0.05$, $\lambda_{\mathrm{BS}} = 0$, $\xi_{\mathrm{BS}} = -4$, $\lambda_{\mathrm{GM}} = 0.1$, $\Delta = 0.08$, $\xi_{\mathrm{GM}} = 5$.*

In Fig. 4.18 we already see that now both, the boson star field (upper plot) and the monopole field (lower plot) are strongly influenced by each other: the repulsive monopole and the attractive boson star in the combined system strongly influence individual configurations.

However, the core mass function as shown in the upper plot of Fig. 4.19 behaves similarly as in the $\xi_{\mathrm{GM}} = 2$ case while the compactness function is enlarged significantly when compared with the sum of the two, as can be seen in the lower plot of Fig. 4.19. Moreover, the maximum compactness in this case is slightly above 0.4, thus a bit larger then the maximum compactness that can be reached

in the case of (non)minimally coupled boson stars (which is about 0.32). The whole system has shrunk as it is obvious from Fig. 4.20 - the combined object is much smaller then its constituents.
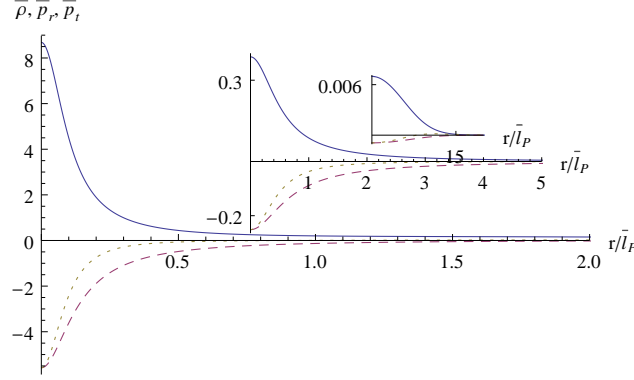

Figure 4.20. *Energy density and pressures for the boson star alone (dotted curves), the global monopole alone (dashed curves) and the combined system of the boson star and the global monopole (solid curves). The parameters are: $\sigma_0 = 0.05$, $\lambda_{\mathrm{BS}} = 0$, $\xi_{\mathrm{BS}} = -4$, $\lambda_{\mathrm{GM}} = 0.1$, $\Delta = 0.08$, $\xi_{\mathrm{GM}} = 5$.*
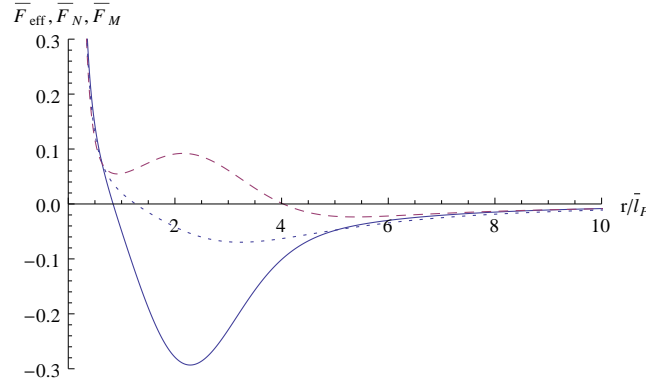

Figure 4.21. *The effective force (D.12) (solid curve), the Newtonian force (C.12) (dotted curve) and the Newtonian force produced by the core mass function (4.48) for the combined system of the boson star and the global monopole. The parameters are: $\sigma_0 = 0.05$, $\lambda_{\mathrm{BS}} = 0$, $\xi_{\mathrm{BS}} = -4$, $\lambda_{\mathrm{GM}} = 0.1$, $\Delta = 0.08$, $\xi_{\mathrm{GM}} = 5$. Also the angular momentum and the energy per unit mass are $\bar{L} = 0.1$ and $\bar{E} = 1$.*

The forces produced by the combined system are also quite strong as shown in Fig. 4.21. Solid curve shows $\bar{F}_{\mathrm{eff}}$, dotted $\bar{F}_N$ and dashed $\bar{F}_M$. When compared with the mild coupling regime in Fig. 4.17, the nonlinear gravitational effects and

the gravitational slip are similar, but amplified.

As ξ_{GM} further increases the object shrinks further and the maximum compactness increases, approaching values comparable to unity which signifies formation of a black hole. To show this, in Fig. 4.22 we plot the compactness for $\xi_{\mathrm{GM}} = 8$, for which the maximum value is slightly above 0.75 (solid curve).

This high value for the combined object is reached although individual maximum compactnesses are quite small: for the monopole alone $\mu_{\mathrm{max}} \simeq 0.05$ while for the boson star alone $\mu_{\mathrm{max}} \simeq 0.1$. In order to find out whether this highly compact object can be a good black hole mimicker, we also show the compactness of a Schwarzschild black hole with a mass that corresponds to the asymptotic mass of the combined system (sparse dashed red curve). A comparison of the two curves shows that up to a radius about a few times the Schwarzschild radius the compactness of the black hole can be well approximated by that of the combined system. This suggests that any physical process that occurs at distances up to a few times the event horizon can be well approximated by this black hole mimicker.
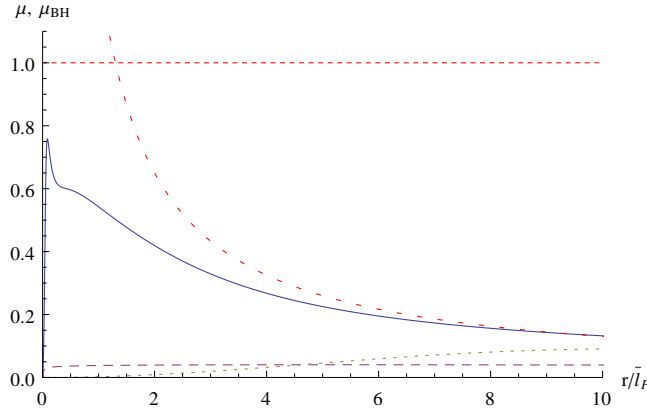

Figure 4.22. *Compactness for the combined system of the boson star and the global monopole (solid curve), the boson star alone (dotted curve) and the global monopole alone (dashed curve). Compactness for a Schwarzschild black hole with the mass equal to the core mass of the combined system (sparse dashed red curve). The parameters are: $\sigma_0 = 0.05$, $\lambda_{\mathrm{BS}} = 0$, $\xi_{\mathrm{BS}} = -4$, $\lambda_{\mathrm{GM}} = 0.1$, $\Delta = 0.11$, $\xi_{\mathrm{GM}} = 8$.*

Of course there is a prize to pay, and there are extremely large effective forces that are developed in the vicinity of the radius where the compactness maximizes, as can be seen in Fig. 4.23. Indeed, the effective force reaches an extremely large

value above 10000, whereby there are no large numbers present in any of the couplings. This can be explained by the large compression exerted on the boson star by the monopole gravitational field. In this process a crucial role is played by the gravitational backreaction as well as by nonlinear effects. This can be seen from the inset in Fig. 4.23, where we show the forces $\bar{F}_N$ (dotted curve) and $\bar{F}_M$ (dashed curve) which are of the order of unity in the relevant region, thence tremendously different from $\bar{F}_{\text{eff}}$. Increasing ξ_{GM} further above 8 leads to a further dramatic increase in the compression of the boson star and the effective force, signaling gravitational instability and formation of a black hole. While we have here managed to form a fine black hole mimicker, the prize was a tuning in the parameters. Namely, for each choice of the coupling there is a critical value of the nonminimal coupling ξ_{GM}, above which a black hole forms, and below which a highly compact object forms with properties close to a black hole.
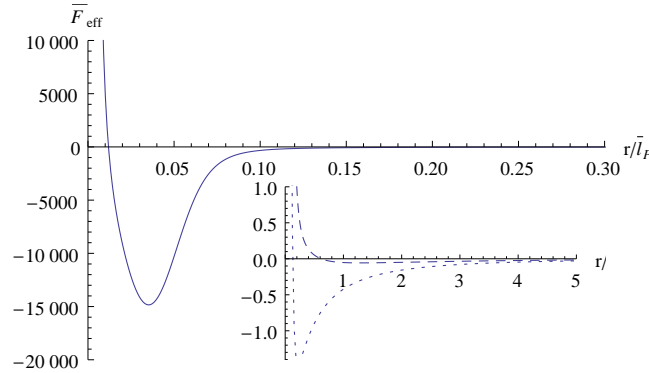

Figure 4.23. *Effective force (D.12) of the combined system of the boson star and the global monopole. Inset: Newtonian force (dotted curve) and the Newtonian force produced by the core mass function (dashed curve). The parameters are: $\sigma_0 = 0.05$, $\lambda_{\text{BS}} = 0$, $\xi_{\text{BS}} = -4$, $\lambda_{\text{GM}} = 0.1$, $\Delta = 0.11$, $\xi_{\text{GM}} = 8$. Also the angular momentum and the xenergy (of the particle) per unit mass are $\bar{L} = 0.1$ and $\bar{E} = 1$.*

4.3   Conclusions and discussion

In this chapter we have considered compact objects composed of nonminimally coupled boson stars and nonminimally coupled monopoles. Three distinct regimes have been identified: weak, mild and strong coupling regimes. The main parameter that determines the regime is the nonminimal coupling of the global monopole.

In the weak coupling regime (when, *e.g.*, $\xi_{\mathrm{GM}} = -1$) nonlinear gravitational effects and the gravitational backreaction are weak, and the resulting compact object can be obtained by summing the energy densities and pressures of the components.

In the mild coupling regime (when, *e.g.*, $\xi_{\mathrm{GM}} = 2$) we have seen that the nonlinear effects and the effects of gravitational slip are present and the resulting object behaves as a boson star with a larger compression and thus with a larger compactness.

In the strong coupling regime, however, (when, *e.g.*, $\xi_{\mathrm{GM}} \gtrsim 5$), a large compression of the composite object takes place such that when $\xi_{\mathrm{GM}} \sim 8$ one can get a highly compact object with the maximum compactness of the order unity. This object represents a good black hole mimicker in that, up to distances close to the black hole event horizon, the compactness profile of the mimicker follows closely that of the black hole. For even larger values of ξ_{GM} we do not get stable configurations. We interpret it as a signal for black hole formation.

It would be of interest to investigate the stability of these highly compact and dense objects, and $M(R)$ stability analysis seems a natural method. We wish to point out that the stability analysis needs to be done with care, since boson stars get largely compressed in the presence of a global monopole, and increasing the boson star mass may lead to a more compact but still stable object. A naive application of $M(R)$ method would suggest instability, while in reality the object may be stable. These thoughts suggest not only the need for a proper stability analysis, but also that it may require a nontrivial modification of standard methods. The result of the last subsection in this chapter indicates that it is the global monopole that stabilizes the monopole-boson star composite system against collapse. Recall that global monopoles are classical field configurations stabilized by topology (of the mapping), while boson stars are stabilized by scalar current density, or equivalently by scalar field charge. With this in mind we make the following conjecture:

> *Compact star objects stabilized by a global charge tend to be more stable than those stabilized by a (local) charge density, and hence are better black hole mimickers.*

In addition to performing a detailed stability analysis, it would be useful to perform a detailed analysis to what extent are the objects composed of a

global monopole and a boson star good black hole mimickers. Here we have only compared in some detail the compactness profiles of the mimickers with those of a true black hole. But of course, there are further comparisons one should investigate, and these include: a detailed comparison of bound (stable and unstable) orbits; the creation and emission of gravitational waves in binary star systems (in which one or two companions is a black hole mimicker); vibrational modes (*i.e.* modes that govern deviations from spherical symmetry) and their decay rates, *etc.* Once such studies are complete we will have a much better idea on to what extent the dense compact objects considered in thesis are good black hole mimickers.

CHAPTER 5

CONCLUSIONS

We have started our journey with a non-perfect-fluid picture of a continuous picture gravastar. This particular dark energy star, due to its large compactness (which is of the order unity) served as a major guideline in building highly compact astrophysical structures. Such a large compactness in gravastars was attributed to the locally negative anisotropic pressures (exhibiting the de Sitter-like core), responsible for the balance of a large amount of matter thus avoiding gravitational collapse. Even though all models describing gravastars are essentially toy models in the sense that their foundation does not stem from fundamental field-theoretic principles, we have shown that all equations of state characterizing gravastar-like objects lead to a radially stable structures (of course with restrictions set on the parameter space). This analysis has been performed rigorously using conventional Chandrasekhar's methods and an eigenvalue problem for the perturbed system (obtained by the linearization of the Einstein equations) has been solved in order to prove radial stability of gravastar configurations. Along with the large compactness, this result motivated search for the akin structures, stemming from the more fundamental Lagrange principle.

One of the most prominent examples of compact object that arose from the fundamental Lagrangian formalism, as a gravitationally bound self-interacting scalar field, is certainly the boson star. It has been known for a while that the concept of anisotropy, which in standard astrophysics has been treated with a great care, is a rather genuine ingredient of the boson star. Besides, it has

been shown that the compression can be quite large (with the compactness up to $\mu_{\max} = 0.32$). However, the de Sitter-like interior does not exist in this setting thus limiting the compactness. For all these reasons in this work we have extended the analysis of boson stars by modifying the Einstein-Hilbert action with a nonminimal coupling of the scalar field to gravity via the Ricci curvature scalar. We have shown that even such a benign extension of classical general relativity already resulted in configurations that resembled more the dark energy stars then the known boson stars. We have also shown that the compactness become significantly larger (up to $\mu_{\max} = 0.50$), and this occurs in the region of negative pressures. Again we could conclude that the scalar field is more compressed in the presence of negative pressures, which obviously helps balance scalar matter against the gravitational collapse. However, within this setting the modified boson star could not approximate xthe black hole configurations arbitrarily close as, we presume, the de Sitter core could not be attained. Besides, the energy conditions are significantly violated in the modified boson star unlike the ordinary boson stars. When we have employed restrictions on matter from the energy conditions we have found that the largest compactness in such a setting was only slightly greater then that in the ordinary boson stars. However, this happens in the region of negative pressures thus again supporting the idea to search for field-theoretic configurations with the de Sitter (like) interior. Instead of "modifying gravity even more", we chose to investigate (modified) boson stars in the presence of gravitationally repulsive global monopole.

Global monopoles are also extensively studied configurations in the context of topological defects and their existence has been tested by modern cosmological observations. Within the framework of general relativity it has been shown that the monopole produces repulsive gravitational effects. This behavior was only locally opposite if the monopole is coupled to gravity nonminimally via the Ricci curvature scalar. Even though the global monopoles which are nonminimally coupled to gravity were considered by other authors in order to prove the existence of bound orbits, a detailed analysis according to which it is possible to trace nonlinear gravitational effects, backreaction of the metric on the matter and the gravitational slip (difference between Newtonian potentials) is lacking. Therefore, in this thesis we have performed an analysis of the effective force which includes all three effects, the linearized Newtonian force which includes the backreaction

of the metric on matter and the Newtonian force produced by the core mass which includes nonlinear effects. An important result of this analysis, in terms of compact objects, was that, independently of the strength of the nonminimal coupling, the global monopole always generates repulsive gravity asymptotically. In this sense it seemed hard to "perceive" a nonminimal global monopole as a viable astrophysical structure on its own.

For these reasons we have coupled a boson star and a global monopole (gravitationally) into one system. We have found three distinct regimes: weak, mild and strong coupling regimes. In the weak coupling regime all three forces are in a qualitative agreement and the resulting compact object arise as a linear combination of its constituents. In the mild coupling regime all three effects are present yielding configurations that behave like a boson star with a larger compression and hence with a larger compactness. In the strong coupling regime, all features from the mild coupling regime are also present but amplified. In this regime a large compression takes place, with maximum compactness slightly above 0.75, and the resulting object represents a good black hole mimicker - that is, up to distances close to the event horizon of a black hole the compactness profile of the mimicker follows closely that of a black hole. When we try to increase the compactness even more we did not get stable configurations which we interpret as a signal for the black hole formation.

The main results of the thesis are as follows:

- a method for testing linear stability of the anisotropic structures with the de Sitter interior is proposed and applied to the gravastar-like objects proving their stability,

- a field-theoretic model for a compact object exhibiting dark energy-like star behaviour is found in modified gravity by means of self-interacting scalar field which is nonminimally coupled to gravity by virtue of the Ricci curvature scalar,

- a field-theoretic model for a highly compact object that mimicks a black hole is found for the combined system of a boson star and a global monopole which are nonminimally coupled to gravity.

Even though some of the issues concerning compact objects have been resolved in this thesis, there are many open, interesting questions that I would like to investigate. Here are some of them:

- Study nonminimally coupled global monopoles with a shell of Dirac fermions. While in the case of bosons the scalar charge is a stabilizing factor, in the case of fermions it will be the Pauli principle, which is automatically embedded into the Dirac equation.

- Study other modifications of gravity that are not at odds with the Ostrogradsky theorem, *i.e.* the corresponding equations of motion contain just two time derivatives. Examples of such theories include the scalar field coupled to the Gauss-Bonnet term, and a coupling to the Einstein curvature tensor.

- Construct a cosmological model that contains many randomly dispersed global monopoles per Hubble volume. I expect that the deficit angle will on large scales generate an average positive spatial curvature. This model can be then put to test against modern cosmological observations.

- Study the observables that could tell compact objects from black holes. Examples of such observables are (a) radial excited states and their decay times; (b) nonspherical vibrational modes and their decay rates; (c) gravitational waves emitted by slightly nonspherical compact stellar objects or by binary systems in which one or both components comprise compact objects. Compare these results with those of standard compact stars such as neutron stars and black holes.

- Study if quantum fluctuations can antiscreen the black hole singularities (see *e.g.* Refs. [109, 110]).

APPENDIX A

CONVENTIONS AND THE TOV EQUATION

In this thesis we work in the spherical symmetry with the coordinates

$$x^\mu = (t, r, \theta, \varphi). \tag{A.1}$$

For the spherically symmetric space-time we use

$$ds^2 = -e^\nu dt^2 + e^\lambda dr^2 + r^2 d\theta^2 + r^2 \sin^2\theta d\varphi^2, \tag{A.2}$$

where in general $\nu = \nu(r,t)$ and $\lambda = \lambda(r,t)$. For this metric, the nonvanishing Christoffel symbols defined as

$$\Gamma^\alpha_{\mu\nu} = \frac{1}{2}g^{\alpha\beta}(\partial_\nu g_{\beta\mu} + \partial_\mu g_{\beta\nu} - \partial_\beta g_{\mu\nu}) \tag{A.3}$$

are

$$\Gamma^r_{rr} = \frac{\lambda'}{2}, \qquad \Gamma^t_{tr} = \frac{\nu'}{2}, \qquad \Gamma^\theta_{\varphi\varphi} = -\sin\theta\cos\theta, \qquad \Gamma^t_{rr} = \frac{\dot\lambda}{2}e^{\lambda-\nu},$$

$$\Gamma^r_{\theta\theta} = -re^{-\lambda}, \qquad \Gamma^r_{tt} = \frac{\nu'}{2}e^{\nu-\lambda}, \qquad \Gamma^\theta_{r\theta} = \Gamma^\varphi_{r\varphi} = \frac{1}{r}, \qquad \Gamma^\varphi_{\theta\varphi} = \cot\theta,$$

$$\Gamma^t_{tt} = \frac{\dot\nu}{2}, \qquad \Gamma^r_{tr} = \frac{\dot\lambda}{2}, \qquad \Gamma^r_{\theta\theta} = -r\sin^2\theta e^{-\lambda}. \tag{A.4}$$

The non-zero components of the Einstein tensor are

$$G^t_t = -e^{-\lambda}\left(\frac{\lambda'}{r} - \frac{1}{r^2}\right) - \frac{1}{r^2}, \tag{A.5}$$

$$G^r_r = e^{-\lambda}\left(\frac{\nu'}{r} + \frac{1}{r^2}\right) - \frac{1}{r^2}, \tag{A.6}$$

$$G^r_t = e^{-\lambda}\frac{\dot{\lambda}}{r}, \tag{A.7}$$

$$G^\theta_\theta = G^\phi_\phi = \frac{1}{2}e^{-\lambda}\left(-\frac{\nu'\lambda'}{2} - \frac{\lambda'}{r} + \frac{\nu'}{r} + \frac{\nu'^2}{2} + \nu''\right)$$
$$-\frac{1}{2}e^{-\lambda}\left(\ddot{\lambda} + \frac{\dot{\lambda}^2}{2} - \frac{\dot{\lambda}\dot{\nu}}{2}\right). \tag{A.8}$$

Tolman-Oppenheimer-Volkoff (TOV) equation for an anisotropic fluid can be obtained i) directly from Einstein equations or ii) from the conservation of the energy-momentum tensor. Conservation of the energy-momentum tensor yield

$$0 = T^\nu_{\mu\,;\nu} = \frac{1}{\sqrt{-g}}\frac{\partial T^\nu_\mu\sqrt{-g}}{\partial x^\nu} - \frac{1}{2}\frac{\partial g_{\nu\delta}}{\partial x^\mu}T^{\nu\delta}, \tag{A.9}$$

or in other "words":

$$\partial_t T^t_\mu + \partial_r T^r_\mu + \partial_\theta T^\theta_\mu + \partial_\varphi T^\varphi_\mu + \frac{\dot{\nu} + \dot{\lambda}}{2}T^t_\mu + \left(\frac{\nu' + \lambda'}{2} + \frac{2}{r}\right)T^r_\mu + \cot\theta T^\theta_\mu$$
$$-\frac{\dot{\nu} + \nu'}{2}T^t_t - \frac{\dot{\lambda} + \lambda'}{2}T^r_r - \frac{1}{r}T^\theta_\theta - \frac{1}{r}T^\varphi_\varphi - \cot\theta T^\varphi_\varphi = 0. \tag{A.10}$$

If we assume now that the energy-momentum tensor depends on t and r only and that the only non-vanishing non-diagonal elements are in $t - r$ direction, we obtain

$$\dot{T}^t_t + \dot{T}^t_r + T^{r\prime}_t + T^{r\prime}_r + \frac{\dot{\nu} + \dot{\lambda}}{2}T^t_r + \frac{\dot{\lambda}}{2}(T^t_t - T^r_r) + \left(\frac{\nu' + \lambda'}{2} + \frac{2}{r}\right)T^r_t$$
$$+\frac{\nu'}{2}(T^r_r - T^t_t) + \frac{2}{r}\left(T^r_r - \frac{1}{2}T^\theta_\theta - \frac{1}{2}T^\varphi_\varphi\right) = 0. \tag{A.11}$$

Tolmann-Oppenheimer-Volkoff equation is obtained from the above equation if we insert the energy-momentum tensor for the anisotropic fluid

$$T_\mu^\nu = \mathrm{diag}(-\rho(r), p_r(r), p_t(r), p_t(r)) \tag{A.12}$$

and for the static metric (*i.e.* $\dot{\nu} = 0 = \dot{\lambda}$), yielding:

$$p_r' = -\frac{1}{2}(\rho + p_r)\nu' + \frac{2}{r}(p_t - p_r). \tag{A.13}$$

APPENDIX B

ENERGY CONDITIONS

Various energy conditions have been proposed as reasonable physical restrictions on matter fields. They originate from the Raychaudhuri equation together with the requirement that gravity should be attractive (see *e.g.* Refs. [22, 51, 68]). When translated to the energy momentum tensor for an anisotropic matter they read

$$\text{The Weak Energy Condition (WEC)} \qquad \rho \geq 0, \quad \rho + p_r \geq 0, \quad \rho + p_t \geq 0,$$
$$\text{The Dominant Energy Condition (DEC):} \qquad \rho - p_r \geq 0, \quad \rho - p_t \geq 0,$$
$$\text{The Strong Energy Condition (SEC):} \qquad \rho + p_r + 2p_t \geq 0. \qquad \text{(B.1)}$$

The weak energy condition imposes the requirement of a positive energy density measured by any observer. Also the energy density plus pressures in any direction needs to be positive. The dominant energy condition requires that the pressures of the fluid do not exceed the energy density, so that the local sound speed in any observable fluid is always less then the speed of light in vacuum. The strong energy condition has very interesting implications. Its violation lead to regions of repulsive gravity such as in cosmological inflation and gravastars. Hence it is reasonable to require that the WEC and DEC are satisfied by a fluid, but that the SEC may be violated.

APPENDIX C

NEWTONIAN LIMIT OF THE EINSTEIN EQUATIONS

In the Newtonian limit, *i.e.* for $c \to \infty$, the metric line element is given with (see *e.g.* Ref. [111])

$$ds^2 = -(1 + 2\phi_N)dt^2 + d\vec{r}^2, \tag{C.1}$$

where ϕ_N is the Newtonian potential. From the Einstein equation

$$G_\mu^\nu = R_\mu^\nu - \frac{1}{2}g_\mu^\nu R = 8\pi G_N T_\mu^\nu \tag{C.2}$$

we can express Ricci scalar R in terms of the energy-momentum scalar T via the trace equation

$$R = -8\pi G_N T \tag{C.3}$$

leading to another form of the Einstein equations

$$R_\mu^\nu = 8\pi G_N \left(T_\mu^\nu - \frac{1}{2}g_\mu^\nu T \right). \tag{C.4}$$

For the given metric (C.1) the only non-vanishing component of the Riemann tensor is R_0^0, thus we have only one Einstein equation in the Newtonian limit

$$R_0^0 = 4\pi G_N (T_0^0 - T_i^i). \tag{C.5}$$

99

Inserting (C.1) in the formula for the Riemann tensor we arrive at

$$R_{00} = -\frac{\partial \Gamma^\alpha_{00}}{\partial x^\alpha} = \Delta \phi_N. \tag{C.6}$$

If we now recall that the energy-momentum tensor for the anisotropic fluid is

$$T^\nu_\mu = \text{diag}(-\rho, p_r, p_t, p_t) \tag{C.7}$$

we arrive at the Poisson equation for the Newtonian potential

$$\Delta \phi_N = 4\pi G_N (\rho + \sum p_i). \tag{C.8}$$

If we now use the following identity ($\phi_N = \phi_N(r)$):

$$\Delta \phi_N = \frac{1}{r^2} \left(r^2 \phi'_N \right)', \tag{C.9}$$

where primes denote derivatives with respect to r, it follows that the Newtonian force is

$$F_N = -\phi'_N = -\frac{1}{r^2} \int_0^r 4\pi G_N (\rho + \sum p_i) \tilde{r}^2 d\tilde{r}. \tag{C.10}$$

Comparing this expression with the standard Newton law, we can read off the *active gravitational mass*

$$M(r) = 4\pi \int_0^r (\rho + \sum p_i) \tilde{r}^2 d\tilde{r}. \tag{C.11}$$

The Newtonian force felt by a test particle with an angular momentum (per unit mass) L is:

$$F_N = -\frac{M(r)}{r^2} + \frac{L^2}{r^3}, \tag{C.12}$$

where $M(r)$ is the active gravitational mass given with the Eq. (C.11).

The geodesic equation

$$\frac{d^2x^\mu}{d\tau^2} + \Gamma^\mu_{\alpha\beta}\frac{dx^\alpha}{d\tau}\frac{dx^\beta}{d\tau} = 0 \tag{D.1}$$

in the metric

$$ds^2 = -e^\nu dt^2 + e^\lambda dr^2 + r^2(d\theta^2 + \sin^2\theta d\varphi^2) \tag{D.2}$$

can be written in terms of its $(x^\mu = t$ and $x^\mu = \varphi)$ components

$$\frac{d^2t}{d\tau^2} + \nu'\frac{dt}{d\tau}\frac{dr}{d\tau} = 0, \tag{D.3}$$

$$\frac{d^2\varphi}{d\tau^2} + \frac{2}{r}\frac{d\varphi}{d\tau}\frac{dr}{d\tau} + 2\frac{\cos\theta}{\sin\theta}\frac{d\theta}{d\tau}\frac{d\varphi}{d\tau} = 0, \tag{D.4}$$

from which we extract the two Killing vectors:

$$K_\mu = (-e^\nu, 0, 0, 0), \tag{D.5}$$

$$F_\mu = (0, 0, 0, r^2\sin^2\theta), \tag{D.6}$$

which lead to the conserved quantities (see *e.g.* [51]):

$$E = -K_\mu\frac{dx^\mu}{d\tau} = e^\nu\frac{dt}{d\tau}, \quad i.e. \quad \frac{d}{d\tau}E = 0, \tag{D.7}$$

$$L = F_\mu\frac{dx^\mu}{d\tau} = r^2\sin^2\theta\frac{d\varphi}{d\tau}, \quad i.e. \quad \frac{d}{d\tau}L = 0. \tag{D.8}$$

Here E is the conserved energy (per unit mass) and L is the conserved angular momentum (per unit mass). Since the direction of the angular momentum is conserved, without loss of generality we can set $\theta = \pi/2$. From the velocity normalization condition $u_\mu u^\mu = -1$ and making use of the conserved quantities E and L we obtain an expression for the radial velocity squared:

$$\left(\frac{dr}{d\tau}\right)^2 = e^{-\nu-\lambda}E^2 - e^{-\lambda}\left(\frac{L^2}{r^2} + 1\right). \tag{D.9}$$

If we rewrite this equation in a slightly different form

$$\frac{1}{2}\left(\frac{dr}{d\lambda}\right)^2 + V_{\text{eff}}(r) = \varepsilon, \tag{D.10}$$

where $\varepsilon = E^2/2$, the effective potential $V_{\text{eff}}(r)$ can be read off:

$$V_{\text{eff}}(r) = \frac{e^{-\lambda}}{2}\left(\frac{L^2}{r^2} + 1\right) + \frac{E^2}{2}\left(1 - e^{-\nu-\lambda}\right). \tag{D.11}$$

The effective force is then

$$F_{\text{eff}} = -\nabla V_{\text{eff}}. \tag{D.12}$$

If the effective potential exhibits a local minimum (node in the effective force) in the radial coordinate then stable bound orbits are possible. If on the other hand, the effective potential has a local maximum (also node in the effective force) then the bound orbits are unstable.

BIBLIOGRAPHY

[1] A.D. Sakharov, Sov. Phys. JETP **22** (1966) 241.

[2] E.B. Gliner, Sov. Phys. JETP **22** (1966) 378.

[3] P.O. Mazur and E. Mottola, "Gravitational Condensate Stars: An Alternative to Black Holes", Proc. Nat. Acad. Sci. **101** (2004) 9545, [arxiv:gr-qc/0109035].

[4] M. Visser and D.L. Wiltshire, "Stable gravastars - an alternative to black holes?", Class. Quantum Grav. **21** (2004) 1135, [arxiv:gr-qc/0310107].

[5] A. DeBenedictis, D. Horvat, S. Ilijić, S. Kloster, and K.S. Viswanathan, "Gravastar solutions with continuous pressures and equation of state", Class. Quantum Grav. **23** (2006) 2303, [arxiv:gr-qc/0511097].

[6] D.J. Kaup, "Klein-Gordon Geon", Phys. Rev. **172** (1968) 1331–1342.

[7] M. Barriola and A. Vilenkin, "Gravitational field of a global monopole", Phys. Rev. Lett. **63** (1989) 341.

[8] P.A.R. Ade *et al.* [Planck Collaboration], arxiv:1303.5085 [astro-ph.CO].

[9] D. Horvat, S. Ilijić and A. Marunović, "Electrically charged gravastar configurations", Class. Quantum Grav. 26 (2009) 025003, [arxiv:gr-qc/0807.2051].

[10] D. Horvat, S. Ilijić and A. Marunović, "Radial stability analysis of the continuous pressure gravastar", Class. Quantum Grav. **28** (2011) 195008, [arxiv:gr-qc/1104.3537].

[11] D. Horvat and A. Marunović, "Dark energy-like stars from nonminimally coupled scalar field", Class. Quantum Grav. **30** (2013) 145006, [arxiv:gr-qc/1212.3781].

[12] B. M. N. Carter, "Stable gravastars with generalized exteriors", Class. Quantum Grav. 22 (2005) 4551, [arxiv:gr-qc/0509087].

[13] F.S.N. Lobo, "Stable dark energy stars", Class. Quantum Grav. **23** (2006) 1525-1541, [arxiv:gr-qc/0508115].

[14] N. Bilić, G.B. Tupper and R.D. Viollier, "Born-Infeld Phantom Gravastars", JCAP **0602** (2006) 013, [arxiv:astro-ph/0503427].

[15] C. Cattoen, T. Faber, and M. Visser, "Gravastars must have anisotropic pressures", Class. Quantum Grav. **22** (2005) 4189, [arxiv:gr-qc/0505137].

[16] I. Dymnikova, "Vacuum nonsingular black hole", Gen. Rel. Grav. **39** (1992) 267-275.

[17] A. DeBenedictis, "Developments in black hole research: clasical, semi-classical, and quantum", Classical and Quantum Gravity Research (2008) 371-462, Nova. Sci. Pub. ISBN 978-1-60456-366-5, [arxiv:gr-qc/0711.2279].

[18] P. Rocha, A.Y. Miguelote, R. Chan, M.F. da Silva, N.O. Santos, and A.Z. Wang, "Bounded excursion stable gravastars and black holes", JCAP **0806** (2008) 025, [arxiv:gr-qc/0803.4200].

[19] R. Garattini, "Wormholes or gravastars?", [arxiv:gr-qc/1001.3831].

[20] S.V. Sushkov and O.B. Zaslavski, " Horizon closeness bounds for static balck hole mimickers", Phys. Rev. D **79** (2009) 067502, [arxiv:gr-qc/0903.1510].

[21] A. DeBenedictis, R. Garattini and F.S.N. Lobo "Phantom stars and topology change", Class. Quantum Grav. **23** (2006) 2303, [arxiv:gr-qc/0511097].

[22] D. Horvat and S.Ilijić, "Gravastar energy conditions revisited", Class. Quantum Grav. **24** (2007) 5637-5649, [arxiv:gr-qc/0707.1636].

[23] F.S.N. Lobo and P. Crawford, "Stability analysis of dynamic thin shells", Class. Quant. Grav. **22** (2005) 4869-4885, [arxiv:gr-qc/0507063].

[24] C.B.M.H. Chirenti and L. Rezzolla, "How to tell a gravastar from a black hole", Class. Quantum Grav. **24** (2007) 4191, [arxiv:gr-qc/0706.1513].

[25] C.B.M.H. Chirenti and L. Rezzolla, "On the ergoregion instability in rotating gravastars", Phys. Rev. D **78** (2008) 084011, [arxiv:gr-qc/0808.4080].

[26] M.E. Gaspar and I. Racz, "Probing the stability of gravastars by dropping dust shells onto them", Class. Quantum Grav. **27** (2010) 185005, [arxiv:gr-qc/1008.0554].

[27] P. Pani, E. Berti, V. Cardoso, Y. Chen and R. Norte, "Gravitational wave signatures of the absence of an event horizon. I. Nonradial oscillations of a thin-shell gravastar", Phys. Rev. D **80** (2009) 124046, [arxiv:gr-qc/0909.0287].

[28] P. Pani, V. Cardoso, M. Cadoni and M. Cavaglia, "Ergoregion instability of black hole mimickers", PoS BHs, GRandStrings 2008:027 (2008), [arxiv:gr-qc/0901.0850].

[29] I. Dymnikova and E. Galaktionov, "Stability of a vacuum non-singular black hole", Class. Quantum Grav. **22** (2005) 2331-2358, [arxiv:gr-qc/0409049].

[30] S. Chandrasekhar, "Dynamical Instability of Gaseous Masses Approaching the Schwarzschild Limit in General Relativity", Phys. Rev. Lett. **12** (1964) 114.

[31] K. Dev and M. Gleiser, "Anisotropic Stars II: Stability", Gen. Rel. Grav. **35** (2003) 1435, [arxiv:gr-qc/0303077].

[32] H. Heintzmann and W. Hillebrandt, "Neutron stars with an anisotropic euation of state: mass, redshift and stability", Astron. Astrophys. **38** (1975) 51.

[33] W. Hillebrandt and K. O. Steinmetz, "Anisotropic neutron star models - Stability against radial and nonradial pulsations", Astron. Astrophys. **53** (1976) 283.

[34] D. Horvat, S. Ilijić and A. Marunović, "Radial pulsations and stability of anisotropic stars with quasi-local equation of state", Class. Quantum Grav. **28** (2011) 025009, [arxiv:gr-qc/1010.0878].

[35] C. W. Misner, K. S. Thorne and J. A. Wheeler, "Gravitation". San Francisco: W.H. Freeman and Co., 1973.

[36] H. Hernandez, L. A. Nunez and U. Percoco, "Nonlocal Equation of State in General Relativistic Radiating Spheres", Class. Quantum Grav. **16** (1999) 871, [arxiv:gr-qc/9806029].

[37] H. Hernandez and L.A. Nunez, "Nonlocal Equation of State in Anisotropic Static Fluid Spheres in General Relativity", Can. J. Phys. **82** (2004) 29, [arxiv:gr-qc/0107025].

[38] J.M. Bardeen, K.S. Thorne and D.W. Meltzer, "A Catalogue of Methods for Studying the Normal Modes of Radial Pulsation of General-Relativistic Stellar Models", Astrophys. J. **145** (1966) 505.

[39] K. D. Kokkotas and J. Ruoff, "Radial oscillations of relativistic stars", Astron. Astrophys. **366** (2001) 565, [arxiv:gr-qc/0011093].

[40] Sergei Yu. Slavyanov and Wolfgang Lay, "Special functions: A unified theory based on singularities", Oxford University Press, Inc., New York, 2000.

[41] T. Singh, G.P. Singh and A. M. Helmi, N. Cim. B **110** (1995) 387.

[42] R. Roy, A.A. Rangwala and N.C. Rana, Indian J. Pure Appl. Math. **27** (1996) 1119.

[43] J. Krishna Rao, M. Annapurna and M.M. Trivedi, Pramana **54** (2000) 215.

[44] L. Herrera and V. Varela, Gen. Rel. Grav. **28** (1996) 663.

[45] Ø. Grøn, Gen. Rel. Grav. **18** (1986) 591.

[46] V. Varela, Gen. Rel. Grav. **39** (2007) 267, [arxiv:gr-qc/0604108].

[47] L. Herrera and J. Ponce de León, J. Math. Phys. **26** (1985) 2302.

[48] S. Ray and S. Bhadra, Phys. Lett. A **322** (2004) 150, [arxiv:gr-qc/0212119].

[49] F.I. Cooperstock and V. de La Cruz, Gen. Rel. Grav. **9** (1978) 835.

[50] J. Ponce de Leon, Gen. Rel. Grav. **25** (1993) 1123.

[51] S. Carroll, "Spacetime and Geometry: An Introduction to General Relativity", Addison Wesley, New York, 2004.

[52] M. Colpi, S.L. Shapiro and I. Wasserman, "Boson Stars: Gravitational Equilibria of Self-Interacting Scalar Fields", Phys. Rev. Letters **57** (1986) 2485.

[53] R. Ruffini and S. Bonazzola, "Systems of Self-Gravitating Particles in General Relativity and the Concept of an Equation of State", Phys. Rev. **187** (1969) 1767.

[54] R. Friedberg, T.D. Lee, Phys. Rev. D **16** (1977) 1096.

[55] T.D. Lee and Y. Pang, Phys. Rept. **221** (1992) 251.

[56] P. Jetzer and J.J. van der Bij, "Charged boson stars", Phys. Lett. B **227** (1989) 341-346.

[57] Edward Seidel and Wai-Mo Suen, "Oscillating soliton stars", Phys. Rev. Lett. **66** (1991) 1659–1662.

[58] Steven S. Liebling and Carlos Palenzuela, "Dynamical Boson Stars", Living Rev. Relativity, **15** (2012) 6.

[59] F.E. Schunck and E.W. Mielke, "General relativistic boson stars", Class. Quantum Grav. **20** (2003) R301–R356.

[60] P. Jetzer, "Boson stars", Phys. Rep. **220** (1992) 163–227.

[61] A.R. Liddle and M.S. Madsen, "The Structure and Formation of Boson Stars", Int. J. Mod. Phys. D **1** (1992) 101–143.

[62] E. Seidel and W. Suen, "Formation of solitonic stars through gravitational cooling", Phys. Rev. Lett. **72** (1994) 2516, [arxiv:gr-qc/9309015].

[63] J. Lee and I. Koh, "Galactic halos as boson stars", Phys. Rev. D **53** (1996) 2236-2239, [arxiv:hep-ph/9507385].

[64] F.S. Guzman and T. Matos, "Scalar fields as dark matter in spiral galaxies", Class. Quantum Grav. **17** (2000) L9.

[65] W. Hu, R. Barkana and A. Guzinov, "Cold and fuzzy dark matter", Phys. Rev. Lett. **85** (2000) 1158-1161, [arxiv:astro-ph/0003365].

[66] F.S.N. Lobo, "Stable dark energy stars", Class. Quantum Grav. **23** (2006) 1525-1541, [arxiv:gr-qc/0508115].

[67] C.R. Ghezzi, "Anisotropic dark energy stars", Astrophys. Space Sci. **333** (2011) 437-447, [arxiv:gr-qc/0908.0779].

[68] F. Rahaman, A.K. Yadav, S. Ray, R. Maulick, R. Sharma, "Singularity-free dark energy star", Gen. Rel. Grav. **44** (2012) 107-124, [arxiv:gr-qc/1102.1382].

[69] S.S. Yazadjiev, "Exact dark energy star solution", Phys. Rev. D **83** (2011) 127501, [arxiv:gr-qc/1104.1865].

[70] G. H. Derrick, "Comments on nonlinear wave equations as models for elementary particles", J. Math. Phys., **5** (1964) 1252-1254.

[71] P. Jetzer and D. Scialom, "On the Stability of Real Scalar Boson Stars", [arxiv:gr-qc/9709056].

[72] A. Arbey, J. Lesgourges and P. Salati, "Galactic halos of fluid dark matter", Phys. Rev. D, **68** (2003) 023511, [arxiv:astro-ph/0301533].

[73] A. Arbey, J. Lesgourges and P. Salati, "Quintessential halos around galaxies", Phys. Rev. D, **64** (2001) 123528.

[74] A. Bernal, J. Barranco, D. Alic and C. Palenzuela, "Multistate boson stars", Phys. Rev. D **81** (2010) 044031.

[75] J. Balakrishna, E. Seidel and W. Suen, "Dynamical Evolution of Boson Stars II: Excited States and Self-Interacting Fields", Phys. Rev. D **58** (1998) 104004, [arxiv:gr-qc/9712064].

[76] U. Ascher, J. Christianse and R. D. Russell, "COLSYS: Collocation software for boundary value ODE's", (1978) [http://www.netlib.org/ode/colsys.f].

[77] X. Hernandez, T. Matos, R.A. Sussman and Y. Verbin, "Scalar field "mini-MACHOs": A new explanation for galactic dark matter", Phys. Rev. D **70** (2004) 043357.

[78] J. Barranco and A. Bernal, "Self-gravitating system made of axions", Phys. Rev. D **83** (2011) 043525.

[79] A. Arbey, J. Lesgourges and P. Salati, "Cosmological constraints on quintessential halos", Phys. Rev. **65** (2002) 083514.

[80] M. Gleiser and R. Watkins, "Gravitational stability of scalar matter", Nucl. Phys. B **319** (1989) 733-746.

[81] T.D. Lee and Y. Pang, "Stability of mini-boson stars", Nucl. Phys. B **315** (1989) 477-516.

[82] P. Jetzer, "Stability of charged boson stars", Phys. Lett. B **231** (1989) 433-438.

[83] S.H. Hawley and M.W. Choptuik, "Boson stars driven to the brink of black hole formation", Phys. Rev. D **62** (2000) 104024.

[84] F.S. Guzman, "Evolving spherical boson stars on a 3D cartesian grid", Phys. Rev. D **70** (2004) 044033.

[85] E. Seidel and W. Suen, "Dynamical evolution of boson stars: Perturbing the ground state", Phys. Rev. D **42** (1990) 384-403.

[86] F.V. Kusmartsev, E.W. Mielke and F.E. Schunck, "Gravitational stability of boson stars", Phys. Rev. D **43** (1991) 3895-3901.

[87] F.S. Guzman, "The three dynamical fates of Boson Stars", Revista Mexicana de Fisica **55** (2009) 321-326.

[88] N. Bilić, R.J. Lindebaum, G.B. Tupper and R.D. Viollier, "On formation of degenerate heavy neutrino stars", Phys. Lett. B**515** (2001) 105, [arxiv:astro-ph/0106209].

[89] Jochum J. van der Bij and Marcelo Gleiser,"Stars of bosons with non-minimal energy-momentum tensor," Phys. Lett. B **194** (1987) 482.

[90] A. DeBenedictis and D. Horvat, "On Wormhole Throats in $f(R)$ Gravity Theory", Gen. Rel. Grav. **44** (2012) 2711-2744.

[91] Matt Visser, "Lorentzian Wormholes: from Einstein to Hawking", AIP, New York 1995.

[92] C. Barcelo and M. Visser, "Scalar fields, energy conditions and traversable wormholes", Class. Quant. Grav. **17** (2000) 3843, [arxiv:gr-qc/0003025].

[93] F. Lobo, "Exotic solutions in General Relativity: Traversable wormholes and 'warp drive' spacetimes", Classical and Quantum Gravity Research, 1-78 (2008) Nova Sci. Pub. ISBN 978-1-60456-366-5, [arxiv:gr-qc/0710.4474].

[94] Pau Amaro-Seoanea, Juan Barrancoa, Argelia Bernala and Luciano Rezzolla, "Constraining scalar fields with stellar kinematics and collisional dark matter", JCAP **11** (2010) 002.

[95] U. Nucamendi, M. Salgado and D. Sudarsky, "An alternative approach to the galactic dark matter problem", Phys. Rev. D. **63** (2001) 125016, [arxiv:gr-qc/0011049].

[96] Xin Shi and Xin-zhou Li, "The gravitational field of a global monopole", Class. Quantum Grav. **8** (1991) 761-767, [arxiv:gr-qc/0903.3085].

[97] I. Cho and A. Vilenkin, "Spacetime structure of an inflating global monopole", Phys. Rev. D **56** (1997) 7621-7626, [arxiv:gr-qc:/9708005].

[98] K.A. Bronnikov, B.E. Meierovich and E.R. Podolyak, "Global monopole in General Relativity", J. Exp. Theor. Phys. **95** (2002) 392-403, [arxiv:gr-qc/0212091].

[99] F. Rahaman, M. Kalam, R. Mondal and B. Raychaudhuri, "Global monopole, dark matter and scalar tensor theory", Mod. Phys. Lett. A **22** (2007) 971-976, [arxiv:gr-qc/0607125].

[100] D. Harari and C. Lousto, "Repulsive gravitational effects of global monopoles", Phys. Rev. D **42** (1990) 2626.

[101] Steven L. Liebling, "Static gravitational global monopoles", Phys. Rev. D **61** (2000) 024030, [arxiv:gr-qc:9906014].

[102] Dieter Maison and Steven L. Liebling, "Some remarks on gravitational global monopoles", Phys. Rev. Lett. **83** (1999) 5218-5221, [arxiv:gr-qc/9908038].

[103] J.C.B. Sanchez and L. Perivolaropoulos, "Topological quintessence", Phys. Rev. D **84** (2011) 123516, [arxiv-gr-qc/1110.2587].

[104] U. Nucamendi, M. Salgado and D. Sudarsky, "Nonminimal global monopoles and bound orbits", Phys. Rev. Lett. **84** (2000) 3037.

[105] Li Xin Zhou, Cheng Hong-Bo and Chung-I Kuo, "D-stars as gravitational lenses", Chin. Phys. Lett. **1** (Vol. 18, 2001) 4.

[106] Xin-zhou Li and Xiang-hua Zhai, "Fermion stars with a global monopole", Phys. Lett. B **364** (1995) 212-215.

[107] Xin-zhou Li, Xiang-hua Zhai and Guang Chen, "Boson D-stars", Astroparticle Physics **2** (Vol. 13, 2000) 245-252.

[108] Jia-mu Li and Xin-zhou Li, "Feature of motion around D-stars", Chin. Phys. Lett. **1** (Vol. 15, 1998) 3.

[109] A. Marunović and T. Prokopec, "Time transients in the quantum corrected Newtonian potential induced by a massless nonminimally coupled scalar field", Phys. Rev. D **83** (2011) 104039, [arxiv:gr-qc/1101.5059].

[110] A. Marunović and T. Prokopec, "Antiscreening in perturbative quantum gravity and resolving the Newtonian singularity", Phys. Rev. D **87** (2013) 104027, [arxiv:hep-th/1209.4779].

[111] L.D. Landau and E.M. Lifshitz, The Classical Theory of Fields (Volume 2 of A Course of Theoretical Physics), Pergamon Press 1971.

Uvod

Jedno od najintrigantnijih rješenja Opće Teorije Relativnosti (OTR) u slučaju kada materija poštuje jaki energijski uvjet (v. Dodatak B) su crne rupe. Crne rupe predstavljaju vakuumska stacionarna rješenja Einsteinovih jednadžbi koja posjeduju horizont događaja i singularitet u središtu koji je *sakriven* horizontom događaja. Ovaj fizikalni singularitet je još uvijek neriješen problem obzirom da implicira kontroverzni problem gubitka informacije prema kojem je informacija na horizontu događaja potpuno izgubljena. Principi gubitka informacije su u konfliktu sa standardnim zakonima kvantne fizike – kao posljedica unitarnosti kvantne fizike, informacija o sustavu u jednom trenutku je dovoljna da se odredi informacija o sustavu u bilo kojem drugom trenutku. Uzimajući u obzir sve navedeno, prirodno se nameće pitanje da li je konačno stanje gravitacijskog kolapsa crna rupa ili neki drugi (još uvijek neotkriveni) gusti objekt koji spriječava daljnji kolaps.

Koncept nesingularnog kolapsa datira još od Saharovljevog razmatranja jednadžbe stanja $p = -\rho$ za jako guste fluide [1] te Glinerove pretpostavke da bi ovakvi fluidi mogli predstavljati konačno stanje gravitacijskog kolapsa [2]. Inspirirani ovim idejama, Mazur i Mottola su kreirali gravastar (*gravitational vacuum star* = gravitacijska vakuumska zvijezda) [3]. Gravastar je anizotropni, kompaktni, astrofizički objekt koji se sastoji od de Sitterove jezgre ($p_r(0) = p_t(0) = -\rho(0)$), te se nastavlja na vanjsku Schwarzschildovu metriku izbjegavajući formiranje horizonta događaja. Zbog svoje visoke komapktnosti (omjer mase i radi-

jusa), gravastar vanjskom promatraču nalikuje na crnu rupu te kao takav predstavlja dobru alternativu crnim rupama. S druge pak strane, opažač koji se nalazi u blizini horizonta događaja jasno raspoznaje gravastar od crne rupe budući gravastar, za razliku od crne rupe, ne posjeduje horizont događaja. Ovisno o strukturi, danas razlikujemo dvije vrste gravastara – prva (originalna) realizacija ima ljuskastu strukturu u kojoj su gustoća energije i tlakovi diskretne funkcije radijalne koordinate, dok su u drugoj realizaciji sve navedene funkcije kontinuirane u prostoru.

Glavna tema ove disertacije je studija mikroskopskih modela koji predstavljaju alternativne konfiguracije crnim rupama, tj. istraživanje stabilnih, kompaktnih, astrofizičkih objekata koristeći Lagrangeove principe klasične teorije polja. Najstariji, i ujedno najviše izučavan astrofiziči model baziran na Lagrangeovom formalizmu je bozonska zvijezda, koja predstavlja kompaktni objekt izgrađen od samointeragirajućeg, gravitacijski vezanog, skalarnog polja [6]. Poznato je da bozonske zvijezde u OTR-u posjeduju određena svojstva karakteristična za gravastar, kao što su anizotropija tlakova te relativno velika kompaktnost ($\mu_{\max} = 0.32$). Međutim, neovisno o jakosti samointerakcije, bozonska zvijezda ne može postići proizvoljno veliku kompaktnost i kao takva ne predstavlja dobru alternativu crnoj rupi. Također, principalni tlakovi ne posjeduju de Sitterovu jezgru, tj. tlakovi u središtu zvijezde su pozitivni. Iz navedenih razloga, u ovoj disertaciji proširujemo analizu bozonskih zvijezda tako što modificiramo gravitaciju uvođenjem neminimalnog vezanja skalarnog polja na gravitaciju preko Riccijevog skalara. Pokazuje se da već ova, minimalna, ekstenzija OTR-a rezultira konfiguracijama koje više nalikuju zvijezdama tamne energije (tzv. dark energy stars) nego "običnim" bozonskim zvijezdama. Također, kompaktnost ovakvih konfiguracija je znatno veća ako materija nije ograničena energijskim uvjetima.

Drugi model u klasičnoj teoriji polja koji se istražuje u ovoj disertaciji uključuje globalne monopole [7] te kombinirani sustav bozonske zvijezde i globalnog monopola. Globalni monopoli spadaju u klasu topoloških defekata koji su se 80-ih i 90-ih u kozmologiji proučavali u kontekstu nastajanja velikih struktura u Svemiru. Iako su moderna opažanja u kozmologiji isključila monopole kao glavni uzrok nastajanja struktura, još uvijek ostaje mogućnost da mali dio termalnih fluktuacija u kozmičkom mikrovalnom zračenju dolazi od topoloških defekata. Najjednostavnija realizacija globalnog monopola u teoriji polja uključuje skalarno polje s

(globalnom) $\mathcal{O}(3)$ simetrijom koja se spontano lomi u $\mathcal{O}(2)$ zbog vakuuma. Unutar OTR-a najistaknutije svojstvo globalnog monopola je gravitacijski odbojna massa jezgre. Međutim, kada se gravitacija modificira uvođenjem neminimalnog vezanja, efektivna sila postaje lokalno privlačna, te u tom slučaju imamo kružne orbite čestice u polju monopola. Zbog svih navedenih zanimljivih svojstava globalnog monopola, razumno je istražiti bozonsku zvijezdu u polju monopola. Zaista, pokazuje se da odbojni gravitacijski efekti monopola stabiliziraju bozonsku zvijezdu tako da rezultirajuća konfiguracija ne posjeduje horizont događaja iako ima veliku gustoću energije, velike (i negativne) principalne tlakove, veliku kompaktnost, velik efektivni potencijal te velike lokalne sile. Kao takva, bozonska zvijezda u polju monopola predstavlja ozbiljnu alternativu crnoj rupi.

Gravitacijske vakuumske zvijezde

Radijalna stabilnost gravastara

Nakon originalnog rada Mazura i Mottole, gravastari kao alternativne konfiguracije crnim rupama su privukle dosta pažnje u području teorijske astrofizike, te je nastao niz radova kao rezultat istraživanja različitih svojstava gravastara. Možda najbitnije fizikalno ponašanje koji svaki ozbiljni astrofizički model mora slijediti jest stabilnost na radijalne perturbacije. Uobičajena metoda ispitivanja stabilnosti nekog sustava uključuje praćenje promjene ponašanja nakon uvođenja *male* smetnje u sustav. U našem slučaju, radimo linearizaciju Einsteinovih jednadžbi oko ravnotežnog položaja. Za prostor-vrijeme uzimamo Schwarzschildovu metriku

$$ds^2 = -e^{\nu(r,t)}dt^2 + e^{\lambda(r,t)}dr^2 + r^2 d\theta^2 + r^2 \sin^2\theta d\phi^2, \qquad (D.13)$$

jer želimo da nakon uvođenja smetnje sustav zadrži sfernu simetriju. Tenzor energije-impulsa prikladan za opis gravastara je

$$T_\mu^\nu = (\rho + p_r)u_\mu u^\nu + g_\mu^\nu p_r - l_\mu l^\nu (p_t - p_r) - k_\mu k^\nu (p_t - p_r). \qquad (D.14)$$

Brzina fluida u radijalnom smjeru $\dot{\xi}$ je definirana kao

$$\dot{\xi} \equiv \frac{dr}{dt} = \frac{u^r}{u^t}, \qquad (D.15)$$

pri čemu ξ označava radijalni pomak elementa fluida, $r \rightarrow r + \xi(r, t)$. Slijedimo Chandrasekharovu metodu [30, 31], tj. pretpostavljamo da sve metričke funkcije i funkcije koje opisuju materiju samo *malo* odstupaju od položaja ravnoteže

$$\lambda(r, t) = \lambda_0(r) + \delta\lambda(r, t), \ \nu(r, t) = \nu_0(r) + \delta\nu(r, t), \quad \text{(D.16)}$$

$$\rho(r, t) = \rho_0(r) + \delta\rho(r, t), \ p_r(r, t) = p_{r0}(r) + \delta p_r(r, t), p_t(r, t) = p_{t0}(r) + \delta p_t(r, t), \quad \text{(D.17)}$$

gdje su s "0" su označene ravnotežne funkcije, a $\delta f(r, t)$ su takozvane Eulerove perturbacije, $f \in \{\lambda, \nu, \rho, p_r, p_t, \}$. Eulerove perturbacije mjere lokalni pomak iz ravnoteže dok Lagrangeove perturbacije mjere pomak iz ravnoteže u sustavu fluida – u linearnoj aproksimaciji Lagrangeove perturbacije imaju uloga potpunog diferencijala i s Eulerovima su povezane preko relacije

$$df(r, t) = \delta f(r, t) + f_0'(r)\xi. \quad \text{(D.18)}$$

Linearizacija Einsteinovih jednadžbi $G_{\mu\nu} = 8\pi G_N T_{\mu\nu}$ ($G_N = 1$) vodi na dva skupa jednadžbi: jedan za ravnotežne (statičke) funkcije, te drugi za perturbirane funkcije. Sustav u ravnoteži se opisuje tzv. Tolman-Oppenheimer-Volkoff (TOV) jednadžbom (v. Dodatak A):

$$p_{r0}' = -\frac{1}{2}\left(\rho_0 + p_{r0}\right)\nu_0' + \frac{2}{r}\Pi_0, \quad \text{(D.19)}$$

gdje je $\Pi_0 = p_{t0} - p_{r0}$ anizotropija u tlakovima. Perturbirane funkcije su opisane skupom jednadžbi:
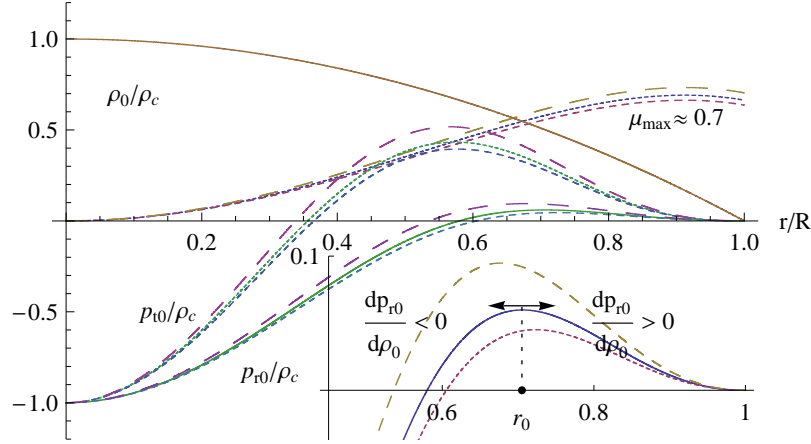
$$\left(re^{-\lambda_0}\delta\lambda\right)' = 8\pi r^2 \delta\rho, \quad \text{(D.20)}$$

$$\delta\nu' = \left(\nu_0' + \frac{1}{r}\right)\delta\lambda + 8\pi re^{\lambda_0}\delta p_r, \quad \text{(D.21)}$$

$$\dot{\delta\lambda}\frac{e^{-\lambda_0}}{r} = -8\pi\dot{\xi}(\rho_0 + p_{r0}), \quad \text{(D.22)}$$

$$e^{\lambda_0-\nu_0}(\rho_0 + p_{r0})\ddot{\xi} + \frac{1}{2}(\rho_0 + p_{r0})\delta\nu' + \frac{1}{2}(\delta\rho + \delta p_r)\nu_0' + \delta p_r' - \frac{2}{r}\delta\Pi = 0. \quad \text{(D.23)}$$

Jednadžba (D.23) je tzv. *pulzacijska jednadžba* koja služi za ispitivanje radijalne stabilnosti sustava. Da bismo riješili ovu jednadžbu, sve perturbirane funkcije se trebaju izraziti preko radijalnog pomaka ξ i ravnotežnih funkcija. Iz Einsteinovih jednadžbi (D.20)-(D.22) slijedi željeni oblik za $\delta\rho$ i $\delta\lambda$, dok se informacija o δp_r i

Slika D.1. *Gustoća energije ρ_0/ρ_c, radijalni tlak p_{r0}/ρ_c, transverzalni tlak p_{t0}/ρ_c i kompaktnost μ_0 kao funkcija r/R za $\{R, n, m\} = \{1, 2, 3\}$. Tri različite vrijednosti centralne gustoće energije $\rho_c = \{0.19, 0.20, 0.21\}$ i njihovih jakosti anizotropije $\beta = \{92.90, 84.77, 76.11\}$ odgovaraju donjoj, srednjoj i gornjoj krivulji, respektivno. r_0 označava radijus na kojem brzina zvuka iščezava (za srednju krivulju).*

$\delta\Pi$ dobiva iz statičkih rješenja.

Statička rješenja za gravastar su opisana diferencijalnom jednadžbom prvog reda (D.19) koja ima tri nepoznanice ρ_0, p_{r0}, p_{t0}. Da bismo riješili danu jednadžbu, slijedimo Ref. [5] te zadajemo gustoću energije i anizotropiju:

$$\rho_0(r) = \rho_c(1 - (r/R)^n), \tag{D.24}$$

$$\Pi_0(r) = \beta\rho_0(r)^m\mu_0(r), \tag{D.25}$$

gdje su n, m (slobodni) parametri, i $\rho_c = \rho_0(0)$ je centralna gustoća energije. β mjeri jakost anizotropije i R je radijus gravastara za koji je $p_{r0}(R) = 0$. $\mu_0(r)$ je kompaktnost definirana kao $\mu_0(r) = 2m_0(r)/r$, gdje je $m_0(r)$ funkcija mase $m_0(r) = 4\pi \int \rho_0(r)r^2dr$. Na Sl. D.1 je prikazano rješenje kontinuiranog modela gravastara. Gustoća energije je pozitivna i monotona. Tlakovi imaju de Sitterovu jezgru, $p_{r0}(0) = p_{t0}(0) = -\rho(0)$. Gravastar također ima atmosferu koja je definirana kao područje u kojem je brzina zvuka, $v_s^2 = dp_{r0}/d\rho_0$, pozitivna. U predstavljenom modelu $\mu_{\max} = 0.7$. Također je vidno da je dominantni energijski uvjet (v. Dodatak B) očuvan.

Koristeći činjenicu da anizotropija ovisi samo o izboru gustoće energije, te

vezu između Eulerovih i Lagrangeovih perturbacija, slijedi

$$\delta p_r = -p'_{r0}\xi + \frac{dp_{r0}(\rho_0)}{d\rho_0}(\delta\rho + \rho'_0\xi), \tag{D.26}$$

$$\delta\Pi = -\Pi'_0\xi + \frac{d\Pi_0[\rho_0]}{d\rho_0}(\delta\rho + \rho'_0\xi), \tag{D.27}$$

gdje je $dp_{ro}(\rho_0)/d\rho_0 = \frac{dp_{ro}/dr}{d\rho_0/dr}$ jer i gustoća energije i radijalni tlak ovise samo o radijalnoj koordinati. Iz (D.19) slijedi

$$\delta\rho = -\rho'_0\xi - (\rho_0 + p_{r0})\frac{e^{\nu_0/2}}{r^2}\left(r^2 e^{-\nu_0/2}\xi\right)' - \frac{2}{r}\Pi_0\xi. \tag{D.28}$$

Kada uvrstimo (D.28) u (D.26) dobivamo perturbaciju za radijalni tlak

$$\delta p_r = -p'_{r0}\xi - (\rho_0 + p_{r0})\frac{dp_{r0}[\rho_0]}{d\rho_0}\frac{e^{\nu_0/2}}{r^2}\left(r^2 e^{-\nu_0/2}\xi\right)' - \frac{2}{r}\Pi_0\frac{dp_{r0}[\rho_0]}{d\rho_0}\xi. \tag{D.29}$$

Da bismo riješili pulzacijsku jednadžbu, koristimo Chandrasekharovu metodu te pretpostavimo da sve metričke funkcije i funkcije materije ovise oscilatorno o vremenu $f(r,t) = e^{i\omega t}f(r)$. Pulzacijska jednadžba sada poprima oblik

$$\mathcal{P}_0\xi'' + \mathcal{P}_1\xi' + \mathcal{P}_2\xi = -\omega^2\mathcal{P}_\omega\xi, \tag{D.30}$$

gdje su $\mathcal{P}_0, \mathcal{P}_1, \mathcal{P}_2$ i $\mathcal{P}_\omega$ polinomi koji ovise o r i statičkim funkcijama. Jednadžba (2.28) predstavlja jednadžbu vlastitih vrijednosti za radijalni pomak ξ (ω^2 je vlastita vrijednost). Rubni uvjeti za ovu jednadžbu su
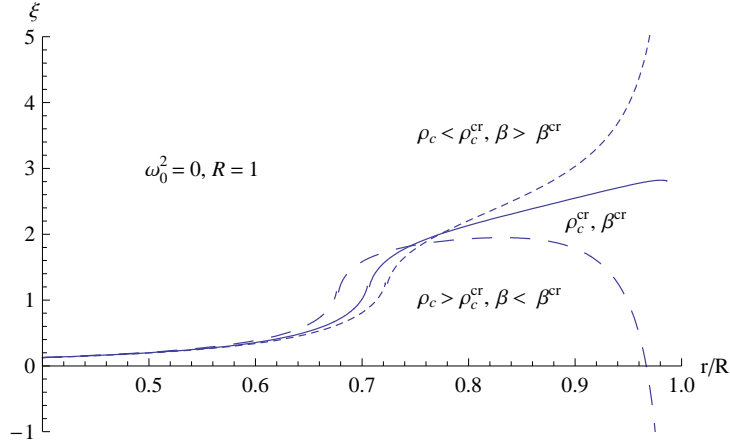
$$\xi = 0 \quad \text{u} \quad r = 0, \tag{D.31}$$

$$\Delta p_r = 0 \quad \text{u} \quad r = R. \tag{D.32}$$

Uz pomoć transformacija

$$\mathcal{P} = e^{\int \mathcal{P}_1/\mathcal{P}_0\,dr} \qquad \text{i} \qquad \mathcal{Q} = \frac{P_2}{P_0}P, \quad \mathcal{W} = \frac{P_\omega}{P_0}\mathcal{P}, \tag{D.33}$$

pulzacijska jednadžba (D.30) se svodi na Sturm-Liouvilleov oblik

$$(\mathcal{P}\xi')' + \mathcal{Q}\xi = -\omega^2\mathcal{W}\xi. \tag{D.34}$$

Slika D.2. *Radijalni pomak $\xi(r)$ za $\{R, n, m\} = \{1, 2, 3\}$ i $\omega^2 = 0$. Tri različite vrijednosti centralne gustoće energije $\rho_c = \{0.19, 0.20, 0.21\}$ i odgovarajuće vrijednosti anizotropije $\beta = \{92.90, 84.77, 76.11\}$ odgovaraju donjoj (nestabilno), srednjoj (granično stabilno) i gornjoj (stabilno) krivulji, respektivno.*

Prema Sturm-Liouvilleovom formalizmu, broj nultočaka od ξ za određeni ω^2 je usko povezan sa stabilnošću sustava: ako za $\omega^2 = 0$, ξ nema nultočke onda je sustav stabilan za sve radijalne modove viših frekvencija; ako pak ξ ima nultočke onda je sustav nestabilan za sve radijalne modove. Za stabilan sustav vrijedi

$$\omega_0^2 < \omega_1^2 < \cdots < \omega_n^2 < \ldots, \tag{D.35}$$

gdje n označava broj nultočaka.

Rješenja i diskusija

S obzirom da je brzina zvuka u gravastaru pozitivna jedino u području gravastarske atmosfere, tj. za $r > r_0$, prilikom ispitivanja radijalne stabilnosti danog sustava, fizikalno je podijeliti cijeli interval na dva dijela: $\mathcal{I}_1 = (0, r_0)$ i $\mathcal{I}_2 = (r_0, R)$. Standardan Sturm-Liouvilleov formalizam se primjenjuje na $\mathcal{I}_2$ dok u $\mathcal{I}_1$ pretpostavljamo da signal eksponencijalno trne budući je brzina zvuka imaginarna.

Ispitivanje stabilnosti bilo kojeg sustava općenito se svodi na traženje graničnih vrijednosti parametara za koji je sustav stabilan. U Sturm-Liouvilleovom formalizmu, granična stabilnost se postiže u slučaju kada je frekvencija fundamentalnog moda ($n = 0$) nula ($\omega_0^2 = 0$). Na Sl. D.2 je prikazan radijalni pomak $\xi(r)$ za $\omega^2 = 0$ za tri različite vrijednosti centralne gustoće energije. Srednja krivu-
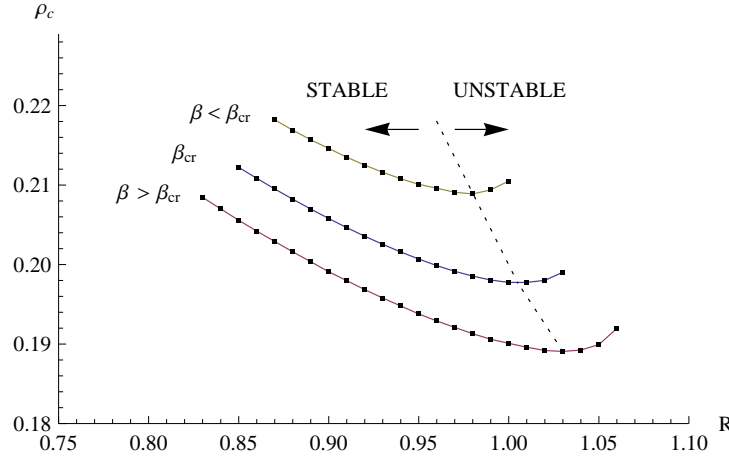
Slika D.3. *Centralna gustoća energije ρ_c u ovisnosti o radijusu R. Za $\{R, n, m\} = \{1, 2, 3\}$ parametar anizotropije $\beta = \{92.90, 84.77, 76.11\}$ je konstantan na svakoj krivulji i fiksiran izborom centralne gustoće energije $\rho_c = \{0.19, 0.20, 0.21\}$ za donju, srednju i gornju krivulju, respektivno. Minimum svake krivulje predstavlja granično stabilne konfiguracije.*

lja odgovara graničnoj stabilnosti, gornja predstavlja stabilnu konfiguraciju jer $\xi(r)$ nema nultočke, dok donja krivulja predstavlja nestabilnu konfiguraciju jer $\xi(r)$ ima nultočke. Izbor parametara odgovara srednjoj, donjoj te gornjoj krivulji na Sl. D.1, respektivno. Na Sl. D.3 je predstavljena krivulja stabilnosti $\rho_c(R)$. Minimumi krivulja odgovaraju graničnoj stabilnosti za određeni parametar anizotropije β. Prilikom povećanja centralne gustoće energije, radijus stabilnih konfiguracija se smanjuje, dok se radijus nestabilnih konfiguracija povećava.

Neminimalne bozonske zvijezde

Iako su gravastarske konfiguracije bazirane na vrlo zanimljivim idejama, svi gravastarski modeli su makroskopski u smislu da njihovi temelji leže u proučavanju Einsteinove teorije za neki fluid koji slijedi fenomenološku jednadžbu stanja, te kao takvi ne počivaju na temeljima teorije polja. Oba modela gravastara, diskontinuirani i kontinuirani, su esencijalno tzv. toy-modeli (toy=igračka) koji su također bitni u proučavanju određenih svojstava gravastara. Međutim, fundamentalno razumijevanje danih objekata je moguće jedino ako ih uspijemo modelirati koristeći mikroskopske principe teorije polja.

Dobar primjer mikroskopskog modela koji sadrži anizotropiju u principalnim tlakovima i relativno veliku kompaktnost je bozonska zvijezda. Bozonske zvijezde su nesingularna rješenja Einstein-Klein-Gordonovog sustava jednadžbi za masivno, kompleksno skalarno polje. Opsežno istraživanje bozonskih zvijezda počelo je s Kaupom [6] koji je razmatrao gravitacijski vezane skalarne čestice. Ruffini i Bonazzola [53] su razmatrali bozonske zvijezde bez samointerakcije dok su efekt samointerakcije uveli u razmatranje Colpi i suradnici [52]. Pokazalo se da iako samointerakcija znatno povećava kompaktnost bozonske zvijezde, anizotropija u principalnim tlakovima je pozitivna, što je u suprotnosti s gravastarima. Iz tog razloga analiza bozonskih zvijezda, u ovoj disertaciji, je proširena uvođenjem neminimalnog vezanja polja na gravitaciju preko Riccijevog skalara. Pokazuje se da čak i ovakva minimalna ekstenzija Einsteinove gravitacije rezultira konfiguracijama koje zbog negativnih tlakova više nalikuju na zvijezde tamne energije nego na "obične" bozonske zvijezde.

Model

Akcija za gravitaciju je standardna Einstein-Hilbertova akcija

$$S_{EH} = \int d^4x \sqrt{-g} \frac{R}{16\pi G_N},$$ (D.36)

gdje je G_N Newtonova konstanta, R je Riccijev skalar, i g je determinantna metričkog tenzora $g_{\mu\nu}$

$$g_{\mu\nu} = \text{diag}(-e^{\nu(r)}, e^{\lambda(r)}, r^2, r^2 \sin^2\theta).$$ (D.37)

Za materiju uzimamo akciju samointeragirajućeg skalarnog polja neminimalno vezanog na gravitaciju

$$S_\phi = \int d^4x \sqrt{-g} \left(-g^{\mu\nu} \partial_\mu \phi^* \partial_\nu \phi - m_\phi^2 \phi^* \phi - \frac{\lambda_\phi}{2}(\phi^*\phi)^2 + \xi R \phi^* \phi \right),$$ (D.38)

gdje je ξ mjera jakosti vezanja skalarnog polja ϕ na gravitaciju, ϕ^* je kompleksno konjugirani ϕ. Tenzor energije-impulsa za kompleksno skalarno polje se dobije

varijacijom akcije po metričkom tenzoru

$$
\begin{aligned}
T_{\mu\nu}^{\phi} &= 2\delta_{(\mu}^{\alpha}\delta_{\nu)}^{\beta}\partial_{\alpha}\phi^{*}\partial_{\beta}\phi - g_{\mu\nu}\left[g^{\alpha\beta}\partial_{\alpha}\phi^{*}\partial_{\beta}\phi + m_{\phi}^{2}\phi^{*}\phi + \frac{1}{2}\lambda_{\phi}(\phi^{*}\phi)^{2}\right] \\
&\quad - 2\xi\phi^{*}\phi G_{\mu\nu} + 2\xi\nabla_{\mu}\nabla_{\nu}(\phi^{*}\phi) - 2\xi g_{\mu\nu}\Box(\phi^{*}\phi).
\end{aligned} \tag{D.39}
$$

Jednadžba gibanja za skalarno polje se dobije varijacijom akcije po ϕ^{*}

$$
\left[\Box - m_{\phi}^{2} - \lambda_{\phi}\phi^{*}\phi + \xi R\right]\phi = 0. \tag{D.40}
$$

Varijacijom ukupne akcije $S = S_{\text{E-H}} + S_{\phi}$ po metričkom tenzoru $g^{\mu\nu}$ dobijemo Einsteinovu jednadžbu

$$
R_{\mu\nu} - \frac{1}{2}g_{\mu\nu}R = 8\pi G_{N}T_{\mu\nu}. \tag{D.41}
$$

Nadalje, biramo oscilatorno polje u vremenu

$$
\phi(r,t) = \phi_{0}(r)e^{-\iota\omega t}, \qquad \phi_{0}(r) \in \mathbb{R}. \tag{D.42}
$$

Da bismo problem riješili numerički zgodno je sve varijable/funkcije izraziti preko bezdimenzionalnih veličina:

$$
\frac{r}{\sqrt{8\pi G_{N}}} \to x, \qquad 8\pi G_{N}\phi_{0}(r)^{2} \to \sigma(r)^{2},
$$
$$
8\pi G_{N}R \to \tilde{R}, \qquad 8\pi G_{N}m_{\phi}^{2} \to \tilde{m}_{\phi}^{2}, \qquad 8\pi G_{N}\omega^{2} \to \tilde{\omega}^{2}. \tag{D.43}
$$

Sada su sve varijable/funkcije izražene u reduciranim Planckovim jedinicama

$$
\begin{aligned}
\bar{m}_{P} &= \sqrt{\frac{\hbar c}{8\pi G_{N}}} = 0.2435 \times 10^{19} \frac{\text{GeV}}{c^{2}} = 0.4341 \times 10^{-8}\ \text{kg}, \\
\bar{l}_{P} &= \sqrt{\frac{\hbar 8\pi G_{N}}{c^{3}}} = 8.1024 \times 10^{-35}\ \text{m}.
\end{aligned} \tag{D.44}
$$

Reskalirane diferencijalne jednadžbe koje rješavamo su

$$\lambda' = \frac{1-e^\lambda}{x} + x\frac{e^\lambda(\tilde{m}_\phi^2 + \tilde{\omega}^2 e^{-\nu} + \frac{\lambda_\phi}{2}\sigma^2)\sigma^2 + (1+4\xi)\sigma'^2 - 2\xi\nu'\sigma\sigma'}{1+2\xi\sigma^2}$$
$$+ \frac{4x\xi e^\lambda(\tilde{m}_\phi^2 - \tilde{\omega}^2 e^{-\nu} + \lambda_\phi\sigma^2 - \xi\tilde{R})\sigma^2}{1+2\xi\sigma^2}, \tag{D.45}$$

$$\nu' = \frac{(e^\lambda - 1)(1+2\xi\sigma^2)/x + xe^\lambda(-\tilde{m}_\phi^2 + \tilde{\omega}^2 e^{-\nu} - \frac{\lambda_\phi}{2}\sigma^2)\sigma^2 + x\sigma'^2 - 8\xi\sigma\sigma'}{1+2\xi\sigma^2 + 2\xi x\sigma\sigma'}, \tag{D.46}$$

$$\sigma'' = -\left(\frac{2}{x} + \frac{\nu' - \lambda'}{2}\right)\sigma' + e^\lambda(\tilde{m}_\phi^2 + \lambda_\phi\sigma^2 - \tilde{\omega}^2 e^{-\nu} - \xi\tilde{R})\sigma, \tag{D.47}$$

s bezdimenzionalnim Riccijevim skalarom

$$\tilde{R} = \frac{2\tilde{m}_\phi^2\sigma^2 + 2(1+6\xi)\left[(\tilde{m}_\phi^2 - \tilde{\omega}^2 e^{-\nu} + \lambda_\phi\sigma^2)\sigma^2 + e^{-\lambda}\sigma'^2\right]}{1+2\xi(1+6\xi)\sigma^2}, \tag{D.48}$$

gdje $'$ označavaju derivacije po x.

Jednadžbe (D.45–D.47) imaju jedinstveno rješenje (koje ovisi o σ_0) za dane rubne uvjete:

$$(1) \quad \lambda(0) = 0, \qquad (2) \quad \nu(\infty) = 0, \qquad (3) \quad \sigma(0) = \sigma_0, \qquad (4) \quad \sigma(\infty) = 0. \tag{D.49}$$

Da bismo problem riješili numerički, potrebno je zadati niz parametara $\{\lambda_\phi, \tilde{m}^2, \tilde{\omega}^2, \xi\}$ reda veličine jedan u reduciranim Planckovim jedinicama. Mi pak znamo da u svim fizikalno zanimljivim situacijama, dani parametri se znatno razlikuju od jedinice. Ovaj problem se rješava tako što prepoznamo da su bezdimenzionalne jednadžbe (D.45–D.48) invarijantne na 'konformnu' transformaciju

$$x \to \beta x, \quad \lambda \to \frac{\lambda}{\beta^2}, \quad \tilde{R} \to \frac{\tilde{R}}{\beta^2}, \quad \tilde{m}^2 \to \frac{\tilde{m}^2}{\beta^2}, \quad \tilde{\omega}^2 \to \frac{\tilde{\omega}^2}{\beta^2}, \quad \sigma \to \sigma, \quad \xi \to \xi. \tag{D.50}$$

Također slijedi

$$M \overset{\sim}{\to} \beta M. \tag{D.51}$$

Na ovaj način možemo generirati astrofizičke objekte različitih veličina: od jako malih kompaktnih objekata do jako velikih (galaktičkih) haloa tamne materije.
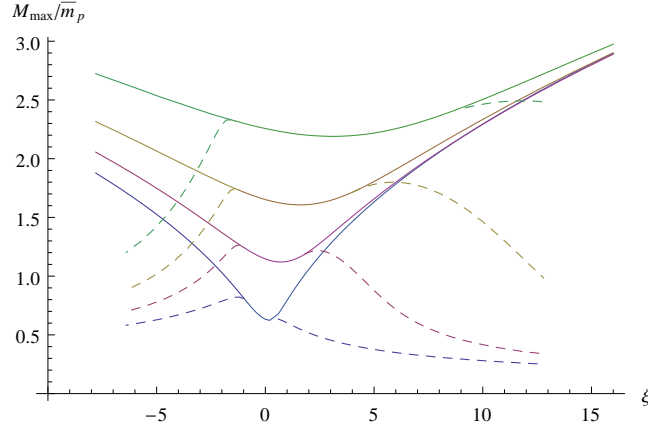
Slika D.4. *Maksimalna masa kao funkcija ξ za $\lambda_\phi = \{0, 20, 50, 100\}$ od dole prema gore. Isprekidane krivulje za $\xi < 0$ opisuju konfiguracije koje poštuju slabi energijski uvjet i za $\xi > 0$ konfiguracije koje poštuju dominantni energijski uvjet. Pune krivulje opisuju konfiguracije koje nisu ograničene energijskim uvjetima. Također $m_\phi^2 = \bar{m}_P^2$.*

Zvijezde tamne energije - efekt neminimalnog vezanja

U slučaju minimalnog vezanja polja na gravitaciju, anizotropija je

$$\Pi = p_t - p_r = -2e^{-\lambda}\phi_0'^2. \tag{D.52}$$

Komponente tenzora energije-impulsa, općenito, za anizotropni fluid su

$$T_\mu^\nu = \text{diag}(-\rho, p_r, p_t, p_t), \tag{D.53}$$

gdje je ρ gustoća energije, p_r je radijalni i p_t je transverzalni tlak ($p_t = p_\theta = p_\phi$). Iz (D.52) sada eksplicitno vidimo da je anizotropija isključivo negativna funkcija radijalne koordinate, iz čega direktno slijedi da se u minimalnom vezanju ne mogu konstruirati strukture s $p_r > p_t$ kao što je to slučaj kod gravastara. Za $\xi \neq 0$, anizotropija poprima oblik:

$$\begin{aligned}
\Pi &= -2e^{-\lambda}\phi_0'^2 - 2\xi(G_\theta^\theta - G_r^r)\phi_0^2 + 2\xi e^{-\lambda}\left(\nu' + \frac{4}{r}\right)\phi_0\phi_0' \\
&- 4\xi\left(m_\phi^2 + \lambda_\phi\phi_0^2 - \omega^2 e^{-\nu} - \xi R\right)\phi_0^2. \tag{D.54}
\end{aligned}$$

Kao što je spomenuto ranije u tekstu, uvođenjem neminimalnog vezanja Π može postati pozitivna za određene radijalne koordinate, što je jako važno svojstvo pri
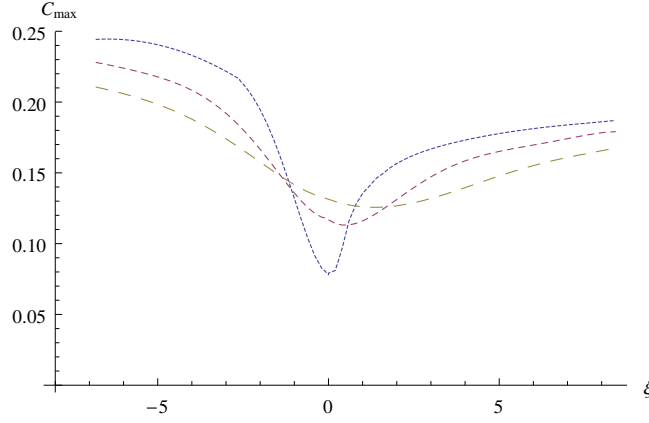
Slika D.5. *Efektivna kompaktnost kao funkcija parametra ξ za $\lambda_\phi = 0$ (točkasta krivulja), $\lambda_\phi = 20$ (kratko-isprekidana krivulja) i $\lambda_\phi = 50$ (dugo-isprekidana krivulja). Takođ̵er $m_\phi^2 = \bar{m}_P^2$.*

kreiranju mikroskopskih objekata s negativnim tlakovima.

Rješenja i diskusija

Kada modeliramo sferno-simetrične, lokalizirane konfiguracije materije, energijski uvjeti (v. Dodatak B) predstavljaju bitan kriterij za fizikalno prihvatljivu materiju. Za $\xi \neq 0$ proizlazi da su slabi i dominantni energijski uvjeti narušeni. Efekt nepoštivanja danih energijskih uvjeta zapisan je u krivulji $\tilde{M}_{\max}(\xi)$ prikazanoj na Sl. D.4 isprekidanim linijama, gdje se $\tilde{M}_{\max}$ za dani ξ dobije kao maksimum u krivulji $\tilde{M}(\sigma_0)$ (lijevo od maksimuma u $\tilde{M}(\sigma_0)$ su stabilne, a desno nestabilne konfiguracije).

Da bismo odredili područje najveće kompaktnosti, definiramo tzv. efektivnu kompaktnost [94]

$$C(\sigma_0, \lambda_\phi) = \frac{M_{99}(\sigma_0, \lambda_\phi)}{R_{99}}, \tag{D.55}$$

gdje je R_{99} radijus na kojem je masa zvijezde jednaka 99% ukupne mase M ($M = m(\infty)$). Kompaktnost je $\mu = 2C$. Na Sl. D.5 je prikazana efektivna kompaktnost u ovisnosti o ξ za tri različite vrijednosti parametra samointerakcije $\lambda_\phi = 0, 20, 50$. Vidimo da se maksimalna kompaktnost postiže u području negativnih ξ tako da $\mu_{\max} \approx 0.5$. Međutim, kada uzmemo u obzir valjanost energijskih uvjeta, efektivna kompaktnost se smanjuje što je prikazano na Sl. D.6, te dostiže svoju maksimalnu vrijednost u području negativnih ξ i nešto je veća od maksimalne
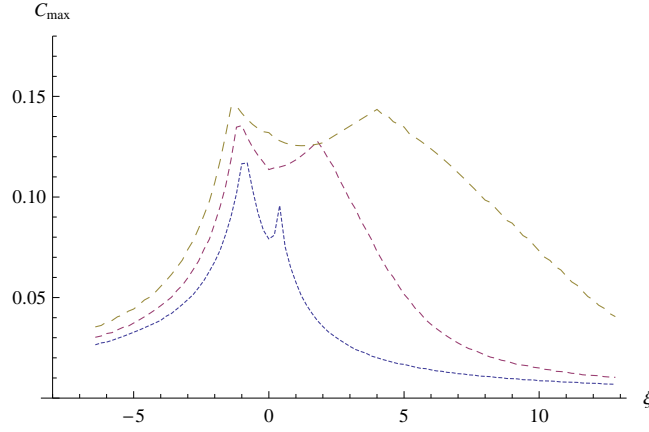
Slika D.6. _Efektivna kompaktnost u ovisnosti o ξ za konfiguracije koje poštuju slabi i dominantni energijski uvjet. $\lambda_\phi = 0$ (točkasta krivulja),$\lambda_\phi = 20$ (kratko-isprekidana krivulja) i $\lambda_\phi = 50$ (dugo-isprekidana krivulja). Također $m_\phi^2 = \bar{m}_P^2$._

kompaktnosti kod običnih bozonskih zvijezda za koje je $\mu_{\max} \approx 0.32$.

Kada promotrimo kako se ponašaju gustoće energije i tlakovi, proizlazi da su principalni tlakovi upravo u području najveće kompaktnosti negativni. Primjer jedne ovakve konfiguracije je dan na Sl. D.7. Jaki energijski uvjet, kao signal odbojne gravitacije, je, nažalost, očuvan za sve ξ.
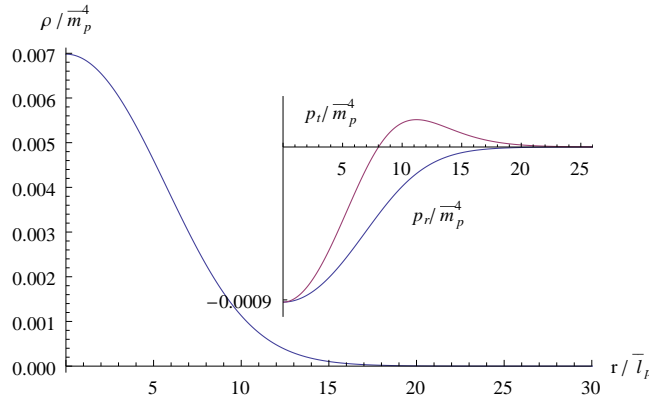
Slika D.7. _Gustoća energije i principalni tlakovi (umetak) za $m_\phi^2 = \bar{m}_P^2$, $\xi = -4$, $\{\lambda_\phi, \sigma_c\} = \{0, 0.050\}$._

Međutim, iako se za negativnu vrijednost parametra samointerakcije mogu pronaći konfiguracije koje blago narušavaju jaki energijski uvjet, ovakva rješenja su generički nestabilna. Također je moguće pronaći konfiguracije s pozitivnim

tlakovima, no one se postižu za pobuđena stanja skalarnog polja koja generiraju oscilatorne funkcije gustoće energije i tlakova, prilikom čega dolazi do narušenja slabog energijskog uvjeta.

Neminimalne bozonske D-zvijezde

Neminimalni globalni monopol

Globalni monopoli, uz kozmičke strune, domenske zidove i kozmičke teksture, spadaju u klasu topoloških defekata koji nastaju spontanim lomljenjem simetrije pri faznom prijelazu u ranom Svemiru. Standardan primjer globalnog monopola je teorija polja koja se sastoji od tri realna skalarna polja čija je akcija $\mathcal{O}(3)$ simetrična, te se termalno induciranim faznim prijelazom lomi u $\mathcal{O}(2)$. Barriola i Vilenkin [7] su prvi razmatrali globalni monopol u gravitaciji. Nadalje su Lousto i suradnici [100] pokazali da globalni monopol ima odbojne gravitacijske efekte. Nucamendi i suradnici [104] su uveli neminimalno vezanje polja na gravitaciju kako bi pokazali postojanje stabilnih kružnih orbita u polju monopola.

Model neminimalnog globalnog monopola

Akcija za globalni monopol koji je neminimalno vezan na gravitaciju je

$$S_\phi = \int d^4x \sqrt{-g}\left(-\frac{1}{2}g^{\mu\nu}(\partial_\mu\phi^a)(\partial_\nu\phi^a) - V(\phi^a) + \frac{1}{2}\xi R(\phi^a\phi^a)\right), \qquad \text{(D.56)}$$

gdje je ϕ^a, $a = 1, 2, 3$, triplet skalarnog polja s globalnom $\mathcal{O}(3)$ simetrijom koja je spontano slomljena u $\mathcal{O}(2)$. Potencijal koji lomi simetriju je

$$V(\phi^a) = \frac{\mu^2}{2}\phi^a\phi^a + \frac{\lambda_\phi}{4}(\phi^a\phi^a)^2 + \frac{\mu^4}{4\lambda_\phi}, \qquad \text{(D.57)}$$

pri čemu je μ maseni član monopola i λ_ϕ je jakost samointerakcije. Veličina ξ mjeri jakost vezanja skalarnog polja i gravitacije (preko Riccijevog skalara R). Tenzor energije-impulsa za globalni monopol se dobije varijacijom akcije po metričkom

tenzoru $g^{\mu\nu}$:

$$
\begin{aligned}
T_{\mu\nu}^{\phi} &= (\partial_\mu \phi^a)(\partial_\nu \phi^a) - g_{\mu\nu} \left[\frac{1}{2} g^{\alpha\beta}(\partial_\alpha \phi^a)(\partial_\beta \phi^a) + \frac{\mu^2}{2} \phi^a \phi^a + \frac{\lambda_\phi}{4}(\phi^a \phi^a)^2 + \frac{\mu^4}{4\lambda_\phi} \right] \\
&\quad - \xi \left(G_{\mu\nu} + g_{\mu\nu}\Box - \nabla_\mu \nabla_\nu \right)(\phi^a \phi^a) .
\end{aligned}
\tag{D.58}
$$

Jednadžba gibanja za skalarno polje dobiva se varijacijom ukupne akcije $S = S_{EH} + S_{GM}$ po ϕ^a:

$$
\Box \phi^a - \frac{\partial V}{\partial \phi^a} + \xi R \phi^a = 0 .
\tag{D.59}
$$

Za polje monopola biramo tzv. jež *Ansatz*

$$
\vec{\phi}(\vec{r}, t) = \phi(r) \left(\sin\theta \, \cos\varphi, \sin\theta \, \sin\varphi, \cos\theta \right) .
\tag{D.60}
$$

Einsteinove jednadžbe $G_{\mu\nu} = 8\pi G_N T_{\mu\nu}$ i jednadžba gibanja za skalarno polje u reduciranim Planckovim jedinicama su

$$
\begin{aligned}
\frac{d\lambda}{dx} &= \frac{1 - e^\lambda}{x} + \Delta \frac{x}{1 + \xi\Delta\tilde{\phi}^2} \Big\{ \frac{1}{2}(1 + 4\xi)\tilde{\phi}'^2 + e^\lambda \frac{\tilde{\phi}^2}{x^2} + e^\lambda \Delta \frac{\lambda_\phi}{4}(1 - \tilde{\phi}^2)^2 \\
&\quad - \xi\nu'\tilde{\phi}\tilde{\phi}' + 2\xi e^\lambda \left(\Delta\lambda_\phi(\tilde{\phi}^2 - 1) + \frac{2}{x^2} - \xi\tilde{R} \right) \tilde{\phi}^2 \Big\} ,
\end{aligned}
\tag{D.61}
$$

$$
\begin{aligned}
\frac{d\nu}{dx} &= \frac{e^\lambda - 1}{x} \frac{1 + \xi\Delta\tilde{\phi}^2}{1 + \xi\Delta\tilde{\phi}^2 + \xi\Delta x\tilde{\phi}\tilde{\phi}'} \\
&\quad - \Delta \frac{x}{1 + \xi\Delta\tilde{\phi}^2 + \xi\Delta x\tilde{\phi}\tilde{\phi}'} \Big\{ -\frac{1}{2}\tilde{\phi}'^2 + 4\xi\frac{\tilde{\phi}\tilde{\phi}'}{x} + e^\lambda \left(\frac{\tilde{\phi}^2}{x^2} + \Delta \frac{\lambda_\phi}{4}(1 - \tilde{\phi}^2)^2 \right) \Big\} ,
\end{aligned}
\tag{D.62}
$$

$$
\frac{d^2\tilde{\phi}}{dx^2} = -\frac{1}{2}\left(\frac{d\nu}{dx} - \frac{d\lambda}{dx} + \frac{4}{x} \right)\tilde{\phi}' + e^\lambda \left[\Delta\lambda_\phi(\tilde{\phi}^2 - 1) + \frac{2}{x^2} - \xi\tilde{R} \right]\tilde{\phi} ,
\tag{D.63}
$$

s Riccijevim skalarom

$$
\tilde{R} = \Delta \frac{(1 + 6\xi)\left[e^{-\lambda}\tilde{\phi}'^2 + 2\frac{\tilde{\phi}^2}{x^2} - \Delta\lambda_\phi\tilde{\phi}^2(1 - \tilde{\phi}^2) \right] + \Delta\lambda_\phi(1 - \tilde{\phi}^2)}{1 + \xi(1 + 6\xi)\Delta\tilde{\phi}^2} .
\tag{D.64}
$$

U limesu $x \to \infty$ ($\tilde{\phi} \to 1$) jednadžbe (D.61) i (D.62) se mogu formalno integrirati, iz čega slijedi

$$e^{-\lambda(x)} = e^{\nu(x)} = 1 - \frac{\Delta}{1 + \xi\Delta} - \frac{2M}{x}. \tag{D.65}$$

gdje je M masa jezgre monopola. Deficitni kut u slučaju neminimalnog vezanja je:

$$\tilde{\Delta} = \frac{\Delta}{1 + \xi\Delta}\,, \tag{D.66}$$

pri čemu je $\Delta = 8\pi G_N \phi_0^0$ deficitni kut, tj. skala lomljenja simetrije i $\tilde{\phi} = \phi/\phi_0$. Rubni uvjeti za jednadžbe (D.61–D.63) su:

$$(1)\ e^{\lambda(0)} = 1, \quad (2)\ e^{\nu(\infty)} = 1 - \tilde{\Delta}\,, \quad (3)\ \tilde{\phi}(0) = 0, \quad (4)\ \tilde{\phi}(\infty) = 1. \tag{D.67}$$

Rezultati i diskusija

U slučaju minimalnog vezanja ($\xi = 0$) polje monopola je pozitivno i monotono, masa jezgre je uvijek negativna, i efektivna (v. Dodatak D) i Newtonova sila (v. Dodatak C) su odbojne na cijelom r-u, gustoća energije je pozitivna i monotona, tlakovi su negativni (uz $p_r > p_t$), te je jaki energijski uvjet narušen. U slučaju neminimalnog vezanja ($\xi \neq 0$), polje monopola je također pozitivno i monotono (v. Sl. D.8), no masa jezgre sada postaje lokalno pozitivna fukcija radijusa (v. Sl. D.9). Efektivna i Newtonova sila također mogu biti lokalno privlačne (v. Sl. D.10), iako su asimptotski ipak odbojne. Iako je masa jezgre lokalno pozitivna za određene vrijednosti ξ, to svojstvo nije uzrokom postojanja lokalno privlačnih sila (te stabilnih kružnih orbita), već (lokalno) poštivanje jakog energijskog uvjeta zbog pozitivnih tlakova i (lokalno) negativne gustoće energije (v. Sl. D.11), koja očito narušava slabi energijski uvjet.

## Neminimalna bozonska zvijezda i globalni monopol

D-zvijezde ili zvijezde s topološkim defektima su *"kompaktni objekti s deficitnim kutem, koji generaliziraju Q-zvijezde uvođenjem kompleksnog skalarnog polja (ili fermionskog polja), Goldstoneovog polja i klasične Einsteinove gravitacije"* [105]. U [106] su se istraživale fermionske D-zvijezde, dok se u [107] provela aproksimativna analiza bozonskih D-zvijezda. Dok su fermionske D-zvijezde pokazale još uvijek neriješene probleme stabilnosti, izučavanje bozonskih D-zvijezda je motivi-
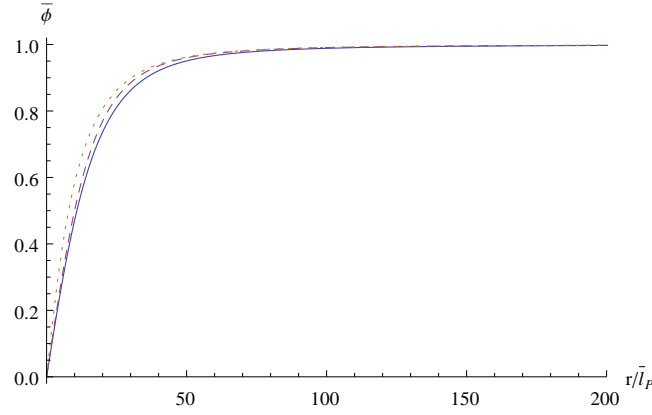
Slika D.8. *Polje monopola $\bar{\phi}$ za $\lambda_\phi = 0.1$, $\Delta = 0.1$, $\xi = -1$ (puna krivulja), $\xi = 1$ (isprekidana krivulja) i $\xi = 2$ (točkasta krivulja).*
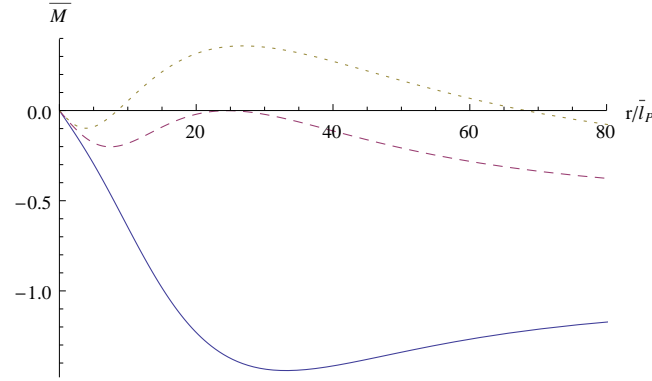
Slika D.9. *Masa jezgre za $\lambda_\phi = 0.1$, $\Delta = 0.1$, $\xi = -1$ (puna krivulja), $\xi = 1$ (isprekidana krivulja) i $\xi = 2$ (točkasta krivulja).*
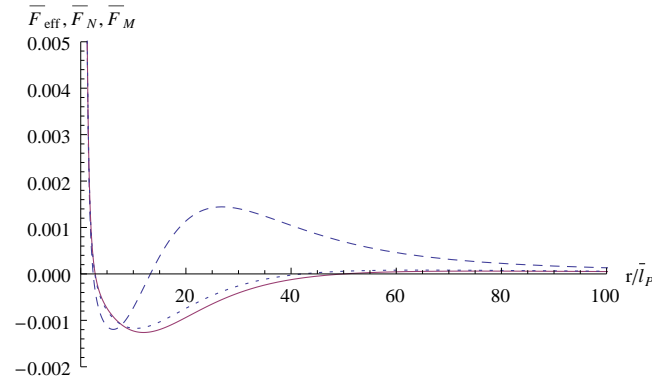
Slika D.10. *Efektivna sile $\bar{F}_{\mathrm{eff}}$ (D.12) (puna krivulja), Newtonova sila $\bar{F}_N$ (C.12) (točkasta krivulja) i Newtonova sila od mase jezgre monopola (4.48) (isprekidana krivulja) za $\xi = -1$, $\lambda_\phi = 0.1$, $\Delta = 0.1$. Kutni moment i energija čestice po jedinici su $\bar{L} = 0.1$ i $\bar{E} = 1$.*
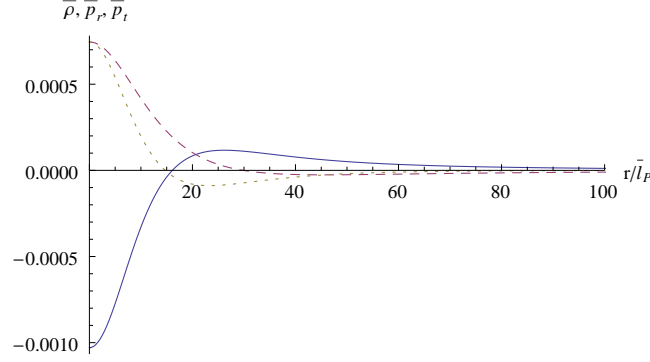
Slika D.11. *Gustoća energije $\bar{\rho}$ (puna krivulja) i principalni tlakovi (isprekidane krivulje, $\bar{p}_r > \bar{p}_t$) kao fukcija $x = r/\bar{l}_P$ za $\lambda_\phi = 0.1$, $\Delta = 0.1$ i $\xi = -1$.*

ralo postojanje crnih rupa s deficitnim kutem. Nadalje, gibanje u polju D-zvijezda se proučavalo u [108], dok su se u [105] razmatrale D-zvijezde kao gravitacijske leće.

U ovoj disertaciji se detaljno analizira sustav koji se sastoji od bozonske zvijezde i globalnog monopola, prilikom čega su oba polja neminimalno vezana na gravitaciju te međudjeluju jedino gravitacijski.

Model

Za materiju uzimamo zbroj akcija za neminimalnu bozonsku zvijezdu (D.38) i neminimalni globalni monopol (D.56)

$$S = S_{BS} + S_{GM}. \tag{D.68}$$

Tenzor energije-impulsa kombiniranog sustava je

$$T_{\mu\nu} = T_{\mu\nu}^{\mathrm{BS}} + T_{\mu\nu}^{\mathrm{GM}}, \tag{D.69}$$

gdje je $T_{\mu\nu}^{\mathrm{BS}}$ dan jednadžbom (D.39) i $T_{\mu\nu}^{\mathrm{GM}}$ jednadžbom (D.58). S indeksom *1* označavamo polje i parametre za bozonsku zvijezdu, a s indeksom *2* polje i parametre za globalni monopol. Jednadžba gibanja za polje bozonske zvijezde je

$$\sigma'' = -\left(\frac{2}{x} + \frac{\nu' - \lambda'}{2}\right)\sigma' + e^{\lambda}(\tilde{m}_1^2 + \lambda_1\sigma^2 - \tilde{\omega}^2 e^{-\nu} - \xi_1\tilde{R})\sigma, \tag{D.70}$$

dok je jednadžba gibanja za monopolsko polje jednaka

$$\tilde{\phi}'' = -\left(\frac{2}{x} + \frac{\nu' - \lambda'}{2}\right)\tilde{\phi}' + e^{\lambda}\left(\lambda_2\Delta(\tilde{\phi}^2 - 1) + \frac{2}{x^2} - \xi_2\tilde{R}\right)\tilde{\phi}. \qquad \text{(D.71)}$$

Iz prve dvije Einsteinove jednadžbe $G_{\mu\nu} = 8\pi G_N T_{\mu\nu}$ slijede diferencijalne jednadžbe za metričke funkcije

$$
\begin{aligned}
\lambda' &= \frac{1 - e^{\lambda}}{x} + \frac{x}{1 + 2\xi_1 + \xi_2\tilde{\phi}^2}\Bigg\{e^{\lambda}\left((\tilde{m}_1^2 + \tilde{\omega}^2 e^{-\nu} + \lambda_1/2)\sigma^2 + \frac{\tilde{\phi}^2}{x^2} + \frac{\tilde{\lambda}_2}{4}\Delta^2(1 - \tilde{\phi}^2)^2\right) \\
&\quad + (1 + 4\xi_1)\sigma'^2 + \frac{1}{2}(1 + 4\xi_2)\tilde{\phi}'^2 - 2\xi_1\nu'\sigma\sigma' - \xi_2\nu'\tilde{\phi}\tilde{\phi}' \\
&\quad + 4\xi_1 e^{\lambda}\left[\tilde{m}_1^2 - \tilde{\omega}^2 e^{-\nu} + \lambda_1\sigma^2 - \xi_1\tilde{R}\right]\sigma^2 \\
&\quad + 2\xi_2 e^{\lambda}\left[\lambda_2\Delta(\tilde{\phi}^2 - 1) + \frac{2}{x^2} - \xi_2\tilde{R}\right]\tilde{\phi}^2\Bigg\} \qquad \text{(D.72)} \\
\nu' &= \frac{x}{1 + 2\xi_1\sigma^2 + 2\xi_1 x\sigma\sigma' + \xi_2\tilde{\phi}^2 + \xi_2 x\tilde{\phi}\tilde{\phi}'}\Bigg\{\frac{-1 + e^{\lambda}}{x^2}(1 + 2\xi_1\sigma^2 + \xi_2\tilde{\phi}^2) \\
&\quad + \sigma'^2 - e^{\lambda}(\tilde{m}_1^2 - \tilde{\omega}^2 e^{-\nu} + \frac{\lambda_1}{2}\sigma^2)\sigma^2 - \frac{8\xi_1\sigma\sigma'}{x} + \frac{\tilde{\phi}'^2}{2} - \frac{4\xi_2\tilde{\phi}\tilde{\phi}'}{x} \\
&\quad - e^{\lambda}\left[\frac{\tilde{\phi}^2}{x^2} + \frac{\lambda_2}{4}\Delta^2(1 - \tilde{\phi}^2)^2\right]\Bigg\}. \qquad \text{(D.73)}
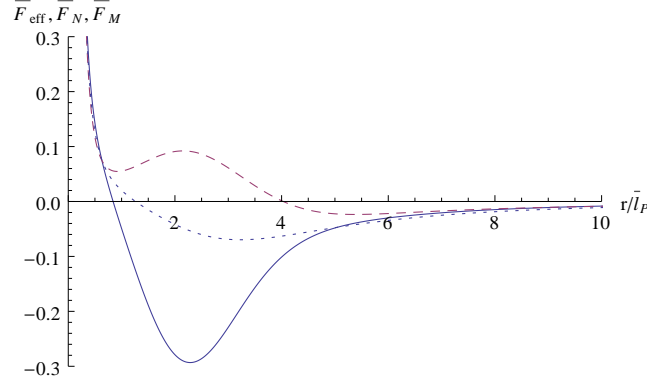\end{aligned}
$$

Reskalirani Riccijev skalar je

$$
\begin{aligned}
\tilde{R} &= \frac{2\tilde{m}_1^2\sigma^2 + 2(1 + 6\xi_1)\left[(\tilde{m}_1^2 - \tilde{\omega}^2 e^{-\nu} + \lambda_1\sigma^2)\sigma^2 + e^{-\lambda}\sigma'^2\right]}{1 + 2\xi_1(1 + 6\xi_1)\sigma^2 + \xi_2(1 + 6\xi_2)\tilde{\phi}^2} \\
&\quad + \frac{\lambda_2\Delta^2(1 - \tilde{\phi}^2) + (1 + 6\xi_2)\left[e^{-\lambda}\tilde{\phi}'^2 + \frac{2\tilde{\phi}^2}{x^2} - \lambda_2\Delta(1 - \tilde{\phi}^2)\tilde{\phi}^2\right]}{1 + 2\xi_1(1 + 6\xi_1)\sigma^2 + \xi_2(1 + 6\xi_2)\tilde{\phi}^2}. \qquad \text{(D.74)}
\end{aligned}
$$

Skup diferencijalnih jednadžbi (D.71-D.73) se rješava uz rubne uvjete

$$
\begin{aligned}
\lambda(0) &= 0, & \nu(\infty) &= 1 - \tilde{\Delta}, \\
\sigma(0) &= \sigma_0, & \sigma(\infty) &= 0, \\
\tilde{\phi}(0) &= 0, & \tilde{\phi}(\infty) &= 1. \qquad \text{(D.75)}
\end{aligned}
$$

Također ćemo koristiti sljedeće skraćenice

$$\xi_{\text{BS}} = \xi_1, \qquad \xi_{\text{GM}} = \xi_2. \tag{D.76}$$

Slika D.12. *Efektivna sila (D.12) (puna krivulja), Newtonova sila (C.12) (točkasta krivulja) i Newtonova sila od mase jezgre monopola (4.48) (isprekidana krivulja) za kombinirani sustav bozonske zvijezde i globalnog monopola. Vrijednosti parametara su: $\sigma_0 = 0.05$, $\lambda_{\text{BS}} = 0$, $\xi_{\text{BS}} = -4$, $\lambda_{\text{GM}} = 0.1$, $\Delta = 0.08$, $\xi_{\text{GM}} = 5$. Također kutni moment i energija po jedinici mase su $\bar{L} = 0.1$ i $\bar{E} = 1$.*
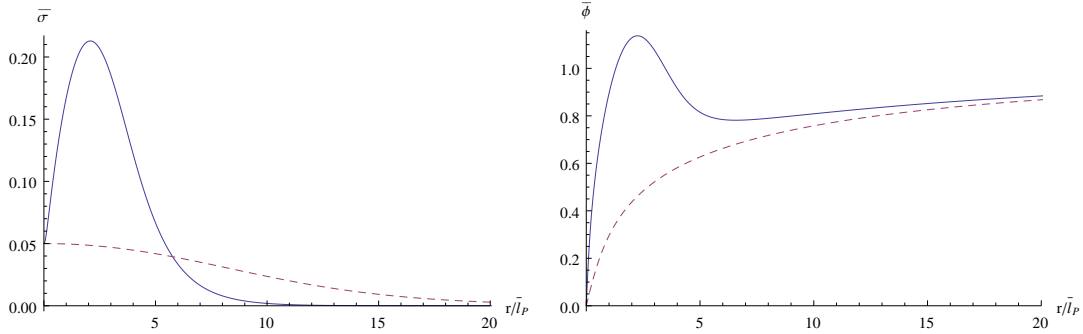
Slika D.13. *Lijevo: polje same bozonske zvijezde (isprekidana krivulja) i polje bozonske zvijezde u prisustvu monopola (puna krivulja). Desno: polje samog globalnog monopola (isprekidana krivulja) i polje globalnog monopola u prisustvu bozonske zvijezde (puna krivulja). Vrijednosti parametara su: $\sigma_0 = 0.05$, $\lambda_{\text{BS}} = 0$, $\xi_{\text{BS}} = -4$, $\lambda_{\text{GM}} = 0.1$, $\Delta = 0.08$, $\xi_{\text{GM}} = 5$.*
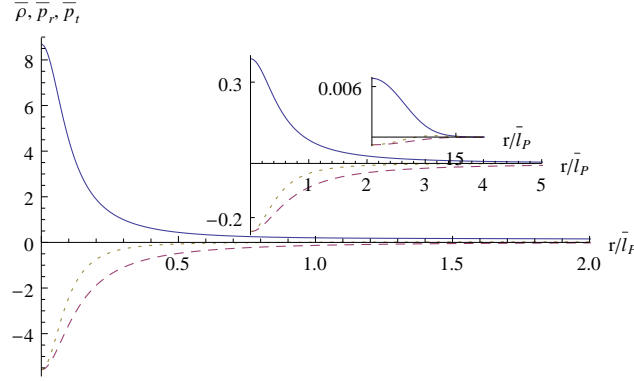
Slika D.14. *Gustoća energije i tlakovi za bozonsku zvijezdu samu (točkasta krivulja), za globalni monopol sam (isprekidana krivulja) i kombinirani sustav bozonske zvijezde i globalnog monopola (puna krivulja). Vrijednosti parametara su: $\sigma_0 = 0.05$, $\lambda_{\text{BS}} = 0$, $\xi_{\text{BS}} = -4$, $\lambda_{\text{GM}} = 0.1$, $\Delta = 0.08$, $\xi_{\text{GM}} = 5$.*

Rješenja i diskusija

U slučaju i bozonske zvijezde i globalnog monopola smo vidjeli da su polja monotona bez obzira na izbor parametara. U kombiniranom sustavu to više nije slučaj: oba polja se rekonfiguriraju ovisno o parametrima. Sukladno tome, razlikujemo tri režima interakcije:

- Režim slabog vezanja: u ovom režimu oba polja zadržavaju svoju monotonost.

- Režim blagog vezanja: u ovom režimu polje bozonske zvijezde blago postaje nemonotono, dok polje monopola ostaje monotono.

- Režim jakog vezanja: u ovom režimu se oba polja znatno rekonfiguriraju te postaju nemonotona. Ovaj režim je posebno zanimljiv jer dolazi do velike kompresije bozonske zvijezde i cijeli sustav dostiže jako veliku kompaktnost, te na taj način rezultirajuća konfiguracije predstavlja dobru alternativu crnoj rupi.

Za bozonsku zvijezdu uzimamo parametre koji odgovaraju maksimalnoj kompaktnosti ($\sigma_0 = 0.05, \lambda_{\text{BS}} = 0, \xi_{\text{BS}} = -4$), dok kod monopola mijenjamo ξ_{GM}.

U režimu slabog vezanja ($\xi_{\text{GM}} = -1$), sve funkcije – gustoća energije, tlakovi, masa jezgre, kompaktnost, efektivne sile – zbrajaju se gotovo linearno.
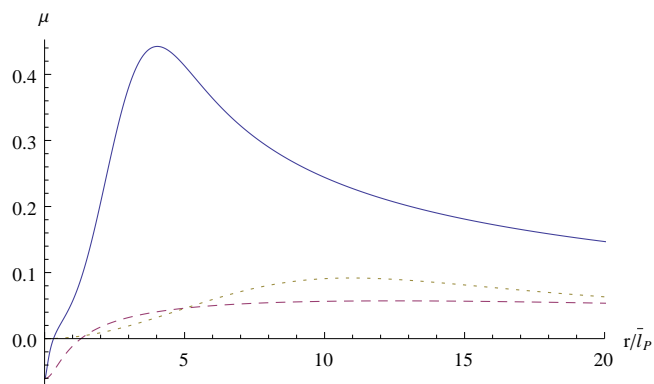
Slika D.15. *Kompaktnost za bozonsku zvijezdu samu (isprekidana krivulja), globalni monopol sam (isprekidana krivulja) i kombinirani sustav (puna krivulja). Vrijednosti parametara su: $\sigma_0 = 0.05$, $\lambda_{\mathrm{BS}} = 0$, $\xi_{\mathrm{BS}} = -4$, $\lambda_{\mathrm{GM}} = 0.1$, $\Delta = 0.08$, $\xi_{\mathrm{GM}} = 5$.*

U režimu blagog vezanja nelinearni efekti su prisutni, te dolazi do umjerene kompresije bozonske zvijezde, tako da su u ovom slučaju sve veličine kombiniranog sustava po iznosu veće od zbroja veličina pojedinih sustava.

U režimu jakog vezanja prisutni su jaki nelinearni efekti koji se mogu pratiti usporedbom efektivne i Newtonove sile (v. Sl. D.12). Oba polja se jako rekonfiguriraju (v. Sl. D.13), dolazi do velike kompresije bozonske zvijezde (v. Sl. D.14) s dosta velikom maksimalnom kompaktnošću (v. Sl. D.15).

Daljnjim povećanjem ξ_{GM}, dobiveni objekt se dodatno smanjuje te se kompaktnost povećava dostižući vrijednosti usporedive s jedinicom, što signalizira formiranje crne rupe. Na Sl. D.16 je prikazana kompaktnost za $\xi_{\mathrm{GM}} = 8$ čija je maksimalna vrijednost nešto iznad 0.75 (puna krivulja). S isprekidanom krivuljom je prikazana kompaktnost za Schwarzschildovu crnu rupu s masom jednakom masi kombiniranog objekta. Zbog jako visoke kompaktnosti ovaj objekt predstavlja dobru altrnativu crnoj rupi.

Zaključak

Glavni rezultati disertacije su:

- metoda za testiranje linearne stabilnosti anizotropnih struktura s de Sitterovom jezgrom je predložena i primijenjena na gravastarske objekte dokazujući njihovu radijalnu stabilnost,
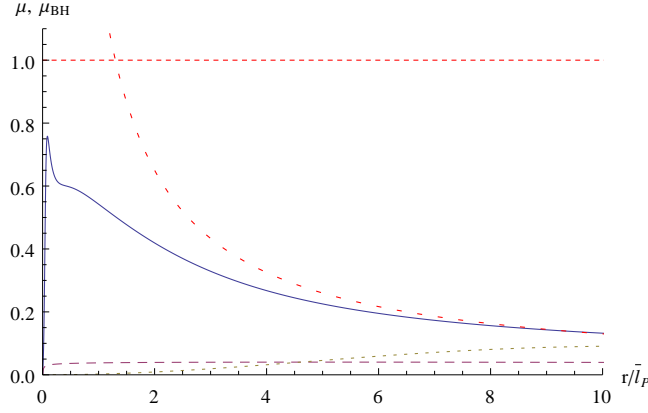
Slika D.16. *Kompaktnost za kombinirani sustav bozonske zvijezde i globalnog mono-
pola (puna krivulja), samu bozonsku zvijezdu (točkasta krivulja) i globalni monopol sam
(isprekidana krivulja). Kompaktnost za Schwarzschildovu crnu rupu s masom jedna-
kom masi kombiniranog sustava (proširena točkasta krivulja). Vrijednosti parametara
su: $\sigma_0 = 0.05$, $\lambda_{BS} = 0$, $\xi_{BS} = -4$, $\lambda_{GM} = 0.1$, $\Delta = 0.11$, $\xi_{GM} = 8$.*

- unutar klasične teorije polja i modificirane gravitacije, iz samointeragi-
  rajućeg skalarnog polja koje je neminimalno vezano na gravitaciju, pronađen
  je model za kompaktni objekt sličan zvijezdama tamne energije,

- unutar klasične teorije polja i modificirane gravitacije, iz kombiniranog sus-
  tava bozonske zvijezde i globalnog monopola čija su polja neminimalno
  vezana na gravitaciju, pronađen je model za visoko kompaktni objekt koji
  predstavlja dobru alternativu crnoj rupi.

CURRICULUM VITAE

Anja Marunović was born on 1979 in Zenica (Bosnia and Herzegovina). She graduated from high school in 1998 at the XV. Gymnasium in Zagreb (major: mathematics). She began undergraduate study in 1998 at the Faculty of Science (Physics) in Zagreb. She graduated in 2006 and from 2007 she has been working at the Department of Applied Physics at the Faculty of Electrical Engineering and Computing as a research assistant. She began postgraduate studies in 2008 at the Department of Physics of Faculty of Science under supervision of prof. Dubravko Horvat. During her PhD studies she attended many international schools and conferences. From 2009 she has an ongoing international collaboration with Utrecht University in the Netherlands. Her research interests lie in the fields of cosmology and gravity. So far she has published six scientific papers.

ŽIVOTOPIS

Anja Marunović rođena je 1979. godine u Zenici (Bosna i Hercegovina). Završila je XV. Gimnaziju u Zagrebu (matematički smjer) 1998. godine. Iste godine upisala je studij Fizike na Prirodoslovno-matematičkom fakultetu u Zagrebu. Diplomirala je 2006. te od 2007. godine radi kao znanstveni novak na Zavodu za primijenjenu fiziku Fakulteta elektrotehnike i računarstva. Doktorski studij je upisala 2008. god. pod mentorstvom prof. Dubravka Horvata. Tijekom poslijediplomskog studija sudjelovala je na brojnim međunarodnim školama i konferencijama. Od 2009. godine ima međunarodnu znanstvenu suradnju sa Sveučilištem u Utrechtu u Nizozemskoj. Njeni glavni znanstveni interesi leže u području gravitacije i kozmologije. Do sada je objavila šest znanstvenih radova.